Persistent trade-offs balance competition and colonization across centuries

Talia Backman*[1], Jiajun Cui*[2], Emma Caullireau*[1], Ella Bleak[1], Ilja Bezrukov[3], Patricia Girardi[1], Aubrey Hawks[1], Jesse R. Lasky[4,5], Sergio M. Latorre[2], Joel M. Erberich[6], Lua Lopez[4,7], Manuela Neumann[3], Allison M. Perkins[1], Efthymia Symeonidi[1], Parastoo Azadi[8], Martin P. Horvath[1], Artur Muszyński[8], Patricia L. M. Lang[9], Talia L. Karasov*[1*†], Hernán A. Burbano*[2†]

Affiliations:
[1]School of Biological Sciences, University of Utah, Salt Lake City, UT 84112, USA.
[2]Centre for Life's Origins and Evolution, Department of Genetics, Evolution and Environment, University College London, London WC1E 6BT, UK
[3]Department of Molecular Biology, Max Planck Institute for Biology Tübingen, Tübingen 72076, Germany
[4]Department of Biology, Pennsylvania State University, University Park, PA 16802, USA
[5]PAC Herbarium, Pennsylvania State University, University Park, PA 16802, USA
[6]Department of Biology, Stanford University, Stanford, CA, USA
[7]Department of Biology, California State University, San Bernardino, California, USA
[8]Complex Carbohydrate Research Center, University of Georgia, Athens, GA 30602, USA
[9]Department of Plant and Microbial Biology, University of California Berkeley, Berkeley, CA 94720, USA

*Equal contribution
†Corresponding author

ORCID:
TB 0000-0002-1967-270X, talia.backman@utah.edu
JC 0009-0009-4453-0744, jiajun.cui.22@ucl.ac.uk
EC 0000-0002-9484-2182, emma.caullireau@utah.edu
EB 0009-0009-3437-9163, u1346590@utah.edu
IB 0000-0003-0420-4329, ilja.bezrukov@tue.mpg.de
PG 0009-0008-1209-1196, patricia.girardi@utah.edu
AH 0000-0001-6061-2584, aubrey.hawks@utah.edu
JL 0000-0001-7688-5296, lasky@psu.edu
SL 0000-0002-5889-0670, s.latorre@ucl.ac.uk
JE 0000-0002-3844-9386, jerberic@stanford.edu
LL 0000-0002-3619-763X, lua.lopezperez@csusb.edu
MN 0000-0003-2778-3028, hoelscher.manuela@gmail.com
AP 0009-0006-8267-9628, allison.perkins@utah.edu
ES 0000-0002-4412-4596, u6030864@umail.utah.edu
PA 0000-0002-6166-9432, azadi@ccrc.uga.edu
MPH 0000-0003-3057-9722, martin.horvath@utah.edu
AM 0000-0003-3497-9977, muszynski@ccrc.uga.edu
PL 0000-0001-6648-8721, plang@berkeley.edu
TLK 0000-0002-3592-6597, t.karasov@utah.edu
HAB 0000-0003-3433-719X, h.burbano@ucl.ac.uk

Abstract

Microbial competition drives rapid adaptation, often forcing organisms to specialize in new ecological niches. Adaptations that improve competitive ability can reduce performance in other environments creating trade-offs. Whether such trade-offs persist in nature—or are eroded as lineages adapt through compensatory changes—remains largely unknown. Here we show that a trade-off between competitive ability and host colonization has been stably maintained in natural *Pseudomonas* populations for centuries. Wild plant-pathogenic *Pseudomonas* compete using

tailocins—phage-derived molecular weapons that bind to specific cell-surface receptors. Genomic surveys and functional assays reveal that the most broadly lethal tailocins remain rare—while the tailocin's production increases competitive killing, it also compromises plant colonization. We determine that the polymorphisms behind this tradeoff are not transient — historical genomes spanning two centuries show that the tradeoff has been maintained for at least 10^5–10^6 generations. Our results demonstrate that, in natural populations, a tradeoff between competition and pathogenicity is fundamental and not easily overcome.

Introduction

Competition between microbes is an ecological and evolutionary force that shapes community structure, resource use, and diversification [1]. Experimental evolution has shown that competition can drive rapid adaptation to new ecological niches [2], yet these adaptive gains often come at a cost in other contexts. The resulting trade-offs—between competitive ability, growth, and colonization—are hypothesized to be pervasive in microbial communities [3]. However, most evidence for such trade-offs comes from experimental evolution in laboratory systems [4], leaving open the question of whether they constrain populations in wild environments and over longer, evolutionary timescales. Do microbes in the wild overcome these trade-offs, optimizing performance across environments, or do they remain trapped by enduring conflicts between competition and colonization?

We address this question in *Pseudomonas viridiflava*, a common plant-pathogenic bacterium that infects *Arabidopsis thaliana* across Europe [5,6]. Within these populations, a pathogenic phylotype named ATUE5 forms a genetically diverse metapopulation in which no single strain dominates [6]. Intraspecific competition within ATUE5 is an important selective pressure [7] mediated by molecular weapons termed tailocins. Tailocins are diffusible protein complexes that resemble phage tails and kill susceptible strains by puncturing their cell membranes [8]. Bacteria are resistant to their own tailocins upon encounter in the environment, allowing producer clones to suppress non-self competitors while sparing their own lineage [9]. Because tailocins are released through cell lysis, the producing cell dies. Consequently, only a fraction of a clonal population produces tailocins, thereby protecting clonemates and suppressing competing strains [9].

The tailocin gene cluster in ATUE5 consists of ~24 collinearly arranged genes, integrated at the same genomic location in all strains, which together assemble the functional tailocin. Each ATUE5 strain encodes one of a few tailocin variants, distinguished by the tail fiber (HTF), a receptor-binding protein that dictates killing specificity [7,8]. The HTF binds to the outer membrane of the target cell, specifically recognizing the O-antigen, a highly variable component of the bacterial lipopolysaccharide (LPS) layer. In ATUE5, *HTF* genes vary in length (1245–1830 bp) and killing spectrum, with distinct length classes corresponding to unique O-antigen biosynthesis gene profiles, suggesting tight linkage between *HTF* variants and their O-antigen receptors within each tailocin-producing bacterium.

Paradoxically, bacteria that produce the most lethal tailocin variant—capable of killing ~80 % of other strains and resistant to ~70 % of others—remain rare in natural populations. Why has the most competitive variant not spread to fixation? We hypothesized that its persistence at low frequency may reflect a trade-off between competitive dominance and host colonization. The O-antigen provides a mechanistic link between these processes [10]. O-antigen diversity influences surface recognition, virulence, and susceptibility to tailocins [11,12] potentially generating an evolutionary tension between success within the host and resistance to microbial attack.

To test for this competition-colonization tradeoff, we combined saturation mutagenesis with functional assays and *in planta* infections. The genetic mutations most important for surviving in the presence of the tailocin also compromised growth in the plant. This experiment showed a short-term tradeoff acting on contemporary bacterial strains. We then examined whether this tradeoff showed evolutionary persistence by analysing 49 historical bacterial genomes recovered from herbarium specimens spanning more than two centuries. Together, the modern and historical population datasets

provide a uniquely powerful framework to identify the association between tailocin and O-antigen polymorphisms underlying the competition-colonization tradeoff, and then to assess whether the trade-off is transient or an enduring feature of bacterial evolution.

Here, we show that O-antigen–dependent trade-offs between pathogenicity and interbacterial competition have persisted for over two centuries in natural *P. viridiflava* populations. O-antigen production enhances virulence but increases susceptibility to tailocin attack. By integrating historical genomics with functional microbiology, we reveal the genetic basis, ecological significance, and remarkable temporal stability of this trade-off. These findings demonstrate that structural constraints on microbial competition and colonization can maintain genetic diversity across evolutionary timescales, illuminating why the most competitive strains do not necessarily dominate in nature.

Results

The growth-defense tradeoff: the O-antigen biosynthesis cluster (OBC) reduces resistance to interbacterial killing by tailocins but enhances colonization *in planta*.

Our previous work established four major *HTF* length variants in *P. viridiflava* populations (1245, 1383, 1803, and 1830 bp) [7]. These *HTF* length variants correlate, within the same bacterial genome, with the presence or absence of specific genes in the O-antigen biosynthesis cluster (OBC) that are critical for tailocin binding. The tight linkage between *HTF* length variants and OBC haplotypes within a bacterial genome suggests that the tail fiber and its O-antigen receptor are evolving in concert in natural populations of *P. viridiflava*. To determine the killing spectrum for each of these *HTF* length variants, we conducted killing assays that included at least one representative from each variant. The individual tailocin preparations were applied to a panel of 50 *P. viridiflava* tester strains that captured the diversity of the focal OBC presence and *HTF* length variants in the metapopulation (**Fig. 1A**). As shown previously, the 1245 bp and 1803 bp *HTF* variants are correlated in the genome of modern strains with OBC^+, whereas the 1383 bp and 1830 bp variants occur only in OBC^- strains [7]. The resulting killing spectra revealed a strong pattern: tailocins from OBC^- strains killed on average 79% of tester strains, while those from OBC^+ strains killed 51% (**Fig. 1B**). These results provide preliminary evidence that OBC^- strains are more successful interbacterial competitors. Despite this apparent advantage, the OBC^- strains represent only ~16% of the population. We thus hypothesized that loss of O-antigen in the OBC^- genotypes leads to reduced fitness in other natural conditions such as during plant infection[13].

To test the colonization hypothesis, we infected *A. thaliana* seedlings with a subset of wild *P. viridiflava* strains that varied in *HTF* length and, therefore, OBC presence. Plant health was quantified using green pixel counts from high-quality plant images, where lower green pixel counts corresponded to a more diseased plant. We found that OBC^+ strains (associated with the 1245 bp and 1803 bp *HTF* haplotypes) caused more severe disease phenotype than OBC^- strains (associated with the 1383 bp and 1830 bp *HTF* haplotypes) (**Fig. 1C**). These results provide preliminary data that suggest that OBC^+ strains may have enhanced aggressiveness in this experimental context. Together, these results suggest a trade-off between interbacterial competition and host colonization: OBC^- strains gain a competitive edge through potent tailocins but suffer reduced virulence *in planta*, whereas OBC^+ strains colonize hosts more effectively but are more vulnerable to tailocin-mediated killing (**Fig. 1D**).

OBC genes mediate a trade-off between tailocin resistance and plant colonization.

We next examined whether disrupting O-antigen biosynthesis within a single genetic background reproduces the population-level trade-off between tailocin resistance and host colonization. We chose to focus on the model *P. viridiflava* strain p25.C2 [7,14] which is OBC^+ and susceptible to the tailocin produced by strain p25.A12 [7]. To systematically identify genes involved in both tailocin susceptibility and fitness *in planta*, we employed high-throughput Random-Barcoded Transposon (Tn) Sequencing (RB-TnSeq) [15]. This approach uses uniquely barcoded transposon mutants to measure each gene's

contribution to fitness across different growth conditions. We previously performed RB-TnSeq fitness in liquid culture of p25.C2 treated with strain p25.A12's tailocin to identify mutations (Tn-insertions) that render P25.C2 resistant to p25.A12's tailocin [7]. Here, we performed RB-TnSeq with the same library in plant infections (*A. thaliana* ecotypes Col-0 and the common German genotype Eyach 1.5-2) to identify mutations that influence fitness in the plant hosts. We tracked the abundance of mutants after growth either in a tailocin environment or in the plants, which provided relative fitness in the presence of tailocins versus within the plant host (**Fig. 2A**). As reported previously, mutants in the OBC significantly increased in abundance following tailocin application, indicating that disruption of these genes confers resistance (**Fig. 2B**, log fold change tailocin > 0) [7].

To determine how these tailocin resistance mutations influence fitness in the host, we plotted each mutant fold-change in abundance during plant colonization (in Eyach 1.5-2; x-axis) against its abundance change under tailocin application (y-axis; **Fig. 2B**). Among the 70 mutations (putative gene knockouts) associated with tailocin resistance [7], 21 significantly reduced bacterial fitness in at least one ecotype, with 13 (61%) showing reduced fitness across both ecotypes (**Fig. 2B**, **Table S1**). We focus on this set of 21 genes, which constitute the "trade-off" genes, for which transposon insertions increases fitness upon tailocin challenge, but decreases fitness during colonization.

We then examined the predicted function of these 21 trade-off candidate genes: seven are found within a single 18-kb operon predicted to synthesize the focal OBC (**Fig. 2C**). These genes encode sugar nucleotide synthases (*rfbB*, *rmlA2_1*, *wfgD*, *rmlC_1*) and glycosyltransferases (*tagG_2*, *tagH_2*, *epsE_4*) responsible for the sequential transfer of sugars involved in O-antigen initiation, elongation, polymerization, or ligation (**Fig. 2D**). Putative knockouts in genes involved in this pathway increased survival under tailocin treatment but reduced fitness during leaf colonization, supporting the hypothesized competition-versus-colonization trade-off, regardless of the phase in O-antigen biosynthesis. The same pattern emerged, although with smaller effect sizes, for additional LPS- and O-antigen-related genes elsewhere in the genome, suggesting that LPS and O-antigen modifications are common for tailocin-resistant mutations that result in reduced colonization (**Table S1**).

The overlap in the RB-TnSeq results in two *A. thaliana* ecotypes validates the predicted trade-off, suggesting that the OBC resistance mechanism is associated with impaired plant colonization, thereby prioritizing the OBC for further functional analysis.

O-antigen mutants alter LPS structure and reduce susceptibility to tailocins and bacterial load *in planta*.

To confirm the contribution of the O-antigen deletion on *P. viridiflava* growth in the plant niche, we generated site-directed deletion mutants. We generated clean deletion mutants via homologous recombination for six candidate OBC genes mutants. These included putative nucleotide sugar biosynthetic enzymes (*wfgD*, *rmlC_1*), and glycosyltransferases (*tagG_2*, *tagH_2*, *epsE_4*, *spsA*; **Fig. 2C**). *spsA* was included in the mutant analysis given its position within the same predicted operon and its prior functional annotation as an O-antigen biosynthetic gene as previously reported [7].

These gene disruptions altered LPS structure, as shown by the electrophoretic profiles of purified LPS (**Fig. 3A**). Five of six mutants (Δ*wfgD*, Δ*tagG_2*, Δ*tagH_2*, Δ*epsE_4*, and Δ*spsA)* lack high-molecular-weight bands relative to WT, consistent with a modification or absence of O-antigen polymer (silver-stained DOC-PAGE, **Fig. 3A**). In contrast, Δ*rmlC_1,* a deletion of a gene with a sequence homolog in the same genome, retained a higher-molecular-weight band, as observed in WT. Chemical compositional analysis further supported these LPS modifications, showing a shift in sugar residues with a marked loss of rhamnose in all mutants except Δ*rmlC_1* (**Table S2**).

Next, tailocin susceptibility of the mutants was assessed using a soft agar overlay assay with partially purified tailocin from p25.A12 (**Fig. 3B**). The five mutants (Δ*wfgD*, Δ*tagG_2*, Δ*tagH_2*, Δ*epsE_4*, and Δ*spsA)* exhibited resistance to tailocin-mediated killing, while Δ*rmlC_1* showed killing zones similar to WT. We then tested whether O-antigen loss affects bacterial growth and disease *in planta*,

194 by flood-inoculating *A. thaliana* seedlings with WT and O-antigen mutants. We additionally assesed
195 bacterial population size dynamics as well as plant health 7 days post-inoculation (dpi). Across both
196 *Arabidopsis* ecotypes, O-antigen mutants generally exhibited reduced bacterial load compared to WT at 7
197 dpi, consistent with a fitness cost of resistance to tailocin (**Fig. 3C**). In Col-0, all six mutants showed
198 significantly lower bacterial load than WT, with highly significant differences observed for all strains
199 after FDR correction (all $p < 0.0001$). In Eyach 1.5-2, three mutants (Δ*spsA*, Δ*tagH_2*, and Δ*wfgD*)
200 exhibited strongly reduced growth relative to WT (FDR-adjusted $p < 0.005$), while Δ*epsE_4*, Δ*rmlC_1,*
201 and Δ*tagG_2* were moderately reduced (FDR-adjusted $p \approx 0.05$). Notably, these results were independent
202 of the inoculation method, as similar outcomes were observed following the syringe infiltration of one
203 O-antigen mutant into plants leaves (**Fig. S1**), suggesting that the role of the O-antigen for colonization
204 extends beyond the leaf surface (epiphytic phase) to the inside of the plant tissue (endophytic phase).
205 Deletion of O-antigen synthesis genes conferred improved plant health outcomes relative to wild-type
206 (WT): in both ecotypes, infections with WT strain frequently resulted in chlorosis or necrosis, whereas
207 infections with O-antigen mutants more often led to asymptomatic, healthy plants (**Fig. S2**). Furthermore,
208 plant health tended to decline overall with increasing bacterial load (**Fig. S3**). Together, these findings
209 validate the function of the insertion mutant candidate genes for an O-antigen-mediated trade-off between
210 tailocin resistance and host colonization with robust and consistent effects across multiple genetic
211 backgrounds.

212 **O-antigen loss affects growth properties *in vitro* but does not affect tolerance to stresses nor host**
213 **immunity activation.**

214 We investigated the biological basis of the reduced bacterial fitness observed *in planta* by testing several
215 hypotheses. Specifically, we considered whether this tradeoff could result from (i) a general physiological
216 defect affecting bacterial growth properties, (ii) a higher susceptibility to antimicrobials or reduced stress
217 tolerance due to membrane permeability, and/or (iii) a stronger activation of host immunity due to a faster
218 pathogen recognition.

219 We first compared the *in-vitro* growth of the WT and O-antigen deletion mutant strains and
220 observed that all mutants, except Δ*rmlC_1*, displayed a growth defect in liquid cultures grown in rich
221 medium (**Fig. S4**). This defect was statistically significant based on several growth parameters, including
222 the growth rates (*k* or *r*), generation time, and the area under the curve (AUC; **Table S3**). We next
223 assessed surface-associated growth of the WT and the O-antigen mutant strains using a 96-well static
224 assay. The WT and Δ*rmlC_1* strains consistently showed no visible aggregate formation, whereas all
225 other O-antigen mutants formed robust surface-associated aggregates in nearly every well after 48 hours
226 of incubation (≥ 95% of replicates, Pearson's $\chi^2 = 241.5$, $p < 2 \times 10^{-16}$; **Fig. S5**). All O-antigen mutants
227 except Δ*rmlC_1* produced significantly more aggregates than the WT (pairwise Fisher's exact test,
228 adjusted $p < 10^{-16}$).

229 Secondly, to test whether O-antigen acts as an antimicrobial barrier during plant colonization, we
230 compared the tolerance of tailocin-resistant O-antigen mutants and the WT to two stressors: the cationic
231 peptide polymyxin B (PMB) and hydrogen peroxide (H_2O_2). No significant difference in growth
232 inhibition was observed between the WT and the O-antigen *P. viridiflava* mutants in PMB disk diffusion
233 assays, regardless of the compound concentration (**Fig. S6A**). Similar results were also observed with
234 another polymyxin (colistin sulfate, **Fig. S6B**). These results indicate that the O-antigen does not
235 contribute detectably to polymyxin tolerance in our strains, in contrast to previous reports describing high
236 sensitivity to PMB of O-antigen mutants in *P. aeruginosa*[16]. Furthermore, growth curves across a gradient
237 of H_2O_2 concentrations revealed that all strains shared the same inhibitory profile, with indistinguishable
238 minimum inhibitory concentrations (MICs; MIC/WT ≈ 1.0 for all strains; **Table S4**) and parallel declines
239 in AUC as H_2O_2 increased (**Fig. S7**). Mixed-effects modeling of five independent replicates confirmed
240 that O-antigen mutants did not differ significantly from WT in their AUC responses or MIC values after

accounting for replicate-level variation.

Finally, we tested whether the O-antigen influences host immunity activation. Focusing on six marker genes associated with early (*FRK1*, *WRKY29*, *NHL10*, *PAD3*) or late (*PDF1.2*, *PR1*) plant defense responses, we monitored their expression from 0 to 72 hours post-infection with either the WT strain or selected O-antigen mutants. We found no evidence of a stronger or faster plant defense activation that could account for the reduced fitness of the O-antigen mutants *in planta* (**Fig. S8**).

Together, these data indicate that the loss of O-antigen (i) generally affects bacterial growth *in vitro* and promotes surface-associated aggregate formation, but is not relevant for (ii) tolerance to reactive oxygen species or cationic peptides under laboratory conditions, and (iii) activation of plant immunity. This suggests that the ecological trade-offs of O-antigen loss observed *in planta* likely result from general physiological changes that lead to altered bacterial growth properties.

Herbarium-derived genomes reveals the persistence of the tradeoff across centuries

Together, our functional and genetic results reveal a clear trade-off: loss of O-antigen confers resistance to tailocins but reduces bacterial fitness during plant colonization. This raises a key evolutionary question: is this trade-off transient, or has it constrained *P. viridiflava* populations over longer, ecological and historical timescales? To investigate this, we used ancient DNA (aDNA) techniques [17] to sequence 49 metagenomic libraries from *A. thaliana* herbarium specimens collected across Europe between 1817 and 2015 (**Fig. 4A**). This ~200 year period corresponds to an estimated 10^5-10^6 generations for *P. viridiflava* [18]. On average, 5.0% (0.2–36.3%) of metagenomic reads mapped to the *P. viridiflava* ATUE5 reference genome (**Fig. S9A**). The herbarium-derived reads covered, on average, 82.5% (59.8–95.1%) of the ATUE5 genome, with an average sequencing depth of 14.7x (1.1-137.4x) (**Fig. S9B**). The *Pseudomonas*-mapped reads showed patterns of DNA damage and fragmentations typical of aDNA [19] (**Fig. S9C; Fig. S10; Fig. S11**) and the distribution of *k*-mer coverage revealed that most historical infections are dominated by a single strain (**Fig. S9D**).

To place the 49 historical *Pseudomonas* draft genomes in the context of contemporary diversity, we constructed a phylogenetic tree that included a subset of 83 contemporary genomes representing the known diversity of *Pseudomonas* segregating in the wild [7]. The tree topology revealed that 43 of the historical draft genomes belong to the ATUE5 phylotype and are broadly distributed across the ATUE5 phylogeny, indicating that historical diversity mirrors contemporary diversity and demonstrating the temporal continuity of ATUE5 over centuries (**Fig. 4A; Fig. S12**).

We then sought to determine the presence of the tailocin cluster and, when present, identify the corresponding *HTF* length variant. The tailocin cluster was detected in all 43 historical genomes (average coverage depth of 17.4x and average proportion of 86.0% of the cluster covered), supporting the idea of a single ancestral insertion shared across the entire ATUE5 population. Due to the high sequence divergence among *HTF* variants, a mapping-based approach was not feasible. We therefore identified the variants using local assembly for high-coverage samples and a unique *k*-mer approach for low-coverage samples. Both approaches yielded congruent results when tested on contemporary ATUE5 short-read data and validated against their corresponding whole-genome assemblies (**Fig. S13A**). Out of the 43 historical *P. viridiflava* draft genomes, we had enough coverage to retrieve reliable *HTF* variants for 38 of the genomes. The local assembly approach permitted the ascertainment of 23 historical *HTF* variants, whereas the approach based on unique *k*-mers allowed us to retrieve 15 additional *HTF* variants (**Fig. S13B**). Our analysis revealed that the four *HTF* length variants have been maintained in European populations over the past 200 years (**Fig. 4A**), suggesting that these variants are subject to long-term selective pressures that contribute to the stability of tailocin-mediated interactions.

Finally, we sought to determine whether the association between *HTF* length variants and O-antigen haplotypes has been maintained over century timescales. To address this, we annotated the

presence or absence of six genes within the O-antigen biosynthesis cluster (OBC) — previously identified as key determinants of tailocin susceptibility in *P. viridiflava* strains [7]. We found that the 1803 bp and 1245 bp *HTF* variants were almost exclusively associated with the presence of the six OBC genes (OBC^+), with only one historical sample deviating from this pattern. Meanwhile, the 1830 bp and 1383 bp *HTF* variants were exclusively associated with the absence of OBC (OBC^-) (**Fig. 4B**). The association between *HTF* variants and OBC haplotypes would be expected if the bacterial chromosome were in strong linkage disequilibrium (LD), but would be unexpected if horizontal gene transfer (HGT) were pervasive and routinely broke down long-range LD. To evaluate this, we calculated pairwise LD between ATUE5 single nucleotide polymorphisms (SNPs) and measured LD decay as a function of the genetic distance between SNPs. We found that LD decays to 50% of its maximum value after only 78 bp (**Fig. S14**). Using an orthogonal, mixture-model–based approach to estimate the relative contributions of recombination and mutation [20], we further estimate that, on average, 96% of SNPs in ATUE5 arise by recombination (**Fig. S15**). These results indicate that HGT-driven recombination is pervasive in ATUE5, making the strong association between *HTF* variants and OBC haplotypes particularly striking, given that the tailocin cluster and the OBC cluster are separated by 1.7 Mb. Our results thus demonstrate that the coupling between tailocin *HTF* length variants and O-antigen haplotypes in *P. viridiflava* has been maintained over a century timescale, likely reflecting the requirement for bacterial self-immunity to their own tailocins. This enduring association suggests that the trade-off between competitive ability and host colonization has persisted for centuries, driven by structural and molecular constraints that restrict the diversification of compatible *HTF*-O-antigen pairs. These constraints preserve functional specificity and prevent deleterious mismatches over evolutionary time. Contemporary data show that *HTF* length variants associated with the absence of O-antigen persist at low frequencies (**Fig. 4C**), likely reflecting the fitness cost imposed by the competition–colonization trade-off. Analysis of historical *HTF* length haplotype frequencies further reveals that none have approached fixation and that their relative abundances fluctuate over time in both the European and German populations (**Fig. 4A-C**), suggesting that the magnitude of the fitness cost associated with the trade-off may vary across ecological or evolutionary contexts.

Discussion

Our results demonstrate that an O-antigen biosynthesis cluster (OBC) mediates a persistent trade-off between tailocin-dependent microbial competition and successful host colonization in *P. viridiflava*. OBC^+ strains colonize *A. thaliana* more successfully but remain more vulnerable to tailocin killing, while OBC^- strains resist tailocins but exhibit reduced growth *in planta*. Previous work has shown O-antigen-dependent costs of phage or tailocin resistance through experimental evolution [21,22]. However, it remains unclear whether such constraints persist in natural populations over extended evolutionary timescales, where environments and clade abundances fluctuate. Here, we extend this body of work, using a time-series of herbarium-derived genomes, to show that this tradeoff is present in natural populations, and long-lived, persisting for more than two centuries or hundreds of thousands of generations.

Tailocin tail fibers recognize O-antigen sugar motifs, with length variation modulating their breadth of killing. The persistence of linkage in OBC-tail fiber associations across both modern isolates and herbarium samples indicates that compensatory evolution to escape this trade-off is constrained, and if it occurs at all, is likely infrequent. It has been hypothesized that evolutionary systems can overcome trade-offs when conflicts are regulatory or ecological—when organisms evolve conditional expression, gene duplication, or context-dependent specialization that separates competing functions [23]. In contrast, structural conflicts embedded in shared molecular architecture are predicted to be less flexible [24]. The O-antigen exemplifies the latter: the same surface structure underlies both host colonization and susceptibility to tailocins, creating an antagonistic pleotropy that makes the trade-off difficult to decouple without compromising either function. We hypothesize that the long-term stability of OBC variants therefore illustrates a case where natural selection is persistently trapped by a structural constraint.

Similar constraints are seen in other systems, such as the conserved flagellin epitope flg22, where mutations that evade host recognition compromise essential motility [25,26]. Our findings suggest that the costs of O-antigen-mediated resistance are lasting features of bacterial physiology rather than short-term fitness deficits that are easily overcome by compensatory mutations.

The continued presence of OBC$^-$ strains in wild populations despite reduced colonization success suggests that ecological factors buffer the costs of O-antigen loss. OBC$^-$ strains may rely on other surface glycans or exopolysaccharides or gain advantages in niches where competition outweighs colonization [27]. Unlike host-microbe interactions in which frequency-dependent selection maintains resistance variation [28], in the tailocin system there is no known frequency dependence of the selection. Instead, variation in host genotype, community composition, or niche context may periodically favor OBC$^-$ lineages, sustaining ATUE5 diversity alongside the structural constraint itself, because no single trade-off state maximizes fitness across all environments [24] Together, these findings show how enduring molecular trade-offs can be stabilized by ecological feedback, producing long-term coexistence rather than evolutionary escape. Understanding such stable constraints could inform antimicrobial strategies that align with, rather than oppose, the predictable evolutionary dynamics of bacterial populations.

Our conceptual model (**Fig. 4D**) synthesizes these results for long-term coevolution between tailocin tail fiber (*HTF*) length and O-antigen structure. *HTF* variants co-occur in wild *Pseudomonas* populations and are associated with differences in tailocin susceptibility and host colonization. We propose that fluctuating ecological contexts of competition versus colonization drive alternating selection for O-antigen variation. Under competitive conditions, tailocin-producing strains with reduced O-antigen gain the fitness advantage, whereas under host-associated contexts, O-antigenic variants perform better. Over time, these opposing forces maintain polymorphism in both *HTF* length and O-antigen composition. This dynamic balance may explain the remarkable temporal persistence of these variants and show how ecological feedback loops can stabilize structural diversity without requiring continuous molecular innovation.

Methods

Bacterial strains, plasmids and growth conditions

The strains used in this study are from Karasov et al. 2018 [6] (ENA: PRJEB24450). Bacteria were grown on Luria-Bertani broth agar (LB agar) and in Luria-Bertani (LB) medium at 28°C for *Pseudomonas spp.* strains and 37°C for *Escherichia coli* strains. All liquid cultures were incubated with shaking at 180 rpm. Antibiotics were used when appropriate at the following concentrations: 50, 100, and 10 µg/ml for kanamycin (Km), nitrofurantoin (NFN), and tetracycline (Tc), respectively. All strains were stored at −80°C in 30% glycerol [v/v]. For plasmid preparation, *E. coli* transformants were cultured in LB. For the selection of the second *P. viridiflava* homologous recombination event, LB supplemented with sucrose (10 g/L tryptone, 5 g/L yeast extract, 10% (W/V) filtered sucrose, 15 g/L agar) plates were used.

Tailocin extraction and partial purification

Methods were adapted from Backman et al. 2024. Overnight cultures were back-diluted into 50 ml of fresh LB to extract and isolate tailocins from the *P. viridiflava* strains. When cultures reached an exponential growth phase [an optical density at 600 nm (OD600) of 0.4 to 0.6), 5 µg/ml MMC (Selleck, catalog no. S8146) was added to induce the bacterial SOS response and tailocin induction. The cultures were then incubated at 28°C for a minimum of 18 hours and then centrifuged at 4°C for 1 hour at 1,400×g to pellet cell debris. The supernatants were sterilized by filtration with 0.2-µm cellulose acetate filters. To precipitate tailocins, 40% (w/v) of ammonium sulfate was slowly added to the filter-sterilized tailocin lysate while stirring on ice. The lysate was left stirring on ice for at least 18 hours. After 18 hours at 4°C, the ammonium sulfate was pelleted by centrifugation at 2,090 × g for 2 hours at 4°C. The supernatant was discarded, and the pellet was resuspended in 500 µl of cold P-buffer (100 mM NaCl, 8 mM MgSO4, 50

385 mM Tris-HCl, pH 7.5) and stored at 4°C. Tailocin lysates were used fresh or for up to 2 weeks and stored
386 at 4°C.
387
388 **Testing bacterial sensitivity to tailocins with spot test phenotypic assays**
389 Methods were adapted from Backman et al. 2024. Briefly, to test the sensitivity of the different bacterial
390 strains to the tailocins, soft agar assays were performed using an adaptation of a protocol from Vacheron
391 et al.[29]. Overnight cultures (750 µl) of each strain were mixed with 25 ml of LB soft agar (0.8%), and the
392 mixture was poured into a square plate and left to harden. Then, aliquots of 3 µl of concentrated tailocins
393 suspension were applied to the agar, along with a control of P-buffer alone and noninduced cultures in
394 serial dilutions. The plates were incubated overnight at 28°C. Bacterial sensitivity or resistance to the
395 tailocins was assessed after 24 hours. No plaques were observed when testing serially diluted tailocins,
396 suggesting that the killing agent is nonreplicative and not a phage. The p25.A12 tailocin can kill p25.C2
397 WT, and was used for mutant spot test phenotypic assays. There were three biological replicates per
398 condition and eight serial dilutions.
399
400 **Plant infections of *Pseudomonas* natural isolates**
401 *A. thaliana* genotypes Eyach 1.5-2 (15-2) and Col-0 were grown axenically and infected with single
402 *Pseudomonas* strains as described in[6]. In brief, seeds were sterilized by overnight incubation at −80°C,
403 followed by 4 hours of bleach treatment at room temperature (seeds in an open 2 mL tube in a desiccator
404 containing a beaker with 40 mL Chlorox and 1 mL HCl (32%)). Seeds were then stratified for three days
405 at 4°C in the dark on ½ MS media. Plants were grown in 3-4 mL ½ MS medium in six-well plates in
406 long-day (16 hours) at 23°C. 12-14 days after stratification, plants were infected with single bacterial
407 strains.
408 *Pseudomonas* overnight cultures were diluted at 1:10 in 5 mL of selective media and grown for
409 an additional three hours. Bacteria were then centrifuged at 3500 g and the pellets diluted to an optical
410 density (OD600) of 0.01 in 10 mM MgSO4. 100 µL of this bacterial suspension was used to
411 drip-inoculate plants, distributing the volume over the whole rosette. Plants were infected with 10 mM
412 MgSO4 as a control. The plates were sealed with parafilm and then returned to the growth chamber.
413 Seven days after infection, pictures of rosettes were taken for green pixel quantification. At least three
414 biological replicates were performed per infection.
415
416 **Plant health quantification with green pixels**
417 For plant health quantification, plates were photographed seven days post-infection, with a
418 tripod-mounted Canon PowerShot G12 digital camera. Individual plants were extracted from whole-plate
419 images as described in [14]. The number of green pixels was determined for each plant and used as a proxy
420 for plant fresh mass. The segmentation of the plant from the background was performed by applying
421 thresholds in LAB color space, followed by a series of morphological operations to remove noise and
422 non-plant objects. Finally, a GrabCut-based postprocessing was applied, and CSV files with plant IDs and
423 green pixel counts were created. The workflow was implemented in Python 3.6 and bash using OpenCV
424 3.1.0 and scikit-image 0.13.0 for image processing operations[14].
425
426 **Competitive mutant fitness assays *in planta***
427 Columbia-0 (Col-0) and Eyach 1.5-2 WT *A. thaliana* plants were grown under long-day conditions (16
428 hours light, 8 hours dark) in an AR41L3 Percival detector with 60% intensity of the SciWhite LED lights.
429 Seedlings were grown in 24-well plates (Greiner Bio-One, catalog no. 6621665). Thirteen-day-old
430 seedlings were used for the infections. Plants were infected with bacterial suspension of the *P. viridiflava*
431 p25.C2 saturation mutagenesis library at an OD_{600} of 0.02. Each plant was infected with 200 µL of
432 bacterial suspension. Each biological sample contained two infected plants. Three days after infection,

433 samples were collected in 2-mL deep-well plates and snap-frozen. Material was ground using two 5-mm
434 glass beads and DNA was extracted using the Puregene extraction kit (QIAGEN Gmbh, Hilden,
435 Germany).
436
437 **RB-TnSeq and analysis of RB-TnSeq data**
438 Methods were adapted from Backman et al. 2024. Briefly, genomic DNA was extracted and barcode PCR
439 was performed as described in[15]. DNA extractions were quantified with NanoDrop 1000 (ThermoFisher
440 Scientific). Barcode sequence data were obtained by multiplexing on a partial NovaSeq X plus lane
441 (Illumina, San Diego, United States) at Novogene (Novogene Corporation Inc., Sacramento, United
442 States). Fitness data were calculated and analyzed from these reads with the DESeq2 R package[30], and
443 scripts can be found on our GitHub page.
444
445 **Construction of the p25.C2 *Pseudomonas* gene deletions**
446 The p25.C2 mutant strains (Δ*OBC*, Δ*wfgD*, Δ*rmlC_1*, Δ*tagG_2*, Δ*tagH_2,* Δ*epsE_4*, and Δ*spsA*) were
447 obtained using the Gateway cloning system with the donor vector pDONR1K18ms (Addgene plasmid no.
448 72644) and the destination vector pDEST2T18ms (Addgene plasmid no. 72647). Briefly, attB-flanked
449 upstream and downstream gene fragments were ordered from TWIST[31] (**Table S5**). BP and LR reactions
450 were conducted in the one-tube format using the attB-flanked fragments. The resulting expression clone
451 was transformed into competent *E. coli* DH5α and then introduced into recipient cells (*P. viridiflava*
452 p25.C2) by conjugation. Recombinant cells (merodiploids) were selected for with the antibiotic resistance
453 conferred by the expression clone and verified with PCR and gel electrophoresis. Positive colonies were
454 purified by streaking onto new plates. Purified merodiploids were grown overnight without the antibiotic
455 conferred by the expression clone to allow for another recombination event and then plated on 10%
456 D-sucrose for *sacB* counterselection. Colonies were examined by PCR and verified by DNA sequencing
457 (GeneWiz). The plasmids for *tagH_2* and *spsA* were ordered directly from TWIST.
458
459 **LPS isolation and purification**
460 Bacteria were grown overnight at 28 °C under vigorous agitation (200 rpm). The suspensions were
461 centrifuged, and the pellets were washed three times in PBS. Wet cell pastes were stored at -70 °C until
462 LPS extraction. The cells were uniformly suspended in deionized water (ratio 1:5 w/v) and the
463 suspensions were brought up to 68 °C with gentle stirring. The extraction was performed by adding an
464 equal volume of preheated to 68 °C 90% liquefied phenol (w/w) and stirring for 20 min at 68 °C,
465 following the Westphal procedure[32] and as previously described[7]. Nucleic acids and proteins were
466 removed by treatment with Benzonase (15 U/mL of LPS stock for 18 h, 37 °C, in the 50 mM $MgCl_2$ and
467 20 mM NaOAc buffer at the pH 7.6), followed by Proteinase K (0.66U/ mL, 18 h, 37 °C), and dialysis
468 (12-14,000 MWCO) at 4 °C against several exchanges of deionized water. Dialyzed fractions were
469 freeze-dried, dissolved, and precipitated three times in cold (-20 °C) 90% EtOH. LPS pellets were
470 freeze-dried again and dissolved in deionized water, and additionally purified by ultracentrifugation at
471 100,000 × g at 4 °C for 16 h. The enzymatic purification and the ultracentrifugation were repeated twice
472 to obtain ultrapure LPS, which was verified by chemical analysis.
473
474 **Analysis of pure LPS by DOC-PAGE**
475 One microgram of purified LPS samples in Laemmli buffer were resolved in 0.75mm-Polyacrylamide gel
476 electrophoresis (PAGE, 4% stacking gel and 18% resolving gel) in the presence of deoxycholic acid
477 (DOC) detergent[33]. for 1 h at 400 V, 30 mA. *Salmonella enterica* ser. *typhimurium* S-type LPS (O-antigen
478 producing strain) was used as a standard. The PAGE was fixed overnight in an aqueous solution of 40%
479 ethanol and 5% acetic acid, and the LPSs were visualized using a silver stain reagent kit (Bio-Rad, CA,
480 USA) after oxidation with sodium periodate.

481
482 **Chemical analysis of pure LPS**
483 Analysis of the glycosyl residues constituting LPS was achieved by derivatizing the samples to
484 O-trimethylsilyl (TMS) methyl glycosides. Briefly, samples were methanolyzed with 1 M HCl-methanol
485 at 80 °C for 18 h, re-N-acetylated at 100 °C for 1 h, and O-trimethylsilylated with Tri-Sil reagent
486 (Thermo-Fisher) at 80 °C for 30 min. Each sample was supplemented with an internal standard of
487 myo-inositol [34,35]. GC-MS analysis of the LPS derivatives was performed on an Agilent AT 7890A GC
488 system interfaced to a 5975B MSD using an Equity-1 (Supelco) fused silica capillary column (30 m
489 length × 0.25 mm ID × 0.25 µm film thickness). The temperature gradient was 80 °C for 2 min, then
490 increased to 140 °C at 20 °C/min with a 2-min hold, followed by an increase to 200 °C at 2 °C/min.
491 Finally, the temperature was increased to 250 °C at 30 °C/min with a 5-min hold. The data were processed
492 using Agilent ChemStation.
493
494 **Plant infection by flood inoculation**
495 To evaluate the growth of p25.C2 WT and O-antigen mutants *in planta*, Columbia-0 and Eyach 1.5-2 WT
496 *A. thaliana* plants were grown under long-day conditions (16 hours light, 8 hours dark) in an AR41L3
497 Percival detector with 60% intensity of the SciWhite LED lights. Seedlings were grown in 24-well plates
498 (Greiner Bio-One, catalog no. 6621665). Thirteen-day-old seedlings were used for the infections. Plants
499 were infected with bacterial suspension of the *P. viridiflava* strain p25.C2, O-antigen mutants, or buffer
500 (10 mM MgSO4). All bacterial strains were tagged with luciferase[14]. Bacteria were grown overnight and
501 diluted 1:10 on the day of the infection. Cells were grown for another 3 hours and then collected and
502 resuspended in 10 mM MgSO4 to a final OD600 of 0.01. The plants were flood-inoculated for 1 min in a
503 randomized manner with 1 mL of treatment (WT, mutant, or buffer).
504
505 **Bacterial fitness evaluation**
506 After flood-inoculation, plants were grown for 7 days and then collected. The collected plants were
507 ground in 1 ml of 10 mM MgSO4 using the Qiagen tissue lyser II, and 200 µl of the suspension was used
508 to measure luciferase activity with a microplate plate reader (Spark®, TECAN, Switzerland). Plants
509 infected with MgSO4 were used as controls. In total, 24 plants were used for each strain or buffer. Plants
510 were blindly scored as healthy (only green, healthy tissue), diseased (chlorosis phenotype, may have some
511 white tissue), or dead (necrosis phenotype, full white tissue).
512 To assess differences in bacterial growth across strains, we used linear mixed-effects models with
513 batch as a random effect and strain as a fixed effect, using the lmer() function in the lme4 R package.
514 Pairwise comparisons between WT and mutant strains were performed using the emmeans() function
515 from the emmeans package. P-values were adjusted for multiple comparisons using the False Discovery
516 Rate (FDR) method, accounting for all pairwise contrasts among strains. This approach enabled us to test
517 for significant differences in colonization while controlling for inflated Type I error rates resulting from
518 multiple tests.
519
520 **Oxidative stress tolerance assays**
521 Methods were adapted from Binesse et al., 2015[36]. To assess sensitivity to reactive oxygen species, we
522 measured growth of WT and O-antigen mutants across a range of hydrogen peroxide (H_2O_2)
523 concentrations using a microplate growth assay. Overnight cultures were diluted into fresh medium and
524 inoculated into 96-well plates containing 0–10 mM H_2O_2 in technical replicates. Optical density (OD_{600})
525 was recorded every 15 minutes for 24 hours at 28°C using a microplate reader (Spark®, TECAN,
526 Switzerland). Four biological replicates were done.
527 For each plate (replicate), raw OD_{600} time series were converted to growth area (AUC) using the
528 trapezoidal rule over 0–24 h. AUC values for each strain were normalized to their respective 0 mM

control to yield AUC_{rel0}. To account for plate-to-plate variation in baseline H_2O_2 potency, we estimated a per-plate WT minimum inhibitory concentration (MIC), defined as the first concentration where mean AUC_{rel0} dropped below 0.1. All H_2O_2 concentrations on that plate were then scaled by the corresponding WT MIC to generate a standardized dose axis (H_2O_2_scaled).

To test for differences in dose-response profiles between WT and O-antigen mutants, we fitted a linear mixed-effects model of log-transformed AUC values, $\log(AUC_{rel0})$ = strain × H_2O_2_scaled + (1 | replicate), using the lmerTest package in R. Estimated marginal means (EMMs) and pairwise contrasts versus WT were computed with the emmeans package on the response scale.

To directly compare MIC values, we also estimated a strain-specific MIC for each replicate using linear interpolation of AUC_{rel0} versus H_2O_2 concentration. A second mixed model of log-transformed MIC values, log(MIC) = strain + (1 ❙ replicate), was used to test for differences in inhibitory thresholds.

Disk diffusion assays

Bacteria were grown for 16 h at 28 °C with vigorous agitation (200 rpm). Suspensions were back-diluted 1:10 in 5 mL of selective liquid medium and grown for an additional 3 h. Suspensions were adjusted to OD600nm = 0.6 and streaked as a thin, uniform layer onto selective solid medium using sterile cotton swabs. Sterile 6 mm filter paper disks were saturated with 20 uL of antimicrobial compound solutions (polymyxin B or colistin sulfate) prepared at concentrations ranging from 0 to 500 ug/mL. Once dried, the disks were placed on the bacterial layer, ensuring sufficient distance between them to prevent overlap of inhibition zones. Inhibition radii were measured after overnight static incubation at 28 °C. The absence of significant differences among strains at each compound concentration was assessed using either one-way ANOVA or Kruskal–Wallis tests, as appropriate.

Aggregation formation assay

Aggregation formation was assessed using a 96-well plate growth assay. Overnight cultures of each strain were grown in LB medium at 28°C with shaking. The following day, cultures were back-diluted 1:10 in fresh LB and grown to an OD_{600} of approximately 0.5. Each culture was then diluted 1:40, and 200 µL of the resulting suspension was added to wells of a sterile, flat-bottom polystyrene 96-well plate (≥10 technical replicates per strain). Wells containing 200 µL of sterile LB served as negative controls. Plates were incubated statically at 28°C for 48 h. Biofilm formation assays were done in three biological replicates.

After incubation, wells were visually blindly scored as aggregation (visible surface-associated growth), no aggregation (turbid growth without surface attachment), or clear (no growth). For statistical analyses, aggregation presence/absence was coded as a binary trait. Proportional differences among strains were first tested with a Pearson's chi-square test, followed by pairwise Fisher's exact tests comparing each mutant to the WT strain (p25.C2). Resulting p-values were adjusted for multiple testing using the Benjamini-Hochberg procedure.

Immune gene expression assessment

Following flood-inoculation, rosettes were collected at 0, 2, 6, 10, 24, 48 and 72 hours post-infection. For each treatment modality at each time point, three individual plants were pooled to form one biological replicate, and this was repeated 3 times to obtain the biological replicates. Samples were snap frozen immediately after collection and stored at -80 °C until RNA extraction. Frozen material was ground using the Qiagen tissue lyser II and total RNA was extracted with TRIzol™ reagent (#15596026; Invitrogen, Thermo Fisher Scientific, MA, USA). RNA concentration, purity and integrity were verified spectrophotometrically and by gel electrophoresis. One microgram of RNA was treated with 1 unit of DNase I (#EN052; Thermo Fisher Scientific, MA, USA) and reverse-transcribed using 50 ng of random hexamers and 200 units of SuperScript™ IV (#18090200; Thermo Fisher Scientific, MA, USA). The

resulting cDNA was treated with 2 units of *E. coli* RNase H (#18090200; Thermo Fisher Scientific, MA, USA) and diluted 1:20 to serve as a template for *PP2A* amplification (27 cycles), confirming successful cDNA synthesis. Samples were diluted 1:50 and used as templates for qPCR reactions performed with Luna® Universal qPCR Master Mix (New England Biolabs, MA, USA), using 20% of cDNA per reaction. All samples from one biological replicate were run on a single 384-well qPCR plate, with three technical replicates per target gene. Amplification was performed on a CFX Opus 384 Real-time PCR system (**Table S6**) and melt curves quality was assessed using the Maestro CX software (Bio-Rad, CA, USA). Amplification data were analysed in RStudio using the chipPCR and qpcR packages. PCR efficiencies were calculated for each individual well and incorporated into the computation of mean normalized expression[37,38]. Expression of *FRK1*, *WRKY29*, *NHL10*, *PAD3*, *PDF1.2*, and *PR1* was quantified over time relative to the housekeeping gene *PP2A*, and normalized to the mock-treated samples at each time point. For each target gene, significant differences between the WT and O-antigen mutants at each time point were assessed using one-way ANOVA or Kruskal–Wallis tests, as appropriate.

DNA extraction, library preparation and sequencing of *A. thaliana* herbarium specimens

Herbarium specimens of *Arabidopsis thaliana* spanning almost two centuries (between 1817 and 2015) were obtained from seven European institutions: Staatliches Museum für Naturkunde Stuttgart (Stuttgart, Germany), the Herbarium Tubingense (Tübingen, Germany), Lund University Botanical Museum (Lund, Sweden), the herbarium at the Biological Museum Oskarshamn (Oskarshamn, Sweden), the herbarium at Real Jardín Botánico (Madrid, Spain), the Herbario de Málaga (Malaga, Spain) and The Natural History Museum's herbarium (London, United Kingdom). Small tissue samples (~0.7 cm^2) were collected for DNA extraction and sequencing, with care taken to minimize visible damage. Each sample specimen was labelled with collection details and internal identifiers, and DNA extraction followed established protocols[17].

DNA from herbarium specimens was extracted and processed into single-stranded Illumina libraries at the UCSC Ancient and Degraded DNA Processing Center following Kapp et al. [39] with suggested modification from Nguyen et al. [40]. Strict contamination control and cleanroom procedures were implemented. Libraries were initially shallow-sequenced on an Illumina NextSeq 550 to assess DNA quality and plant endogenous DNA content, then sequenced on a NovaSeq X Plus (2x150 bp), while adjusting per-sample concentration in the DNA pools to finally achieve an average depth around 9x for the host *A. thaliana* genome of each sample. All sequencing reads have been deposited in the European Nucleotide Archive (ENA) under project ID: PRJEB98841.

Historical reads processing, mapping and authentication

We identified *Pseudomonas*-derived reads in 49 *A. thaliana* herbarium specimens collected across Europe between 1817 and 2015, comprising two previously published datasets [41,42] and 31 newly sequenced herbarium samples from this study (**Table S7**). Before read mapping, we used AdapterRemoval v2.3.3 [43] to trim adapters, remove low-quality bases, and collapse overlapping paired-end reads. Host-derived reads were removed by mapping all merged reads to the *A. thaliana* TAIR10 reference genome [44] using BWA aln v0.7.17 [45], with the seed disabled to improve alignment of damaged historical reads [17]. For each library, reads that could not be merged due to long insert sizes were mapped independently as forward and reverse reads. Subsequently, merged and unmerged reads were combined into a single BAM file per library. The remaining unmapped reads were then mapped to the *P. viridiflava* ATUE5 p25.C2 reference genome[6] using the same approach. PCR duplicates were removed, and mapped reads were filtered for mapping quality ≥ 20 using samtools v1.11[46]. To authenticate the historical nature of both *A. thaliana*- and *Pseudomonas*-mapped reads we used mapDamage2 v2.20 [47], which generated misincorporation patterns and length distributions typical of ancient DNA.

625 **Phylogenetic placement of historical *Pseudomonas* in the context of modern diversity**
626 To determine the phylogenetic placement of the 49 historical *Pseudomonas* strains in the context of
627 modern diversity, we used a set of 83 contemporary genomes representing the known diversity of
628 *Pseudomonas* segregating in wild populations. Single Nucleotide Polymorphisms (SNPs) were identified
629 using bcftools v1.11 with the parameter -ploidy 1 [46], filtered for quality (QUAL >= 20), merged across
630 samples, and restricted to biallelic sites with no missing data. A maximum-likelihood tree was constructed
631 from 3,095 biallelic SNPs detected in at least 95% of isolates using IQ-TREE v2.1.4 [48] applying
632 TVM+F+ASC+R3 as the best substitution model [49]. Historical strains clustering within the modern
633 ATUE5 clade were classified as ATUE5. To examine the diversity within the ATUE5 lineage, we
634 constructed a phylogeny using 53 modern and 43 historical ATUE5 genomes. SNPs were identified and
635 filtered as described above, yielding a total of 8,184 biallelic SNPs. A maximum likelihood tree was
636 constructed also using IQ-TREE v2.1.4 [48] applying TVM+F+ASC+R4 as the best substitution model [49].
637
638 **Ascertainment of tail fiber assembly (TFA) and hypothetical tail fiber (HTF) haplotypes in**
639 **historical samples**
640 To capture reads representing the full spectrum of tailocin genetic diversity, we extended the *P. viridiflava*
641 p25.C2 reference genome with six major haplotypes of the highly polymorphic tail fiber (*HTF*) and tail
642 fiber assembly (*TFA*) genes [7]. Historical *P. viridiflava* reads were then mapped to this extended reference
643 as described above. Reads mapping to the tailocin cluster between the flanking genes *trpE* and *trpG*, as
644 well as all reads mapping to any haplotype of the *HTF* and *TFA* genes were used for *de novo* assembly
645 using SPAdes v3.15.0 [50]. Collinearity between the resulting assemblies and the reference *HTF* and *TFA*
646 genes was assessed using Minimap2 v2.28 [50,51], and the best-matching *HTF* and *TFA* variants for each
647 assembly were identified by ranking the proportion of coverage obtained from the Minimap2 mapping.
648 To determine *HTF* haplotypes in historical strains that had insufficient coverage for *de novo* assembly of
649 the *HTF* gene, we performed *k*-mer–based classification of *HTF* sequences. Reference sets of unique
650 *k*-mers (k = 31) were constructed from the seven *HTF* variants (**Fig. S16**). Only *k*-mers exclusive to any
651 of the *HTF* haplotypes and absent from whole-genome backgrounds were retained. To enhance the
652 discriminatory power of our analysis, we filtered *k*-mers across haplotypes to ensure a minimum edit
653 distance of ≥2 between them. The only exception was the haplotype with the smallest *k*-mer set
654 (HTF_p23.B8), for which *k*-mers were removed only from the larger overlapping sets. Using this set of
655 filtered *HTF* haplotype *k*-mers, we queried *k*-mer match counts for each historical isolate with Jellyfish
656 v2.2.10 [52] (**Fig. S17**) (all additional *k*-mer profiles are available on GitHub). Additionally, we removed
657 *k*-mers with a fold coverage less than the genome-wide mean minus 0.5 standard deviations. For each
658 isolate, we calculated the proportion of *k*-mers matching each haplotype and assigned the haplotype with
659 the highest proportion as the dominant one (**Table S8**). In cases where multiple haplotypes displayed
660 similar dominant proportions, potential co-infections were recorded and confirmed through inspection of
661 genome-wide *k*-mer profiles (**Fig. S17**). Modern high-quality reads were used as benchmarks to validate
662 the *k*-mer approach and compare it with the local assembly method (**Fig. S13**).
663
664 **O-antigen biosynthesis cluster (OBC) gene presence/absence analysis**
665 We determined the presence of six O-antigen biosynthesis genes (*wfgD, rmlC_1, tagG_2, tagH_2, spsA,*
666 and *epsE_4*) [7]. A gene was considered present if it met both of the following criteria: (i) a breadth of
667 coverage ≥ 65% and (ii) a mean depth ≥ the genome-wide average minus 0.25 standard deviations of each
668 isolate; otherwise, it was considered absent.
669 The *epsE_4* locus required additional analysis because of its extended length (~4.5 kb) and high
670 allelic divergence (**Table S8; see GitHub**). For a fraction of modern strains the mapping to the *P.*
671 *viridiflava* p25.C2 *epsE_4* reference resulted in the full recovery of the *epsE_4* gene. In other modern
672 strains, we resorted in the previously published de novo assemblies [7] to extend from the conserved

673 mapped region on the assembled contig. This process generated a set of diverse modern *epsE_4* variants.
674 For historical isolates lacking whole-genome assemblies, the modern haplotype set was used as a
675 reference for local assembly. Reads mapping to any variant were extracted and assembled locally using
676 SPAdes v3.15.0. [50]. Assembled contigs were then aligned against the modern haplotypes with Minimap2
677 v2.28 [51] to identify the best-matching variant.
678 For both modern and historical datasets, rescued *espE4* sequences were translated into amino
679 acids using ExPASy [53] and EMBOSS Transeq [54]. Amino acid sequences were then aligned with Clustal
680 Omega [55]. The resulting multiple sequence alignments and allele length distributions are provided in the
681 supplementary materials (**Table S8; see GitHub**).
682
683 **Linkage disequilibrium and recombination analysis**
684 To evaluate the impact of recombination on the association between *HTF* length variants and OBC
685 haplotypes, we quantified genome-wide linkage disequilibrium (LD) and recombination across
686 *Pseudomonas viridiflava* ATUE5. Variant calling was performed on 53 modern ATUE5 genomes using
687 bcftools v1.11 [46], following the same procedure used for phylogenetic reconstruction. A total of 298,977
688 SNPs were retained and reformatted to include only the genotype (GT) field for LD estimation. Pairwise
689 LD (r^2) was computed using VCFtools v0.1.17 with the --hap-r2 function [56]. LD decay was calculated for
690 SNP pairs separated by 0–2 kb using all SNPs, whereas for 2–2000 kb using a random subset of 2% to
691 reduce computation time. The median r^2 values were calculated after binning SNP pairs by distance (5 bp
692 bins for short-range and 10 kb bins for long-range intervals).
693 To further quantify genome-wide recombination, the same 53 modern genomes were analysed
694 using Recophy [20] with the *P. viridiflava* p25.C2 reference genome under default settings. Recophy
695 mixture-model–based approach to estimate whether SNPs across all pairwise genome comparisons arise
696 via mutation (clonal fraction) or recombination (recombining fraction), from which the ratio of
697 recombined to clonal SNPs was calculated.
698
699 **Plant infection by syringe-infiltration and bacterial population size assessment**
700 Bacteria were grown for 16 h at 28 °C with vigorous agitation (200 rpm). Suspensions were back-diluted
701 1:10 in 5 mL of selective liquid medium and incubated for an additional 3 h. Cells were centrifuged and
702 pellets were washed 3 times with 10 mM MgSO4 (5 mL). Suspensions were adjusted to OD600nm = 0.1
703 (10^8 CFU/mL), 0.01 (10^7 CFU/mL) and 0.001 (10^6 CFU/mL). Ten-week-old *Arabidopsis thaliana*
704 plants of the Eyach 1.5-2 and Col-0 ecotypes, grown under long-day conditions (16 h light, constant 23
705 °C), were used for the infiltration, selecting two leaves at the same phenological stage from 3 individual
706 plants for each treatment. Using a tip-less 1mL-syringe, half of each leaf was infiltrated on the abaxial
707 face with either mock solution (10 mM MgSO4) or bacterial suspension (final volume = *ca.* 5-15 uL).
708 Infiltrated plants were returned to the growth chamber and incubated under a transparent plastic lid to
709 maintain high humidity. At two and five days post-infiltration, infiltrated leaves were collected and
710 ground in 1 mL of 10 mM $MgSO_4$. Homogenates were serially diluted (five 1:10 dilutions), and three 10
711 µL drops of each dilution were spotted onto selective solid medium. After 48 h of static incubation at 28
712 °C, colonies were counted in each drop to estimate bacterial population size. Significant differences
713 between the WT and O-antigen mutant for each condition were assessed using a Student's t-test, Welch's
714 t-test, or Wilcoxon rank-sum test, as appropriate.
715
716 **Bacterial growth *in vitro***
717 Bacteria were grown overnight at 28 °C with vigorous agitation (200 rpm). Cells were centrifuged and
718 overnight pellets were washed three times with PBS. Suspensions were adjusted to OD600nm = 0.01 in
719 liquid LB. Two hundred microliters of suspensions were aliquoted in a 96-well flat transparent plate,
720 considering 4 technical replicates per strain. LB media with no inoculum (sterile) provided the reference

721 for optical density measurements The plate was placed in a humidity cassette and then loaded into the
722 microplate reader (Spark®, TECAN, Switzerland) where it was continuously shaken and incubated at 28
723 °C, and optical density at 600 nm was measured every 15 minutes for 24 h. Statistical analysis was
724 performed with three independent biological replicates. Growth curve parameters were extracted using the
725 growthcurver R package and differences were assessed by one-way analysis of variance (ANOVA1)
726 followed by Tukey's post hoc test for each parameter.
727
728 **Contributions**
729 TB, JC, EC, MH, TLK and HAB devised the study. IB and MN developed the pipeline for analyzing plant
730 growth. TB, EC, EB, ES, PG and AP performed plant growth and tailocin treatment experiments. TB, JC,
731 EC, SL, TLK and HAB. analysed the data. SL, LL, JL, JE, GM, HAB and PL generated and provided the
732 historical genomes data. EC, PA and AM designed the LPS assays and conducted the characterization.
733 AH developed the RB-TnSeq pipeline. TB, JC, EC, MH, TLK and HAB wrote the paper.
734
735 **Acknowledgements**
736 Haim Ashkenazy and Detlef Weigel for discussions and for providing access to the genome data. We are
737 also grateful to the Max Planck Society for supporting the infection experiments, and to Jiyeon Hyun and
738 Heejin Yoo for providing the primers used for PR1 amplification in qPCR. We thank Dominique
739 Bergmann (Stanford) for hosting and supporting PL and JE's generation of historical *A. thaliana*
740 genomes. JRL and some herbarium sequencing was supported by NIH R35GM138300. We thank Aida
741 Andrés, Gemma Murray and members of their labs for input in data analyses and valuable discussions.
742 We further thank Joy Bergelson, Sophien Kamoun, Johannes Krause, Dmitri Petrov and Max Reuter for
743 valuable discussions. This work would not be possible without historical herbarium collections and their
744 curators. We are grateful to Anette Rosenbauer and Mike Thiv at the Staatliches Museum für Naturkunde
745 Stuttgart (Stuttgart, Germany), Oliver Bossdorf and Uta Grünert at the Herbarium Tubingense (Tübingen,
746 Germany), Arne Thell and Ulf Arup from Lund University Botanical Museum (Lund, Sweden), Åke
747 Rühling at the herbarium at the Biological Museum Oskarshamn (Oskarshamn, Sweden), Leopoldo
748 Medina from the herbarium at Real Jardín Botánico (Madrid, Spain), Jose García Sánchez at the Herbario
749 de Málaga (Malaga, Spain) and John Hunnex, Fred Rumsey and Mark Carine from The Natural History
750 Museum's herbarium (London, United Kingdom) for their generous specimen loans and the kind
751 permission to sample specimens. We are further grateful for all help received over the last five years from
752 the California Academy of Sciences Botany Department staff, and for their support with obtaining loans
753 from numerous international institutions, in particular to Collection Manager Emily Magnaghi, past
754 Collection Manager Debra Trock, and past McAllister Chair of Botany Nathalie Nagalingum.
755
756 **Funding**
757 TB was supported by the NIH Training Program in Microbial Pathogenesis (grant T32 AI055434). JME
758 was supported by funds from the US National Institutes of Health (T32GM007276). PL was supported by
759 Human Frontiers Science Fellowship (LT000330/2019-L), and is supported by the University of
760 California Berkeley. TLK and the work in the TLK lab was supported by the NIH award
761 R35GM150722-01, NSF 2422727, USDA-NIFA 10074268. HAB and the work in the HAB Lab was
762 supported by the Royal Society (grant RSWF\R1\191011) and the UK Biological Sciences Research
763 Council (BBSRC) (grant number UKRI359: 2024BBSRC-NSF/BIO). This work was supported in part by
764 the U.S. Department of Energy, Office of Science, Basic Energy Sciences, Chemical Sciences,
765 Geosciences and Biosciences Division, under award DE-SC0015662 to DOE Center for Plant and
766 Microbial Complex Carbohydrates at the CCRC and NIH R24GM137782 award to National
767 Glycoscience Resource-CCRC Service and Training to PA. This research was also supported in part by
768 grant NSF PHY-2309135 and the Gordon and Betty Moore Foundation Grant No. 2919.02 to the Kavli

Institute for Theoretical Physics (KITP). This work was also supported by a NIH award R35GM138300 to JRL. DB is an investigator of the Howard Hughes Medical Institute.

Competing interests

The authors declare that they have no competing interests.

Data and materials availability

All data and code are available in the supplementary materials and have been deposited in the following repositories. Historical sequencing read data have been deposited in the NCBI Sequence Read Archive under BioProject accession PRJEB98841 and in two public datasets [41,42]. Code has been deposited to GitHub:
(https://github.com/JiajunCui-jjc/HTF_OBC_historical_analysis.git,
https://github.com/talia-backman/Ps1524_tailocin_tradeoffs).

References

1. Rainey, P. B. & Travisano, M. Adaptive radiation in a heterogeneous environment. *Nature* **394**, 69–72 (1998).
2. Meyer, J. R. & Kassen, R. The effects of competition and predation on diversification in a model adaptive radiation. *Nature* **446**, 432–435 (2007).
3. Livingston, G. *et al.* Competition-colonization dynamics in experimental bacterial metacommunities. *Nat. Commun.* **3**, 1234 (2012).
4. Experimental evolution: Trends in Ecology & Evolution.
5. Karasov, T. L. *et al.* Continental-scale associations of Arabidopsis thaliana phyllosphere members with host genotype and drought. *Nat. Microbiol.* **9**, 2748–2758 (2024).
6. Karasov, T. L. *et al.* Arabidopsis thaliana and Pseudomonas Pathogens Exhibit Stable Associations over Evolutionary Timescales. *Cell Host Microbe* **24**, 168–179.e4 (2018).
7. Backman, T. *et al.* A phage tail–like bacteriocin suppresses competitors in metapopulations of pathogenic bacteria. *Science* **384**, eado0713 (2024).
8. Ghequire, M. G. K. & De Mot, R. The Tailocin Tale: Peeling off Phage Tails. *Trends Microbiol.* **23**, 587–590 (2015).
9. Granato, E. T., Meiller-Legrand, T. A. & Foster, K. R. The Evolution and Ecology of Bacterial Warfare. *Curr. Biol.* **29**, R521–R537 (2019).
10. Erbs, G. & Newman, M.-A. The role of lipopolysaccharide and peptidoglycan, two glycosylated bacterial microbe-associated molecular patterns (MAMPs), in plant innate immunity: Glycosylated bacterial MAMPs. *Mol. Plant Pathol.* **13**, 95–104 (2012).
11. Ivanov, I. E. *et al.* Relating the physical properties of Pseudomonas aeruginosa lipopolysaccharides to virulence by atomic force microscopy. *J. Bacteriol.* **193**, 1259–1266 (2011).
12. Van Oosten, B. & Harroun, T. A. A MARTINI extension for Pseudomonas aeruginosa PAO1 lipopolysaccharide. *J. Mol. Graph. Model.* **63**, 125–133 (2016).
13. Vacheron, J. *et al.* Molecular and evolutionary basis of O-antigenic polysaccharide-driven phage sensitivity in environmental pseudomonads. *Microbiol. Spectr.* **11**, e0204923 (2023).
14. Duque-Jaramillo, A. *et al.* The genetic and physiological basis of Arabidopsis thaliana tolerance to Pseudomonas viridiflava. *New Phytol.* **240**, 1961–1975 (2023).
15. Wetmore, K. M. *et al.* Rapid quantification of mutant fitness in diverse bacteria by sequencing randomly bar-coded transposons. *MBio* **6**, e00306–15 (2015).
16. Fernández, L. *et al.* Characterization of the polymyxin B resistome of Pseudomonas aeruginosa. *Antimicrob. Agents Chemother.* **57**, 110–119 (2013).
17. Latorre, S. M., Lang, P. L. M., Burbano, H. A. & Gutaker, R. M. Isolation, library preparation, and bioinformatic analysis of historical and ancient plant DNA. *Curr. Protoc. Plant Biol.* **5**, e20121 (2020).
18. Sarkar, S. F. & Guttman, D. S. Evolution of the Core Genome of Pseudomonas syringae, a Highly Clonal, Endemic Plant Pathogen. *Appl. Environ. Microbiol.* **74**, 1961–1961 (2008).
19. Weiß, C. L. *et al.* Temporal patterns of damage and decay kinetics of DNA retrieved from plant

821 herbarium specimens. *R Soc Open Sci* **3**, 160239 (2016).
822 20. Sakoparnig, T., Field, C. & van Nimwegen, E. Whole genome phylogenies reflect the distributions of
823 recombination rates for many bacterial species. *Elife* **10**, (2021).
824 21. Burmeister, A. R., Sullivan, R. M. & Lenski, R. E. Fitness Costs and Benefits of Resistance to Phage
825 Lambda in Experimentally Evolved Escherichia coli*. *Evolution in Action: Past, Present and Future*
826 123–143 (2020).
827 22. Heiman, C. M. *et al.* Pivotal role of O-antigenic polysaccharide display in the sensitivity against
828 phage tail-like particles in environmental Pseudomonas kin competition. *ISME J.* **16**, 1683–1693
829 (2022).
830 23. Garland, T., Jr, Downs, C. J. & Ives, A. R. Trade-offs (and constraints) in organismal biology.
831 *Physiol. Biochem. Zool.* **95**, 82–112 (2022).
832 24. Ferenci, T. Trade-off Mechanisms Shaping the Diversity of Bacteria. *Trends Microbiol* **24**, 209–223
833 (2016).
834 25. Parys, K. *et al.* Signatures of antagonistic pleiotropy in a bacterial flagellin epitope. *Cell Host*
835 *Microbe* **29**, 620–634.e9 (2021).
836 26. Colaianni, N. R. *et al.* A complex immune response to flagellin epitope variation in commensal
837 communities. *Cell Host Microbe* **29**, 635–649.e9 (2021).
838 27. Barrett, L. G., Bell, T., Dwyer, G. & Bergelson, J. Cheating, trade-offs and the evolution of
839 aggressiveness in a natural pathogen population. *Ecol. Lett.* **14**, 1149–1157 (2011).
840 28. Stahl, E. A., Dwyer, G., Mauricio, R., Kreitman, M. & Bergelson, J. Dynamics of disease resistance
841 polymorphism at the Rpm1 locus of Arabidopsis. *Nature* **400**, 667–671 (1999).
842 29. Vacheron, J., Heiman, C. M. & Keel, C. Live cell dynamics of production, explosive release and
843 killing activity of phage tail-like weapons for Pseudomonas kin exclusion. *Commun Biol* **4**, 87
844 (2021).
845 30. Love, M. I., Huber, W. & Anders, S. Moderated estimation of fold change and dispersion for
846 RNA-seq data with DESeq2. *Genome Biol.* **15**, 550 (2014).
847 31. Hartley, J. L., Temple, G. F. & Brasch, M. A. DNA cloning using in vitro site-specific
848 recombination. *Genome Res.* **10**, 1788–1795 (2000).
849 32. Westphal, O. & Jann, K. Bacterial Lipopolysaccharides Extraction Phenol-Water Further
850 Applications Procedure. *Methods Carbohydrate Chemistry* **5**, 83–91 (1965).
851 33. Krauss, J. H., Weckesser, J. & Mayer, H. Electrophoretic analysis of lipopolysaccharides of purple
852 nonsulfur bacteria. *Int. J. Syst. Bacteriol.* **38**, 157–163 (1988).
853 34. York, W. S., Darvill, A. G., McNeil, M., Stevenson, T. T. & Albersheim, P. Isolation and
854 characterization of plant cell walls and cell wall components. in *Methods in Enzymology* 3–40
855 (Elsevier, 1986).
856 35. Bhat, U. R., Mayer, H., Yokota, A., Hollingsworth, R. I. & Carlson, R. W. Occurrence of lipid A
857 variants with 27-hydroxyoctacosanoic acid in lipopolysaccharides from members of the family
858 Rhizobiaceae. *J. Bacteriol.* **173**, 2155–2159 (1991).
859 36. Binesse, J., Lindgren, H., Lindgren, L., Conlan, W. & Sjöstedt, A. Roles of reactive oxygen
860 species-degrading enzymes of Francisella tularensis SCHU S4. *Infect. Immun.* **83**, 2255–2263
861 (2015).
862 37. Pfaffl, M. W. A new mathematical model for relative quantification in real-time RT-PCR. *Nucleic*
863 *Acids Res.* **29**, e45 (2001).
864 38. Simon, P. Q-Gene: processing quantitative real-time RT-PCR data. *Bioinformatics* **19**, 1439–1440
865 (2003).
866 39. Kapp, J. D., Green, R. E. & Shapiro, B. A Fast and Efficient Single-stranded Genomic Library
867 Preparation Method Optimized for Ancient DNA. *J Hered* **112**, 241–249 (2021).
868 40. Nguyen, R., Kapp, J. D., Sacco, S., Myers, S. P. & Green, R. E. A computational approach for
869 positive genetic identification and relatedness detection from low-coverage shotgun sequencing data.
870 *J Hered* **114**, 504–512 (2023).
871 41. Lang, P. L. M. *et al.* Century-long timelines of herbarium genomes predict plant stomatal response to
872 climate change. *Nat Ecol Evol* **8**, 1641–1653 (2024).
873 42. Lopez, L. *et al.* Museum Genomics Reveals Temporal Genetic Stasis and Global Genetic Diversity
874 in Arabidopsis thaliana. *Mol Ecol* **34**, e70081 (2025).
875 43. Schubert, M., Lindgreen, S. & Orlando, L. AdapterRemoval v2: rapid adapter trimming,

876 identification, and read merging. *BMC Res Notes* **9**, 88 (2016).
877 44. Swarbreck, D. *et al.* The Arabidopsis Information Resource (TAIR): gene structure and function
878 annotation. *Nucleic Acids Res* **36**, D1009–14 (2008).
879 45. Li, H. & Durbin, R. Fast and accurate short read alignment with Burrows-Wheeler transform.
880 *Bioinformatics* **25**, 1754–1760 (2009).
881 46. Danecek, P. *et al.* Twelve years of SAMtools and BCFtools. *Gigascience* **10**, giab008 (2021).
882 47. Jónsson, H., Ginolhac, A., Schubert, M., Johnson, P. L. F. & Orlando, L. mapDamage2.0: fast
883 approximate Bayesian estimates of ancient DNA damage parameters. *Bioinformatics* **29**, 1682–1684
884 (2013).
885 48. Minh, B. Q. *et al.* IQ-TREE 2: New Models and Efficient Methods for Phylogenetic Inference in the
886 Genomic Era. *Mol Biol Evol* **37**, 1530–1534 (2020).
887 49. Kalyaanamoorthy, S., Minh, B. Q., Wong, T. K. F., von Haeseler, A. & Jermiin, L. S. ModelFinder:
888 fast model selection for accurate phylogenetic estimates. *Nat Methods* **14**, 587–589 (2017).
889 50. Prjibelski, A., Antipov, D., Meleshko, D., Lapidus, A. & Korobeynikov, A. Using SPAdes De Novo
890 Assembler. *Curr. Protoc. Bioinformatics* **70**, e102 (2020).
891 51. Li, H. Minimap2: pairwise alignment for nucleotide sequences. *Bioinformatics* **34**, 3094–3100
892 (2018).
893 52. Marçais, G. & Kingsford, C. A fast, lock-free approach for efficient parallel counting of occurrences
894 of k-mers. *Bioinformatics* **27**, 764–770 (2011).
895 53. Gasteiger, E. *et al.* ExPASy: The proteomics server for in-depth protein knowledge and analysis.
896 *Nucleic Acids Res* **31**, 3784–3788 (2003).
897 54. Rice, P., Longden, I. & Bleasby, A. EMBOSS: the European Molecular Biology Open Software
898 Suite. *Trends Genet* **16**, 276–277 (2000).
899 55. Sievers, F. *et al.* Fast, scalable generation of high-quality protein multiple sequence alignments using
900 Clustal Omega. *Mol Syst Biol* **7**, 539 (2011).
901 56. Danecek, P. *et al.* The variant call format and VCFtools. *Bioinformatics* **27**, 2156–2158 (2011).

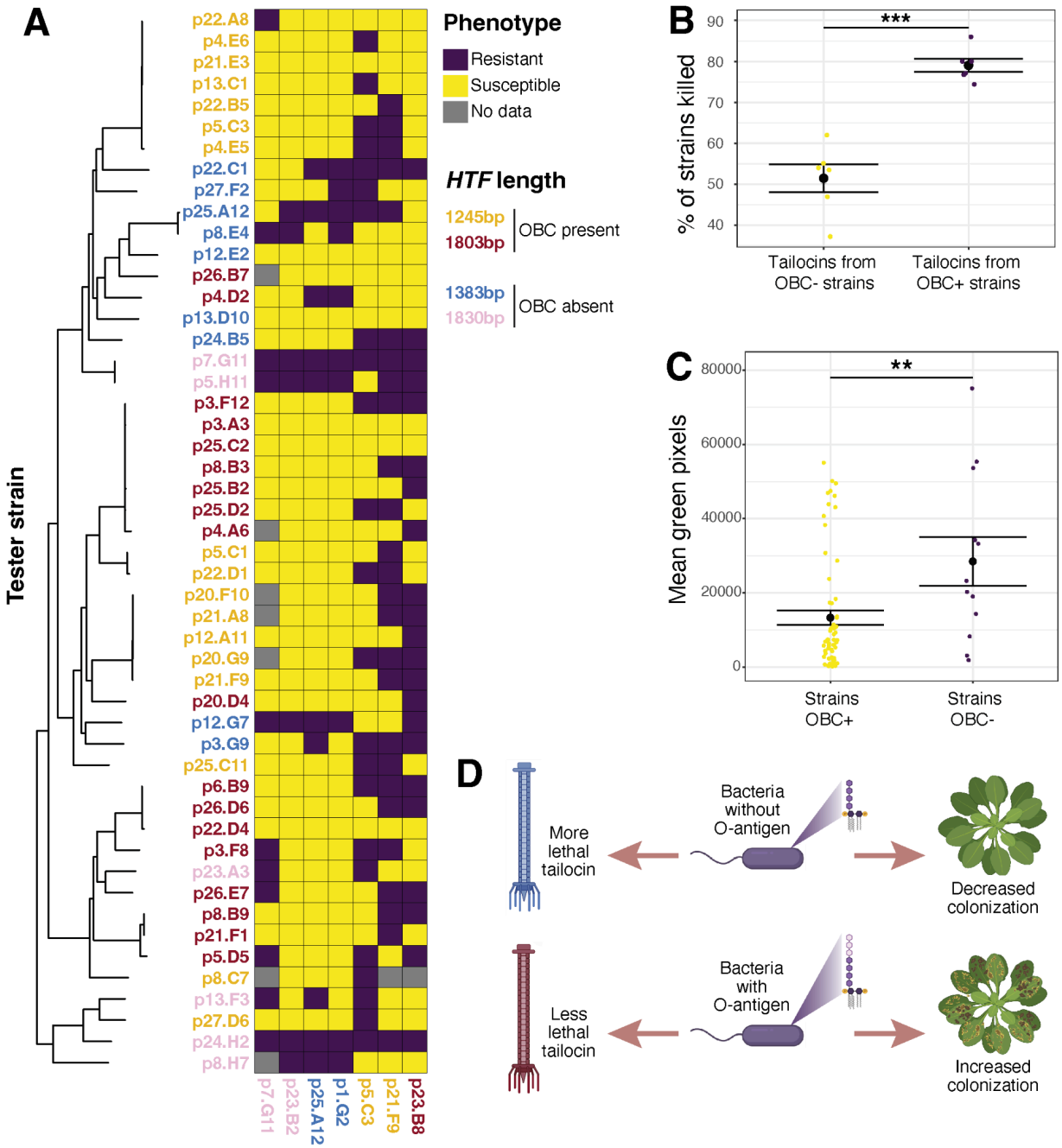

Figure 1: Decreased tailocin activity and increased virulence are associated with the presence of the focal O-antigen Biosynthesis Cluster (OBC) in wild populations of *P. viridiflava*. A. Tailocin killing matrix showing sensitivity (yellow), resistance (purple), or missing data (gray) across a panel of 50 *P. viridiflava* strains. Each row is a tester strain, and each column represents a tailocin from a naturally co-occurring producer strain, annotated below the heatmap and colored by its tail fiber (HTF) length variant. There are representative tailocins from all four HTF length variants previously characterized. **B.** Tailocins from OBC- strains exhibit significantly broader killing spectra than those from OBC+ strains, killing a higher proportion of

tester strains (two-sided Wilcoxon rank-sum test, $p < 0.001$; data derived from A; mean ± SEM). **C.** Infections with OBC- strains resulted in significantly higher mean green pixel counts compared to OBC+ strains, indicating reduced disease severity (n = 93 strains; two-sided Wilcoxon rank-sum test, $W = 1539$, $p = 4.2 \times 10^{-8}$; mean ± SEM). **D.** Schematic describing the hypothesis for why we see variation in the success of competitors and colonizers in wild plant populations. Created in https://BioRender.com**.**

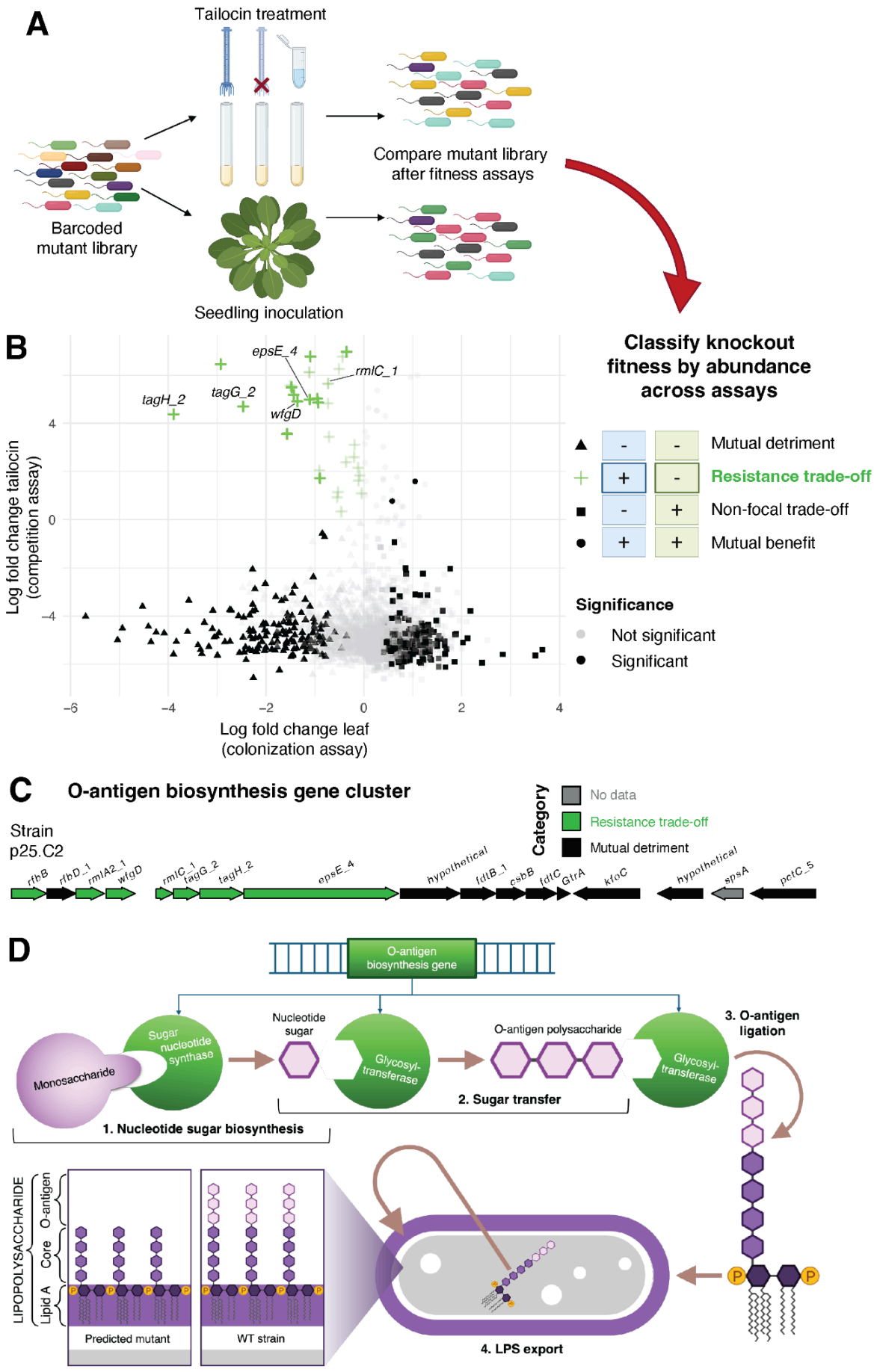
A
Tailocin treatment
Barcoded mutant library
Compare mutant library after fitness assays
Seedling inoculation
B
Classify knockout fitness by abundance across assays
epsE_4
rmlC_1
tagH_2
tagG_2
wfgD
Log fold change tailocin (competition assay)
Log fold change leaf (colonization assay)
Mutual detriment
Resistance trade-off
Non-focal trade-off
Mutual benefit
Significance
Not significant
Significant
C
O-antigen biosynthesis gene cluster
Strain p25.C2
Category
No data
Resistance trade-off
Mutual detriment
rfbB
rfbD_1
rmlA2_1
wfgD
rmlC_1
tagG_2
tagH_2
epsE_4
hypothetical
fdtB_1
gshB
fdtC
GtrA
kfoC
hypothetical
spsA
pctC_5
D
O-antigen biosynthesis gene
Monosaccharide
Sugar nucleotide synthase
Nucleotide sugar
Glycosyl-transferase
O-antigen polysaccharide
Glycosyl-transferase
1. Nucleotide sugar biosynthesis
2. Sugar transfer
3. O-antigen ligation
LIPOPOLYSACCHARIDE
O-antigen
Core
Lipid A
Predicted mutant
WT strain
4. LPS export

Figure 2: Tailocin resistance mutations in the OBC impair bacterial colonization in *Arabidopsis thaliana*. A. Schematic of the RB-TnSeq experimental design. A barcoded transposon mutant library of *P. viridiflava* strain p25.C2 was subjected to two separate treatments: (i) tailocin exposure in liquid culture (data from Backman et al. 2024), and (ii) leaf infiltration into *A. thaliana* ecotypes Eyach 1.5-2 and Col-0. Mutant fitness was inferred from barcode abundance post-selection, and each gene was categorized based on relative fitness across both conditions together: –/– = mutually detrimental, +/+ = mutually beneficial, +/– = resistance trade-off, –/+ = mon-focal trade-off. **B.** Scatterplot of the $\log_2$ fold change in barcode abundance during leaf colonization in Eyach 1.5-2 (x-axis) versus tailocin treatment (y-axis). Each point represents one gene (mean across barcodes). Significance is indicated by opacity: opaque points mark genes significant in both ecotypes ($p < 0.05$), while lighter points indicate nonsignificance in at least one condition. Shapes denote fitness outcome categories (mutual benefit, mutual detriment, non-focal trade-off, or resistance trade-off in both ecotypes). Labeled genes correspond to focal O-antigen biosynthesis cluster resistance trade-off genes. **C.** Gene diagram of the OBC on the *P. viridiflava* strain p25.C2 chromosome. Genes are colored based on statistical significance in each assay: resistance trade-off (green), mutual detriment (black), or no data (grey). **D.** Simplified schematic of O-antigen biosynthesis. (1) Nucleotide sugars are synthetized from phosphorylated monosaccharide precursors. (2) Sugars are sequentially transferred onto a lipid carrier, forming the O-antigen repeat unit and eventually the O-antigen polymer. (3) The O-antigen is ligated to the lipid A-core oligosaccharide to produce lipopolysaccharide (LPS), which is transported across the outer membrane (4). Resistance trade-off genes encode sugar nucleotide synthases and glycosyltransferases involved in these steps, indicating that disrupting any part of this pathway can confer tailocin resistance at the cost of reduced colonization. Created in https://BioRender.com.

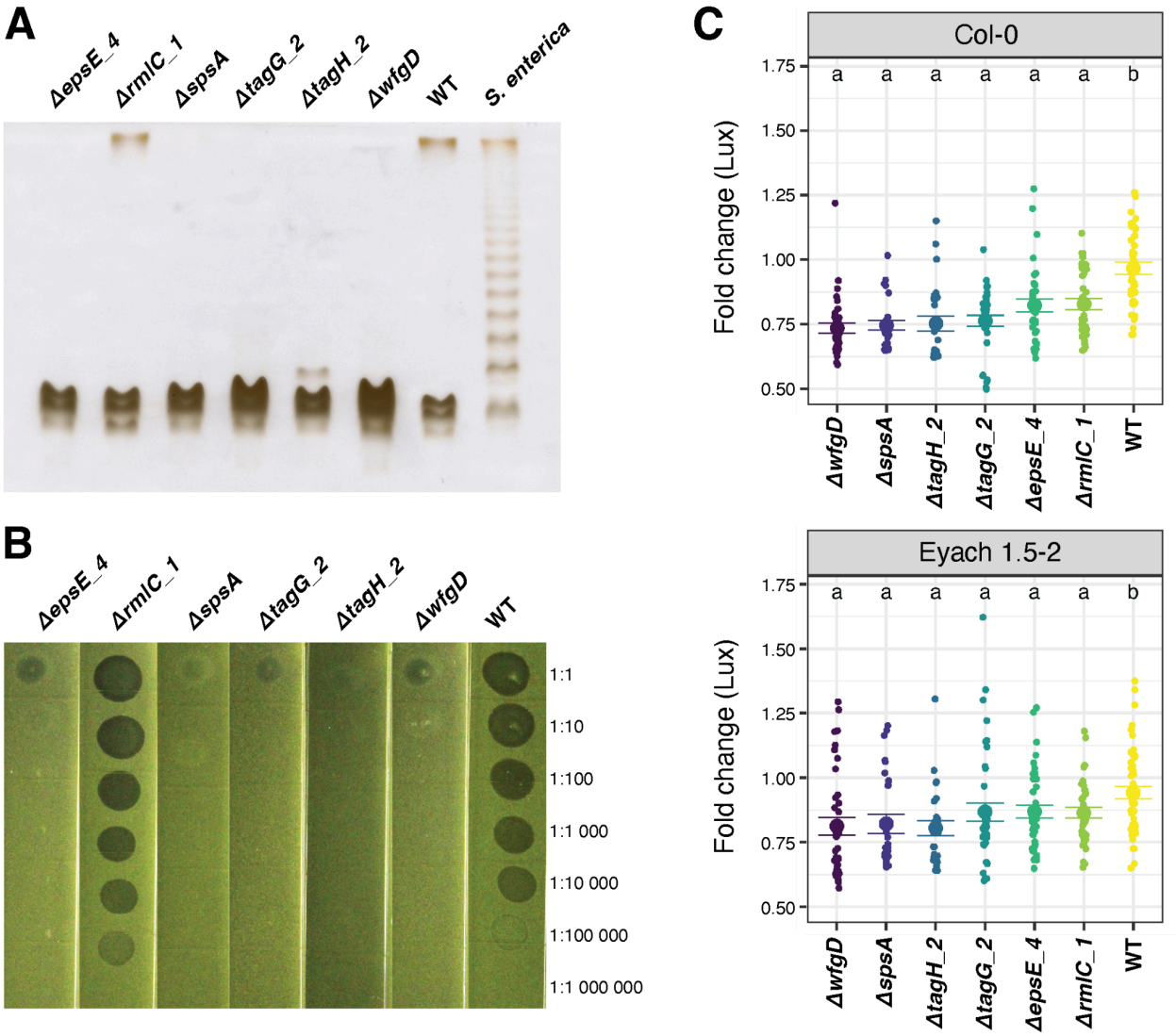

Figure 3: O-antigen mutants lack O-antigen chains, proliferate less *in planta*, and improve plant health outcomes. A. The LPS of the O-antigen knockouts were extracted and visualized with a silver-stained DOC-PAGE gel. Some mutants lack the high molecular weight O-antigen band, while Δ*rmlC_1* still has the O-antigen band. **B.** Tailocin killing assay using partially purified tailocin from p25.A12 applied to soft agar with each O-antigen mutant or wild-type (WT). Killing is shown by zones of inhibition. Six mutants exhibit resistance to tailocin-mediated killing. Δ*rmlC_1* appears to be even more sensitive than WT. Representative results from three GRGbiological replicates are shown. **C.** *Pseudomonas* strains tagged with luciferase were flood-inoculated onto *Arabidopsis thaliana* seedlings (Col-0 or Eyach 1.5-2 background). Bacterial load was quantified by luminescence 7 days post-infection (dpi). Points represent replicate measurements of fold change in Lux signal from 0 dpi to 7 dpi (log-transformed). Mutants generally showed reduced bacterial growth compared to wild-type (WT). Horizontal bars indicate mean ± standard error; letters indicate statistical groupings by a linear mixed model with random intercept for batch.

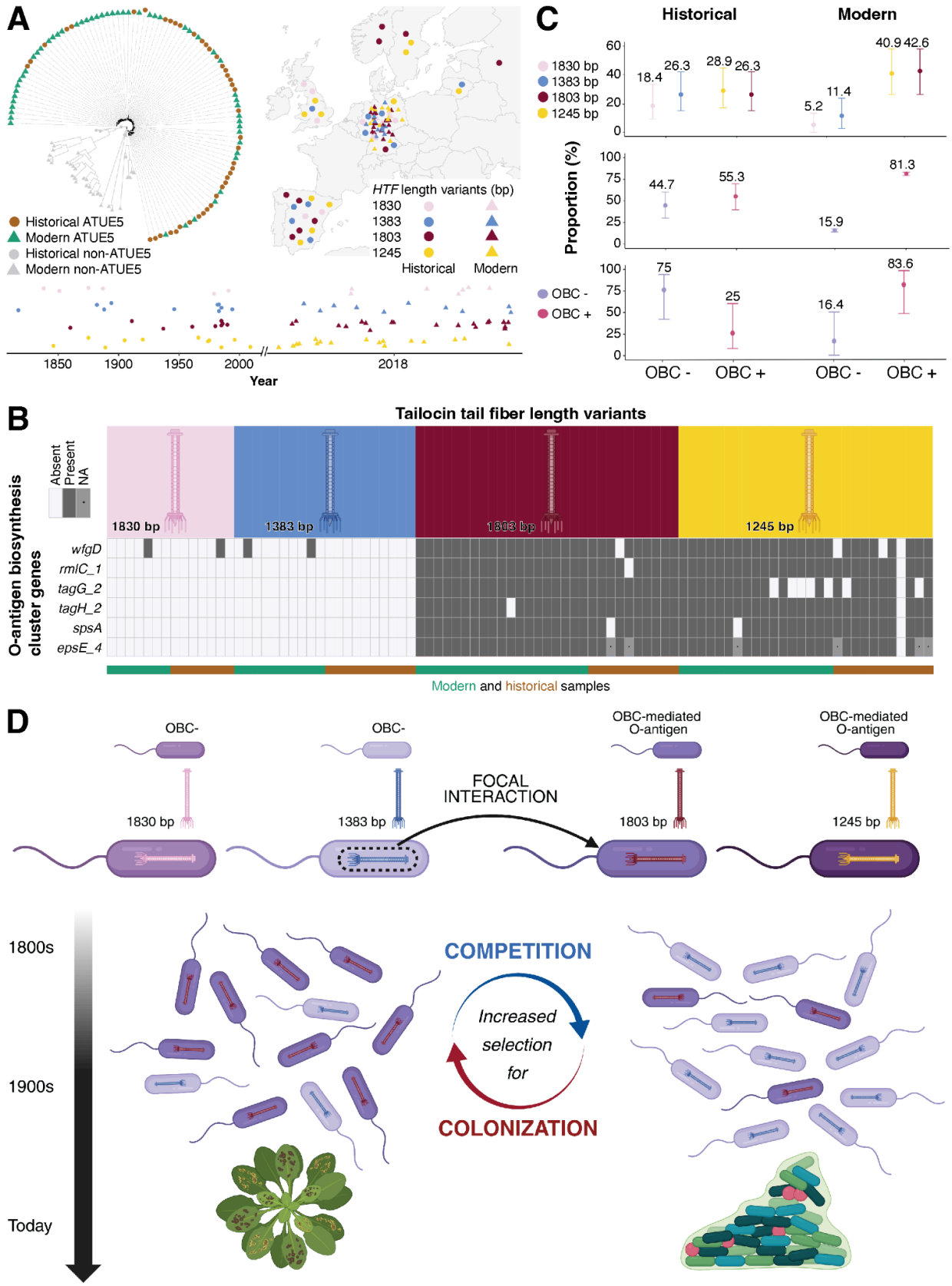
A
Historical ATUE5
Modern ATUE5
Historical non-ATUE5
Modern non-ATUE5
HTF length variants (bp)
1830
1383
1803
1245
Historical
Modern
1850
1900
1950
2000
2018
Year
C
Historical
Modern
1830 bp
1383 bp
1803 bp
1245 bp
Proportion (%)
18.4
26.3
28.9
26.3
5.2
11.4
40.9
42.6
44.7
55.3
15.9
81.3
OBC -
OBC +
75
25
16.4
83.6
OBC -
OBC +
OBC -
OBC +
B
Tailocin tail fiber length variants
Absent
Present
NA
1830 bp
1383 bp
1803 bp
1245 bp
O-antigen biosynthesis cluster genes
wfgD
rmlC_1
tagG_2
tagH_2
spsA
epsE_4
Modern and historical samples
D
OBC-
OBC-
OBC-mediated O-antigen
OBC-mediated O-antigen
FOCAL INTERACTION
1830 bp
1383 bp
1803 bp
1245 bp
1800s
1900s
Today
COMPETITION
Increased selection for
COLONIZATION

Figure 4. Century-long association between tailocin and O-antigen variants in *P. viridiflava*. **A.** Temporal and geographic distribution of historical and modern *Pseudomonas* genomes. The maximum-likelihood tree includes 83 modern *Pseudomonas* strains representing the known diversity segregating in wild populations, together with 49 historical herbarium-derived strains. The type of strain and its phylogenetic classification are indicated in the inset. The map shows the country of origin of each strain, with point locations placed arbitrarily within each country. The type of strain and its corresponding tail fiber (*HTF)* length variant are also indicated in the inset. The temporal distribution of historical and modern samples is shown below, with shape and color codes matching those in the map. Historical strains are positioned according to their collection dates, whereas a horizontal jitter was applied to modern samples (collected in 2018) for visualization. A random vertical jitter was applied to all samples for visual clarity. **B.** Patterns of presence and absence of six OBC genes and their association with *HTF* length variants in historical (brown) and modern (green) genomes. **C.** Proportion of *HTF* length variants and their association with the presence or absence of the O-antigen biosynthesis cluster (OBC). The upper panel shows the frequency of *HTF* length variants in historical and modern strains, the middle panel groups *HTF* length haplotypes according to their association with the presence or absence of the OBC, while the lower panel compares the distribution of *HTF* length variants between German historical strains (n = 8) and modern strains downsampled to the same sample size. **D.** Conceptual model of long-term HTF-O-antigen coevolution in natural *Pseudomonas* populations. This schematic illustrates how fluctuating selection between competitive and colonization contexts may maintain diversity in tailocin tailfiber (HTF) and O-antigen variants over time. Four major *HTF* length variants (1245 bp, 1383 bp, 1803 bp, and 1830 bp) co-occur in natural populations, each represented by a distinct color (yellow, blue, dark red, and pink, respectively). Strains with 1245 bp and 1803 bp *HTF* possess the OBC-mediated O-antigen, while 1383 bp and 1830 bp variants lack OBC genes, reflecting differences in tailocin susceptibility and colonization potential. The lower panel depicts how ecological conditions cyclically favor different strategies: under competitive conditions, strains producing tailocins with the 1383-bp *HTF* variant gain advantage, whereas under host-associated or colonization-favoring conditions, variants with the OBC-mediated O-antigen perform better. These opposing pressures have likely acted for at least 200 years, maintaining polymorphism in *HTF* length and associated O-antigen. Created in https://BioRender.com**.**

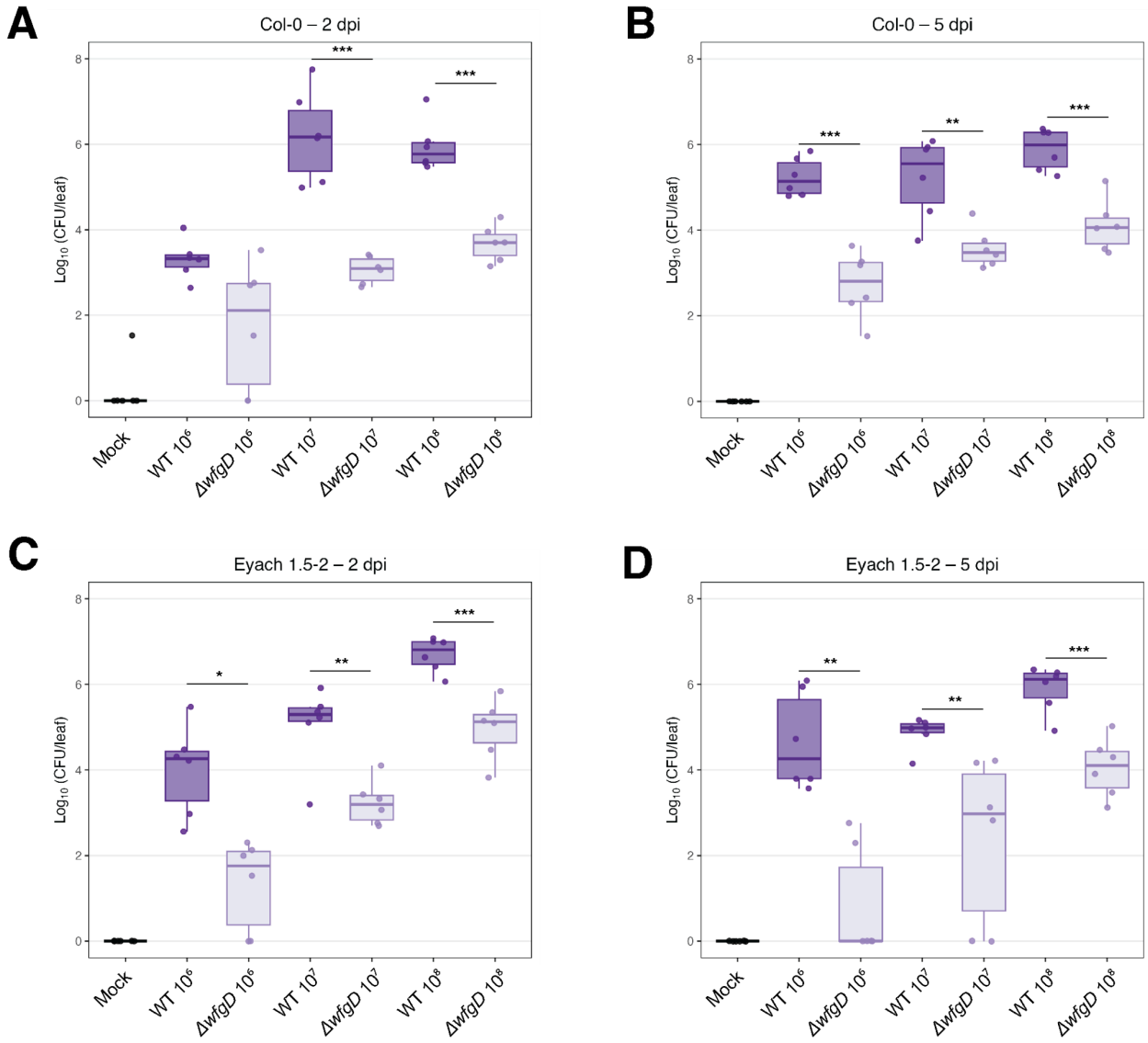

Figure S1: Bacterial population size of p25.C2 WT and O-antigen mutant *ΔwfgD* in Col-0 and Eyach 1.5-2 at 2 and 5 days post-infiltration (dpi) at different inoculum concentrations. The population size of the WT strain was significantly smaller than that of the *ΔwfgD* mutant in all but one condition. Differences between the two strains were assessed using a Student's t-test, Welch's t-test, or Wilcoxon rank-sum test, as appropriate (p-values: *** < 0.001, ** < 0.01, * < 0.05). Data represent 3 technical replicates per condition across 6 biological replicates.

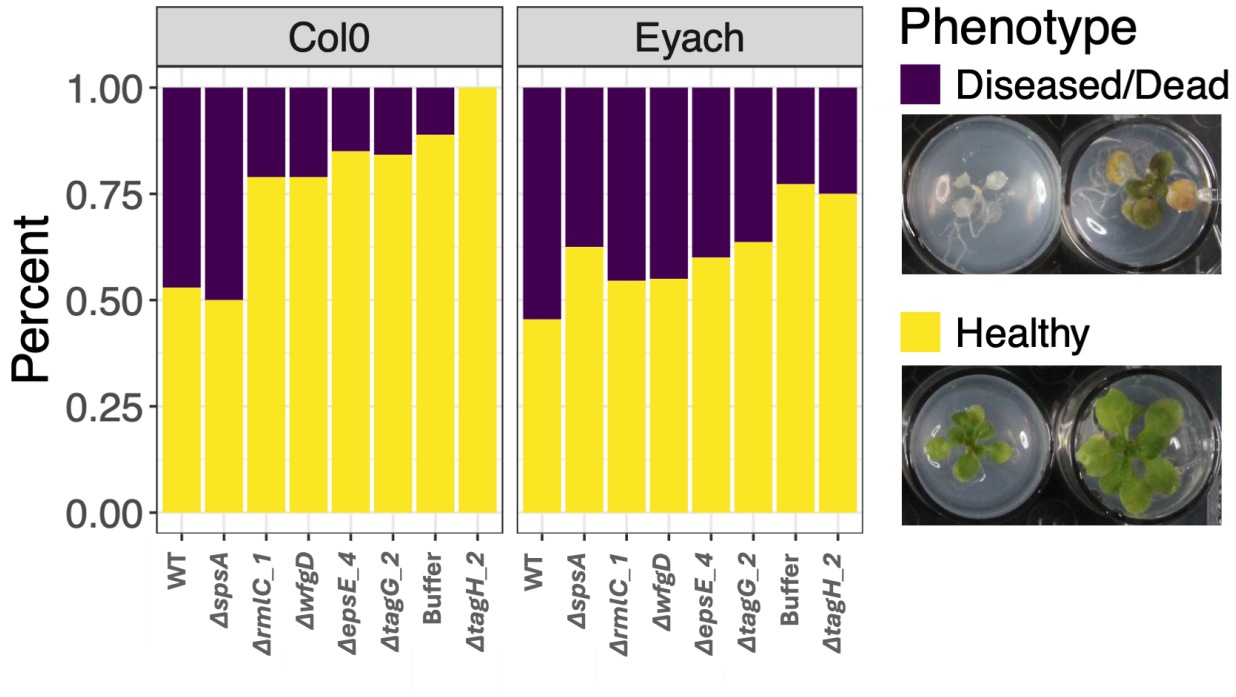

Figure S2: Proportion of plants exhibiting diseased/dead (purple) or healthy (yellow) phenotypes 7 dpi. Across both ecotypes, O-antigen mutants tended to show a higher proportion of healthy plants than WT, although differences were not statistically significant after multiple testing corrections. WT caused disease more frequently but not uniformly, indicating variability in pathogenic outcomes or flood inoculation. Photos of representative diseased, dead, and healthy plants are shown below the legend. Each well is 1.5 cm across.

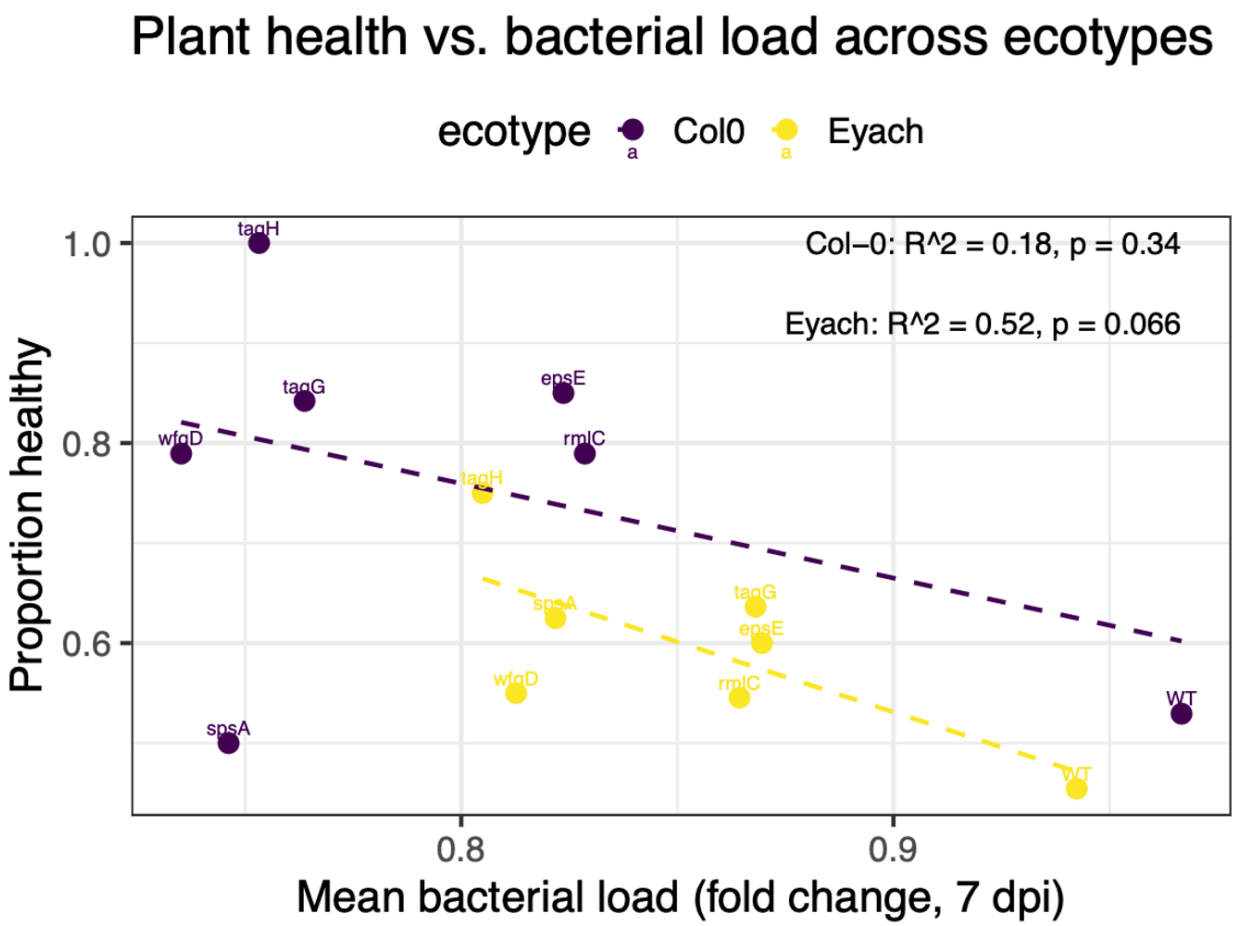

Figure S3: Mean bacterial load (x-axis) is negatively associated with plant health (y-axis) across strains. Each point represents a strain's average 7 dpi fold change (from Fig. 4C) and the corresponding proportion of healthy plants (from Fig. S2). Linear regressions are shown for each ecotype. Across all strains, higher bacterial load tended to predict reduced plant health (pooled model $R^2 = 0.45$, $p = 0.037$; slope $p = 0.086$), although this trend was not significant within Col-0 ($R^2 = 0.18$, $p = 0.34$) and only slightly in Eyach 1.5-2 ($R^2 = 0.52$, $p = 0.066$), reflecting background-specific variation in the relationship between colonization and disease severity.

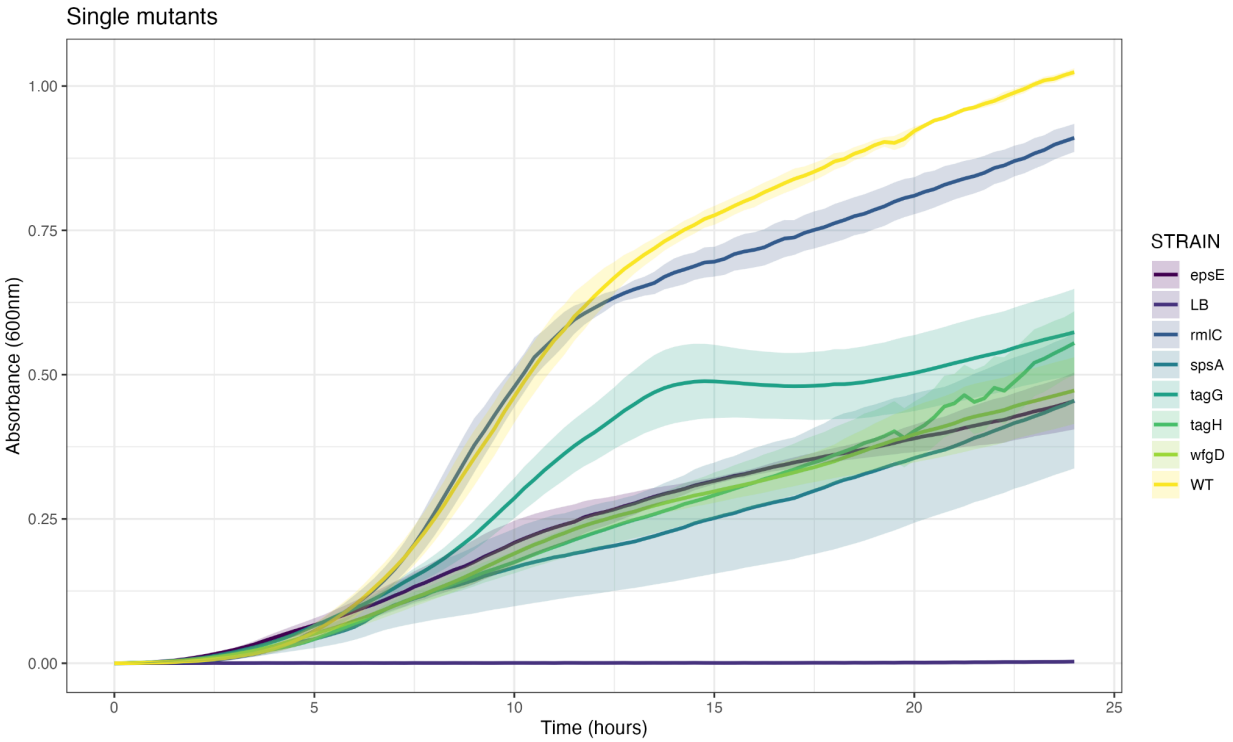

Figure S4: Growth curves *in vitro* of p25.C2 (WT) and the O-antigen mutants. Overnight cultures were adjusted to OD600nm = 0.01 in rich medium (LB) and absorbance was measured for 24 h. Data represent 4 technical replicates per strain across 3 independent biological replicates. Significant differences among strains are reported in Table S3.

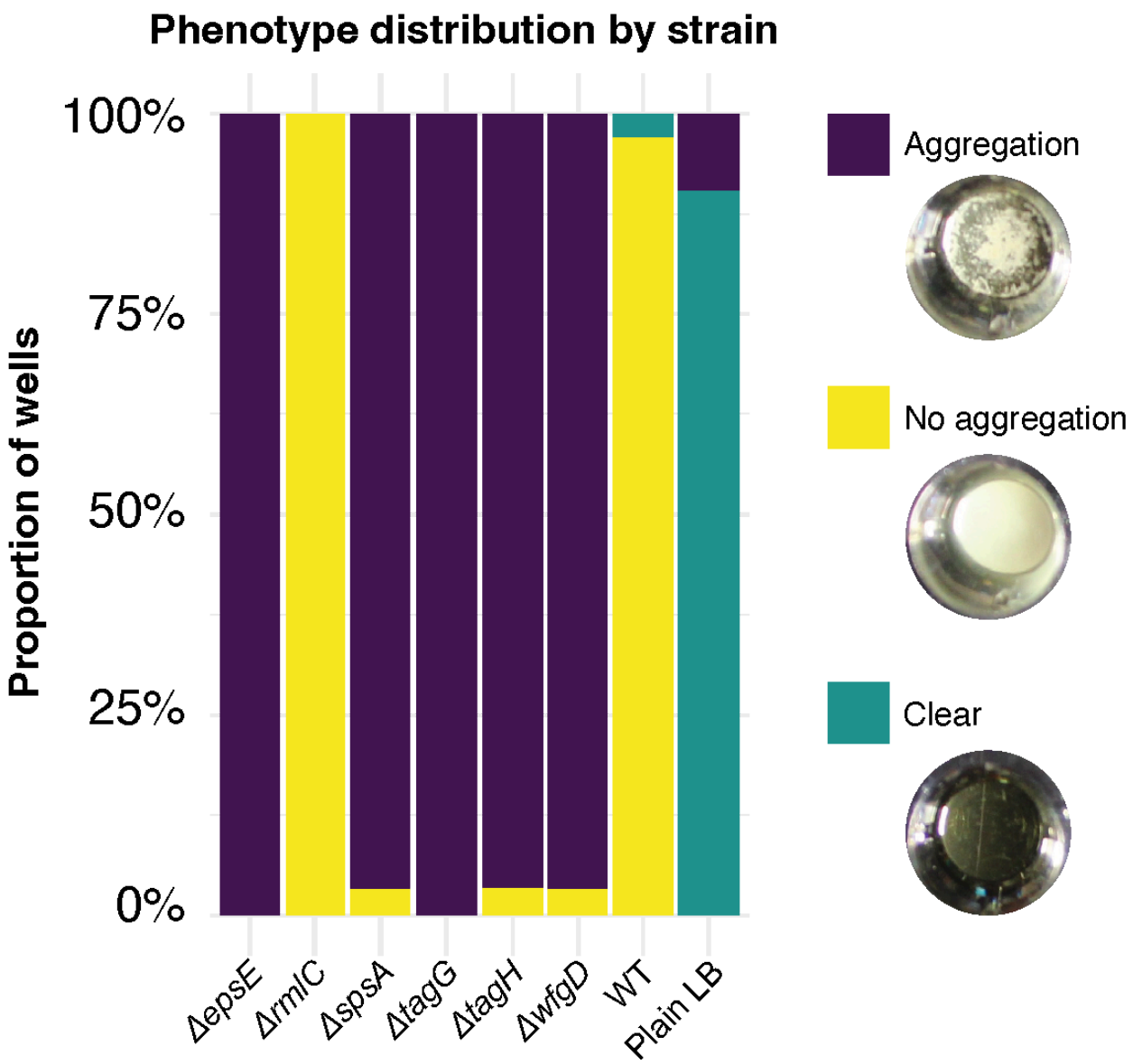

Figure S5: Proportion of wells displaying visible aggregation phenotypes after 48 hours of static incubation at 28°C. Wells were categorized as clear (no growth), growth with no aggregation, or growth with aggregation. All O-antigen mutants except Δ*rmlC* showed significantly higher aggregation frequency than the WT strain (p25.C2; Fisher's exact test, Benjamini–Hochberg-adjusted $p < 10^{-16}$). Data represent 10 technical replicates per strain across 3 biological replicates. Representative photographs illustrate each phenotype category: clear, growth without aggregation, and growth with aggregation.

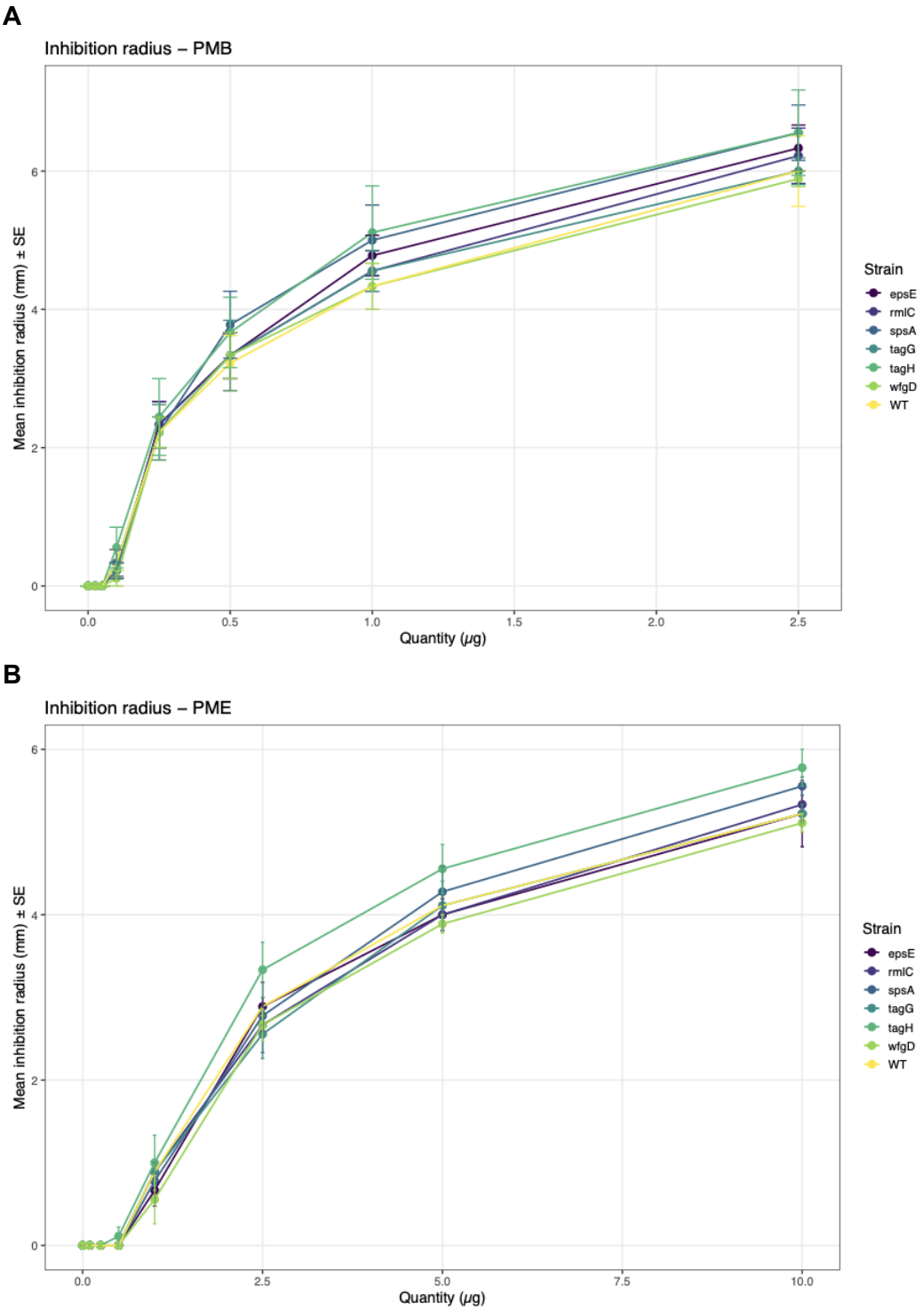

Figure S6: Sensitivity to polymyxin B (A) and polymyxin E (B) in p25.C2 (WT) and the O-antigen mutant. Filter paper disks were saturated with varying quantities of each polymyxin and placed onto freshly streaked bacterial lawns on rich agar medium (LB). Inhibition radii were measured after overnight static incubation at 28 °C. Data represent 3 technical replicates per condition across 3 biological replicates. The absence of significant difference among strains at each compound concentration was assessed using one-way ANOVA or Kruskal–Wallis tests, as appropriate.

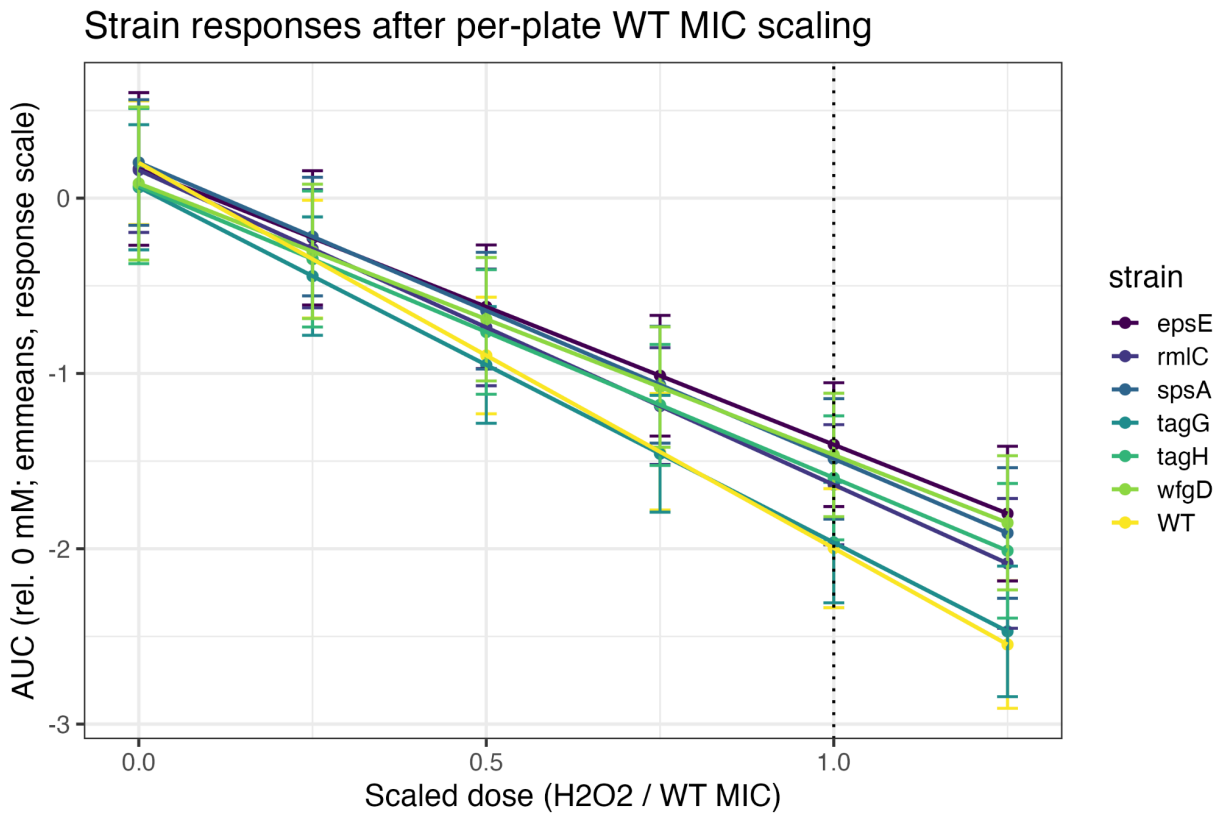

Figure S7: O-antigen mutants and WT exhibit equivalent tolerance to oxidative stress. Area-under-the-curve (AUC) values from growth curves at increasing H_2O_2 concentrations were normalized to 0 mM for each strain and replicate. Each plate's doses were scaled by its WT minimum inhibitory concentration (MIC) to correct for between-experiment variation. Mixed-effects modeling with emmeans contrasts revealed no significant differences between any OPS mutant and WT ($p > 0.05$). Lines show estimated marginal means ± 95% confidence intervals from four replicates.

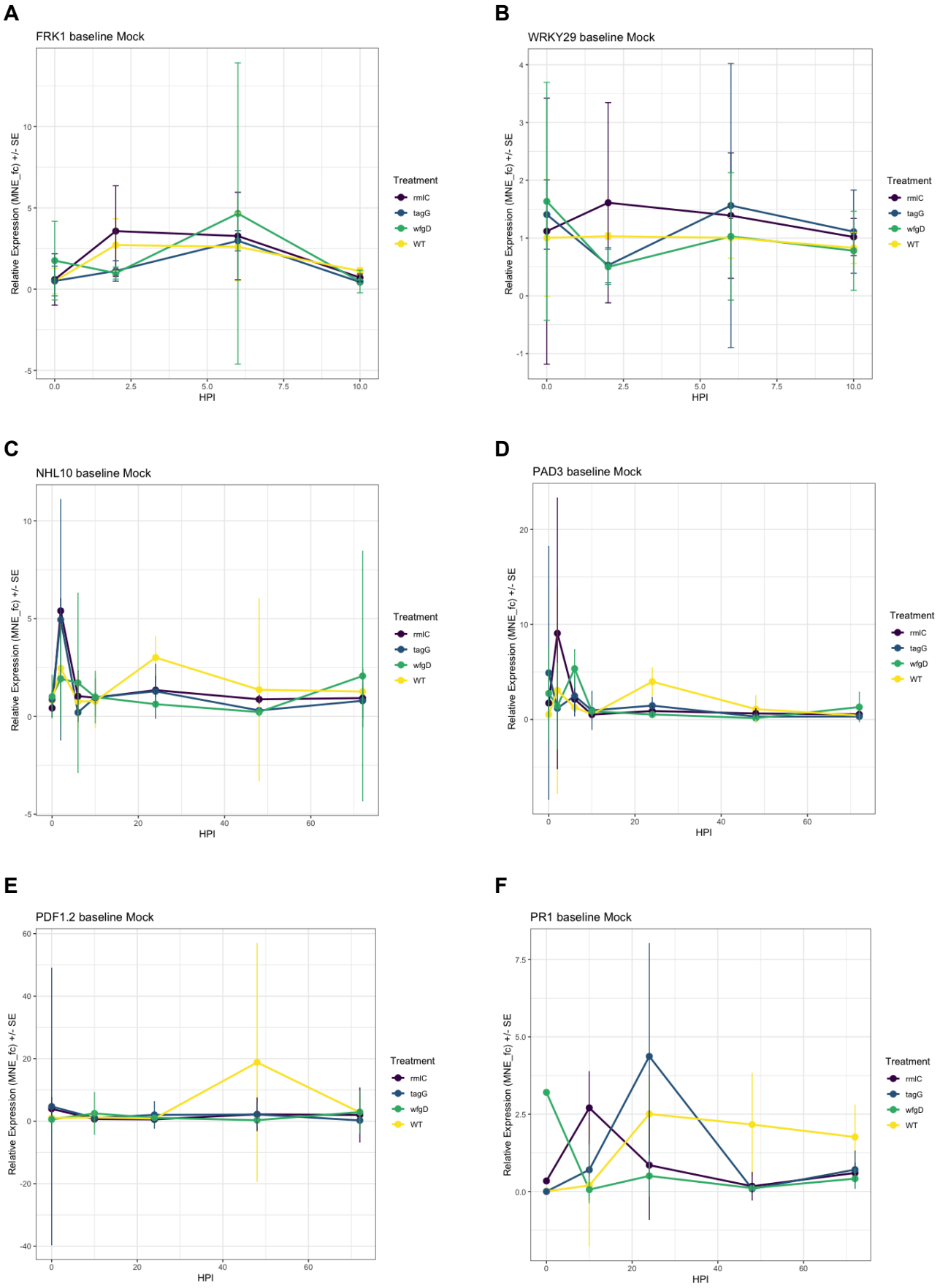
A
FRK1 baseline Mock
Relative Expression (MNE_fc) +/- SE
HPI
Treatment
rmlC
tagG
wfgD
WT
B
WRKY29 baseline Mock
Relative Expression (MNE_fc) +/- SE
HPI
Treatment
rmlC
tagG
wfgD
WT
C
NHL10 baseline Mock
Relative Expression (MNE_fc) +/- SE
HPI
Treatment
rmlC
tagG
wfgD
WT
D
PAD3 baseline Mock
Relative Expression (MNE_fc) +/- SE
HPI
Treatment
rmlC
tagG
wfgD
WT
E
PDF1.2 baseline Mock
Relative Expression (MNE_fc) +/- SE
HPI
Treatment
rmlC
tagG
wfgD
WT
F
PR1 baseline Mock
Relative Expression (MNE_fc) +/- SE
HPI
Treatment
rmlC
tagG
wfgD
WT

Figure S8: Immunity induction in *Arabidopsis thaliana* Col-0 following infection with p25.C2 (WT) and O-antigen mutants. Plants were flood-inoculated, and expression of immune marker genes *FRK1* (A), *WRKY29* (B), *NHL10* (C), *PAD3* (D), *PDF1.2* (E), and *PR1* (F) was assessed at 0, 2, 6, 10, 24, 48, and 72 hours post-infection (HPI). Expression was normalized to the housekeeping gene *PP2A* and expressed as fold change (fc, relative to mock) of the mean normalized expression (MNE), accounting for PCR efficiency. Data represent three technical replicates per condition across three biological replicates. The absence of significant difference among strains at each time point was assessed for each target using one-way ANOVA or Kruskal–Wallis tests, as appropriate.

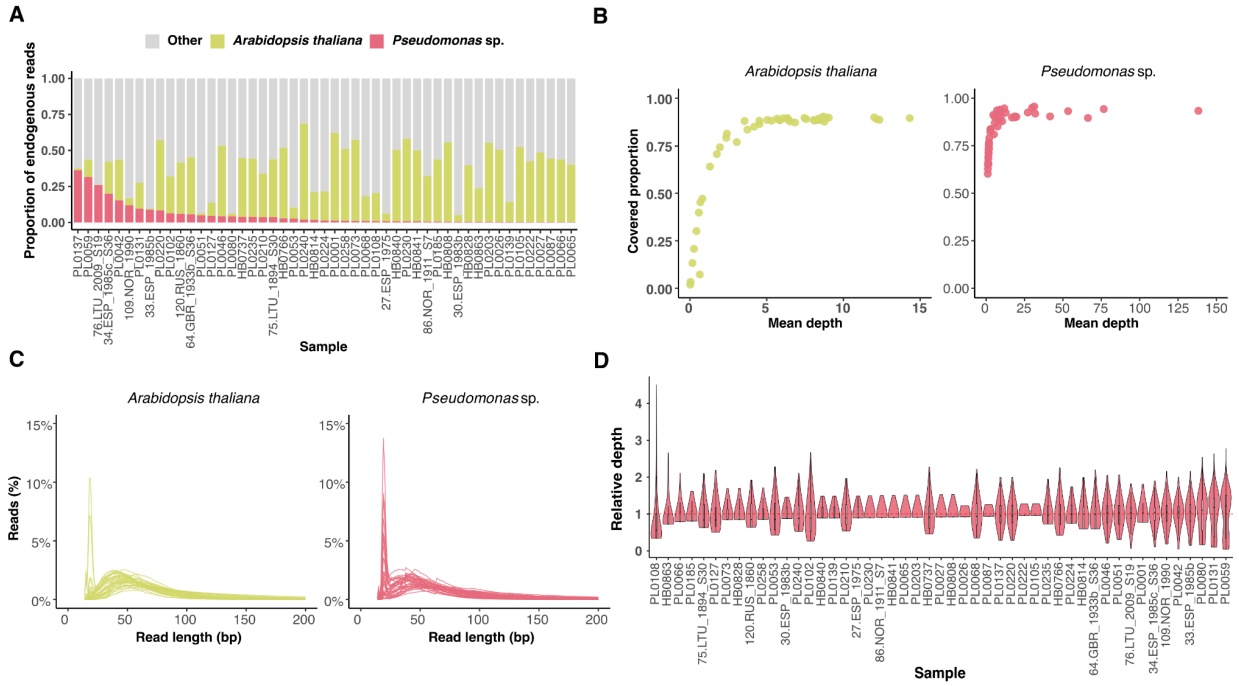

Figure S9. Endogenous DNA profiles reveal variation in historical pathogen representation. A. Endogenous read composition across all 49 historical metagenomic libraries. Stacked bars represent the proportion of reads assigned to *Arabidopsis thaliana* (olive-yellow), *Pseudomonas* sp. (red), and other taxa (grey) within each metagenome. **B.** A scatterplot showing the genome-wide mean read depth (x-axis) vs the breadth of genomic coverage (y-axis) for the *A. thaliana* (olive-yellow) and *Pseudomonas* sp. (red) genomes. Each point represents one historical sample. **C.** Read length distributions of *A. thaliana* (olive-yellow) and *Pseudomonas* sp. (red) reads from 39 historical samples. X-axis was limited to read lengths ≤ 200 bp to provide higher resolution. The remaining ten samples from Lopez et al. (2025) are shown separately in Fig. S10. **D.** Violin plots of *Pseudomonas* sp. whole-genome k-mer depth across historical isolates. The x-axis represents individual samples, and the y-axis shows k-mer depth normalized to each genome's mean depth (mean = 1). The distributions reveal that most historical infections were dominated by a single *Pseudomonas* strain.

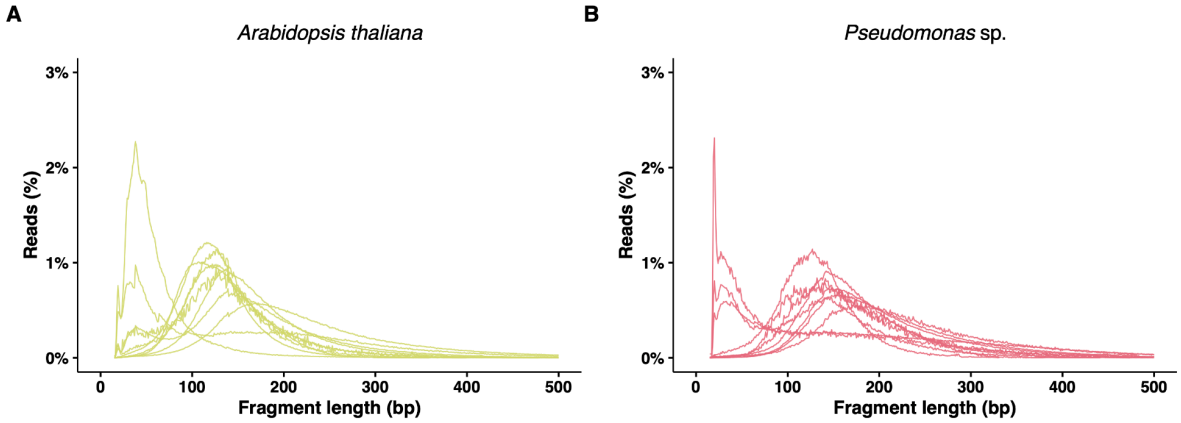

Figure S10. A-B. Read length distributions of reads mapped to *Arabidopsis thaliana* (olive-yellow) and *Pseudomonas* sp. (red) for the ten historical metagenomes from Lopez et al. (2025). X-axis was limited to read lengths ≤ 500 bp to provide higher resolution.

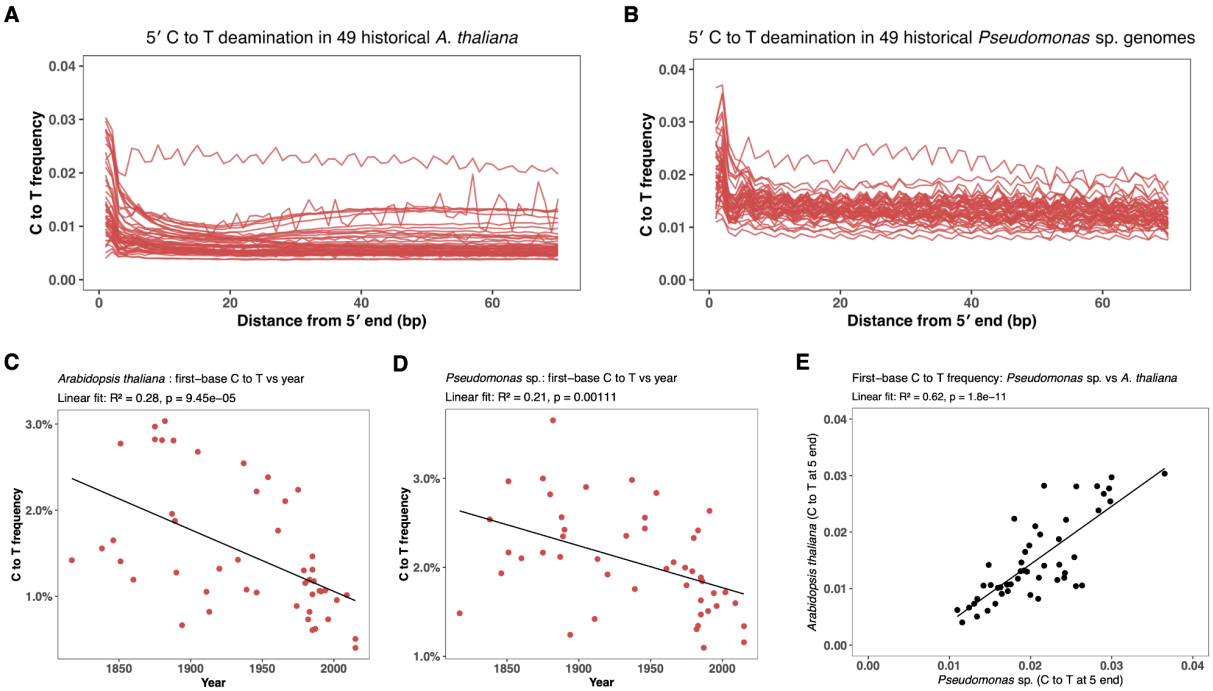

Figure S11. DNA damage patterns in host and pathogen reads support the authenticity of historical metagenomes. Accumulated C-to-T frequencies at the 5′ ends of sequencing reads for 49 *Arabidopsis thaliana* (**A.**) and 49 *Pseudomonas* sp. genomes (**B.**). The y-axis represents C-to-T substitution frequency, and the x-axis shows positions in base pairs from the 5′ end of each read. Both datasets exhibit a typical C-to-T substitutions pattern decaying from the 5′ ends, consistent with historical DNA damage. **C-D.** Scatter plots showing the relationship between the proportion of C-to-T substitutions at the first base (y-axis) and the collection year of each sample (x-axis) for *A. thaliana* (**C.**) and *Pseudomonas* sp. (**D.**). Linear regressions reveal significant negative correlations (*A. thaliana*: R^2=0.28, p value=9.45×10^{-5}; *Pseudomonas* sp.: R^2=0.21, p value=1.11×10^{-3}), indicating that older samples exhibit higher levels of cytosine deamination. Sample PL0087 was excluded due to missing year information. **E.** Correlation between C-to-T substitution frequencies at the 5′ first bases of reads mapped to *Pseudomonas* sp. vs *A. thaliana*. A significant positive correlation confirms that DNA damage signatures are acquired at similar rates between hosts and pathogens.

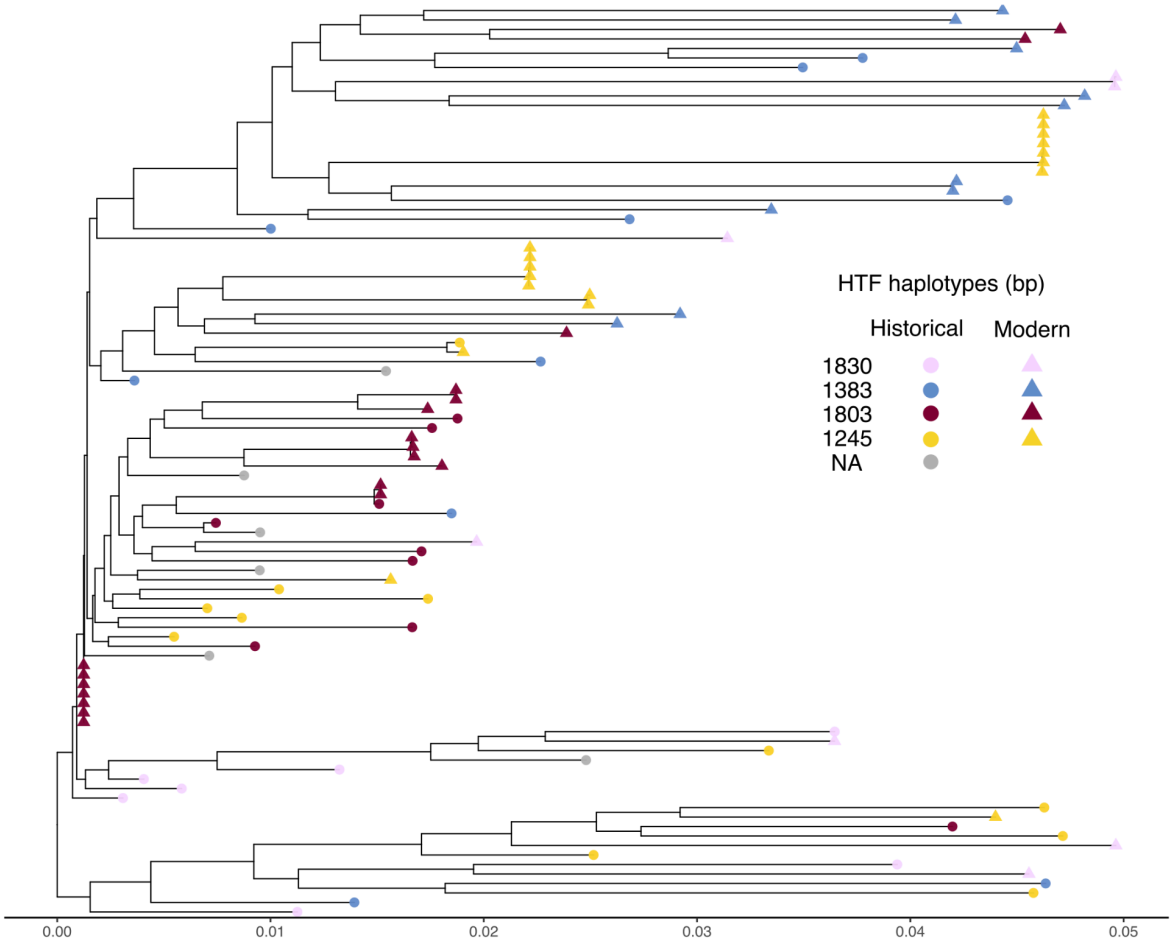

Figure S12. Historical and modern ATUE5 reveal phylogenetic continuity over centuries. Midpoint-rooted maximum-likelihood tree of 43 historical (circles) and 53 modern (triangles) *Pseudomonas viridiflava* ATUE5 genomes. Tip colours indicate the four dominant *HTF* length variants: 1830 bp (pink), 1383 bp (blue), 1803 bp (red) and 1245 bp (yellow). Historical *HTF* variants are broadly distributed across all major branches of the ATUE5 phylogeny, indicating long-term temporal continuity within the lineage.

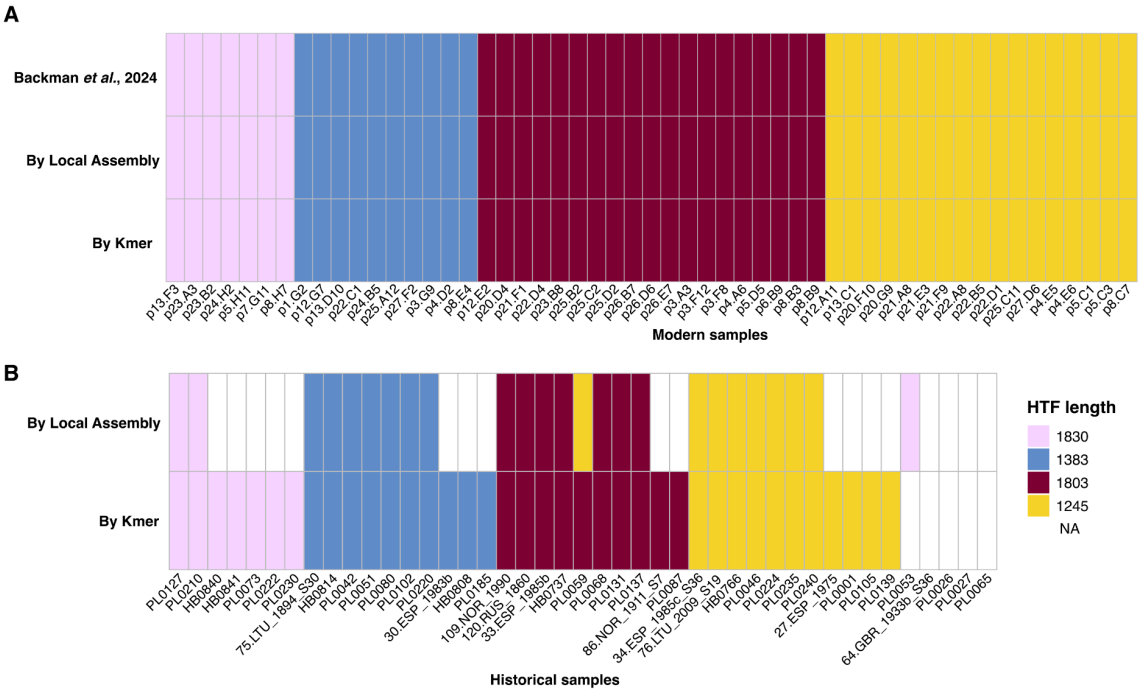

Figure S13. High concordance between k-mer and local assembly methods validates HTF haplotype reconstructions in historical genomes. A. All 53 modern genomes yielded fully concordant haplotype calls across both methods, consistent with previous assignments (Backman *et al*., 2024), which validated the robustness of our approach. **B.** Of 43 historical genomes, 25 haplotypes were assigned by local assembly, and 38 by the k-mer method. Concordance among haplotypes assigned by both methods was 96% (23 of 24), with one sample (PL0059) showing conflicting haplotypes (1245 bp vs. 1803 bp), likely due to coinfection (Fig. S15). We used the 23 concordant and 15 additional k-mer–derived haplotypes for downstream analyses.

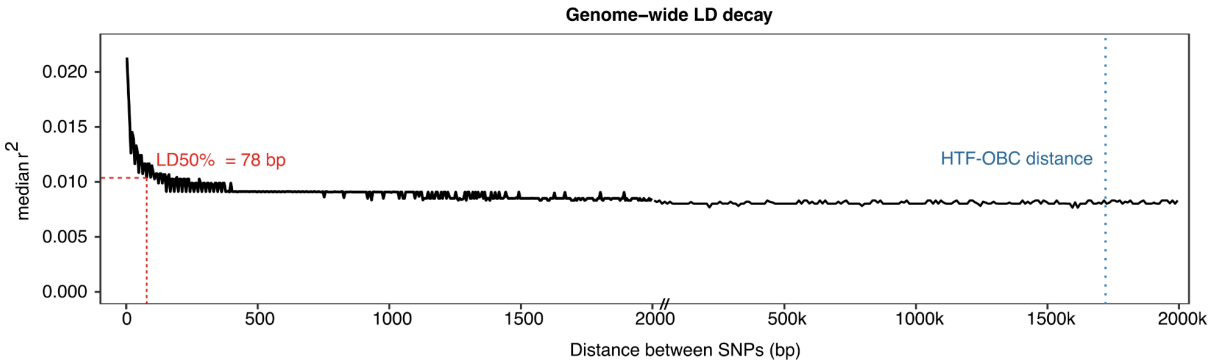

Figure S14. Genome-wide LD decay in *Pseudomonas viridiflava* ATUE5. Pairwise linkage disequilibrium (LD; median r^2) between biallelic SNPs was calculated across 53 modern ATUE5 genomes and plotted against SNP distance. LD was estimated for SNP pairs spanning 0–2 kb using all SNPs, and for 2–2000 kb using a random 2% subset to reduce computation time. LD decays to 50% of its maximum value at 78 bp (LD50; red dashed lines) and reaches background levels by < 2 kb. The genetic distance between the HTF and OBC loci (1.7 Mb; blue dashed line) is shown for reference.

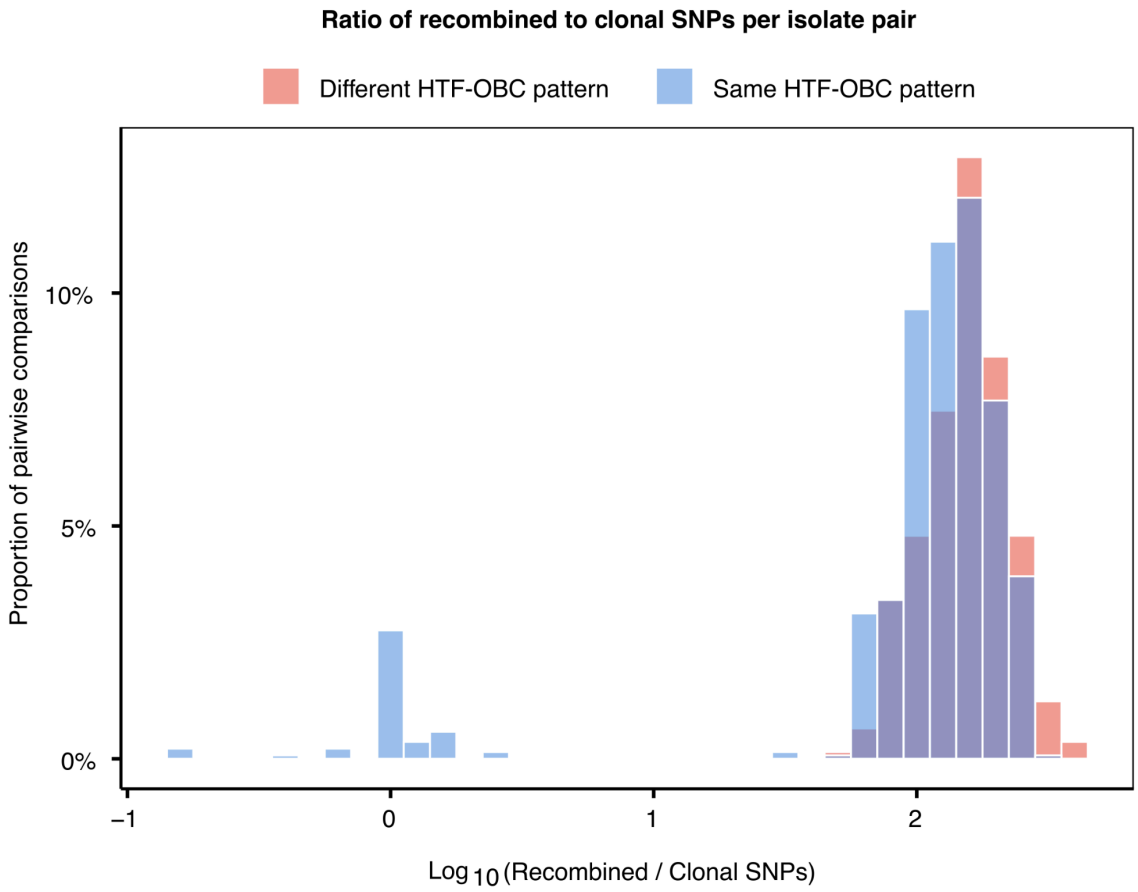

Figure S15. Ratio of recombined to clonal SNPs in pairwise comparisons of *Pseudomonas viridiflava* ATUE5. Distribution of $\log_{10}$(Recombined / Clonal SNPs) across 1,378 pairwise comparisons among 53 modern ATUE5 genomes. Bars indicate the proportion of pairs sharing the same (blue) or different (red) HTF–OBC pattern. 1,318 pairs (95.6%) exhibited $\log_{10}$(Recombined / Clonal SNPs) > 1, indicating that recombination generated more than tenfold the number of clonal SNPs. On average, recombination accounted for 96% of SNPs per isolate.

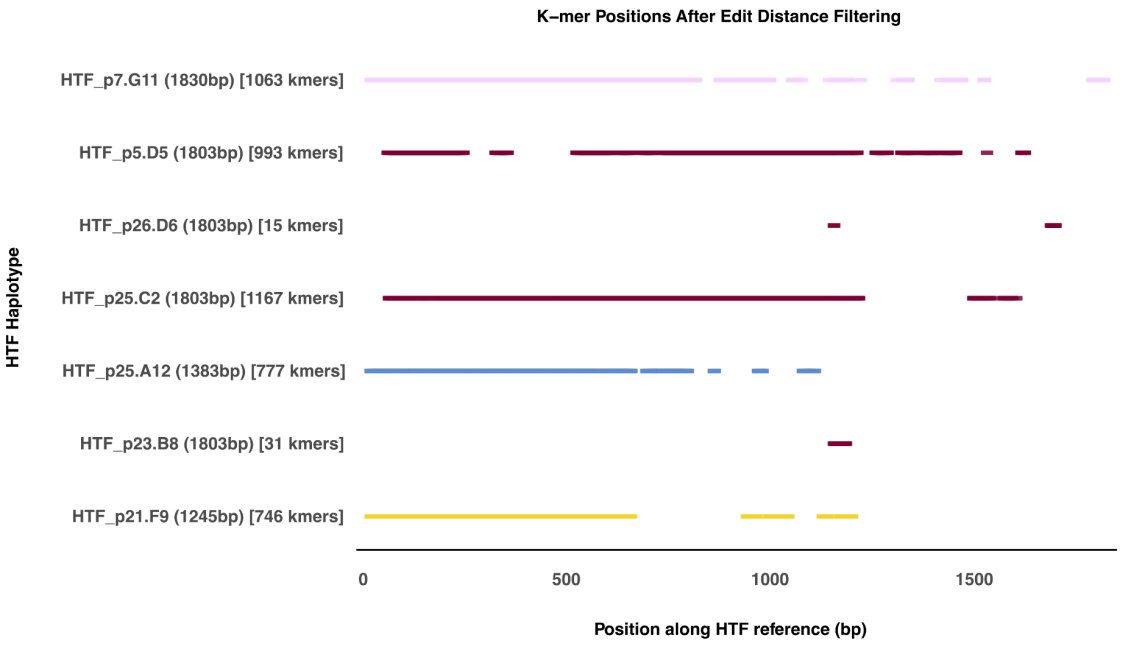

Figure S16. Distribution of diagnostic k-mers across HTF reference sequences. Each tick represents the position of a k-mer along the *HTF* nucleotide sequences (x-axis) after applying an edit-distance filter (>=2). Y-axis labels show *HTF* haplotype names, and the total number of retained k-mers per haplotype.

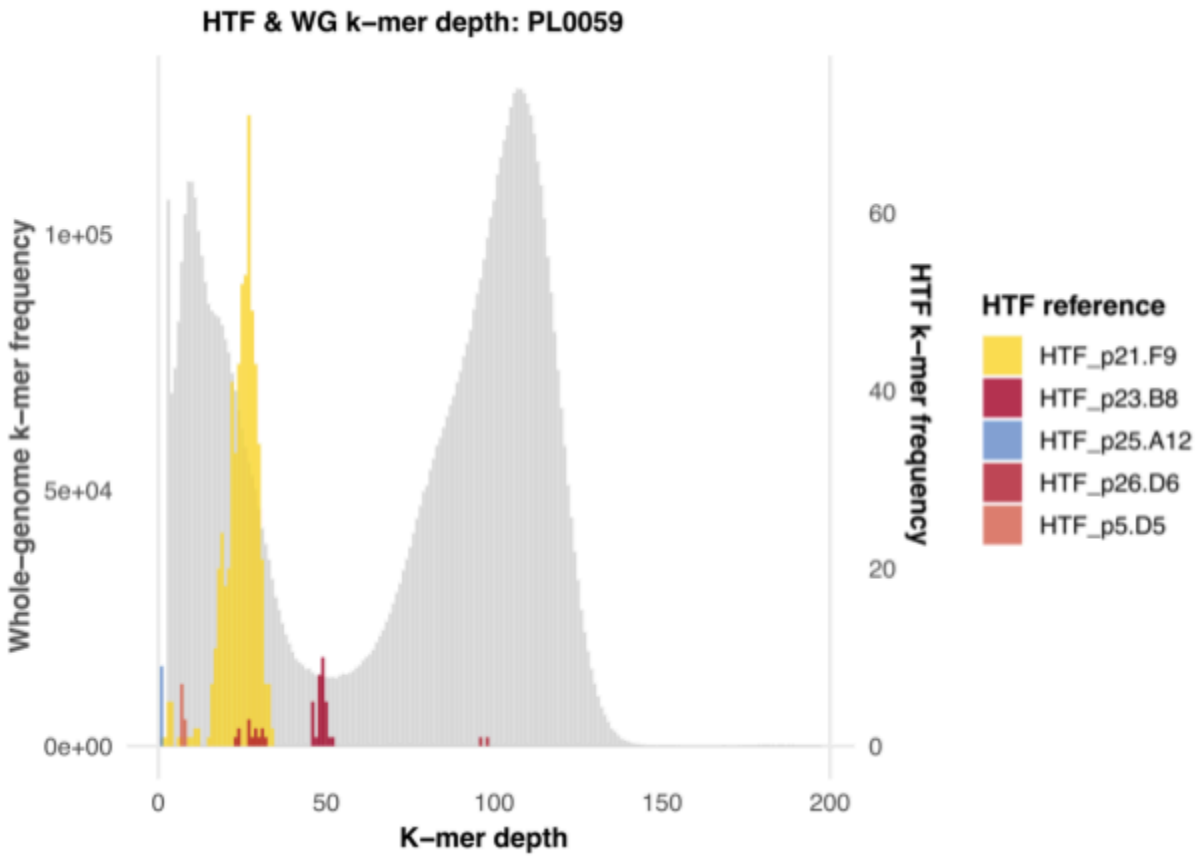

Figure S17. Bimodal k-mer depth distribution of PL0059 suggests coinfection. The histograms represent k-mer depth distributions. The grey background shows the whole-genome distribution, and the colored histograms represent the distribution for each of the diagnostic *HTF* haplotype k-mers. The bimodal pattern in the whole genome *k*-mer distribution indicates potential coinfection in PL0059. *K*-mer distributions for other isolates are available on GitHub.

Table S1: RB-TnSeq significant resistance trade-off genes.

Barcode ID	Log_2 (fold change) in Col-0	p-value Col-0	Log (fold change) after tailocin treatment	p-value tailocin assay	Log_2 (fold change) in Eyach1.5-2	p-value Eyach 1.5-2	Name gene or product	Significance in both ecotypes
BJEIHDPM_02277	-2.284	1.09E-06	3.560	1.38E-15	-1.570	7.8E-04	*chpB*	Both
BJEIHDPM_03520	-0.790	0.023	0.633	0.035	0.140	0.685	*yciF*	Col-0 only
BJEIHDPM_02879	-1.281	0.023	2.396	1.69E-09	-0.365	0.512	BolA-like protein	Col-0 only
BJEIHDPM_04292	-0.092	0.759	3.436	7.25E-16	-0.710	0.025	Hypothetical protein	Eyach 1.5-2 only
BJEIHDPM_01314	-1.152	0.024	5.499	5.78E-33	-1.479	0.005	Glycosyltransferase	Both
BJEIHDPM_01216	0.083	0.826	1.199	1.46E-06	-0.907	0.021	*ureC_2*	Eyach 1.5-2 only
BJEIHDPM_00728	-0.775	0.018	0.704	0.006	0.155	0.638	*ugpC_1*	Col-0 only
BJEIHDPM_03096	-0.709	0.022	0.530	0.030	0.063	0.838	*cmoB*	Col-0 only
BJEIHDPM_03578	-0.807	0.006	1.719	8.36E-15	-0.900	0.003	*flgE*	Both
BJEIHDPM_00926	-0.964	0.035	5.653	3.2E-29	-0.731	0.117	*rmlC_1*	Col-0 only
BJEIHDPM_00922	-0.379	0.026	6.969	3.02E-41	-0.355	0.040	*rfbB*	Both
BJEIHDPM_00925	-1.200	2E-09	4.909	2.38E-29	-1.363	2.09E-11	*wfgD*	Both
BJEIHDPM_00927	-2.879	7.87E-13	4.696	8.7E-23	-2.469	1.27E-09	*tagG_2*	Both
BJEIHDPM_00929	-0.747	7.4E-04	4.991	1.01E-34	-1.107	8.12E-07	*epsE_4*	Both
BJEIHDPM_00928	-3.293	5.98E-14	4.377	8.78E-20	-3.892	1.87E-16	*tagH_2*	Both
BJEIHDPM_00924	-1.212	8.23E-06	6.776	5.76E-40	-1.092	7.84E-05	*rmlA2_1*	Both
BJEIHDPM_00535	-0.200	0.526	2.040	1.74E-17	-0.909	0.005	*dapL*	Eyach 1.5-2 only
BJEIHDPM_03394	-1.276	1.2E-04	5.187	2.43E-28	-1.436	2.27E-05	*tagO*	Both
BJEIHDPM_03395	-1.018	2.79E-07	5.024	3.51E-29	-0.955	2E-06	*pglF*	Both
BJEIHDPM_01313	-1.324	1.3E-09	4.865	7.59E-30	-0.934	2.32E-05	O-antigen ligase domain-containing protein	Both
BJEIHDPM_01315	-2.185	1.55E-06	6.460	2.76E-33	-2.926	1.52E-09	Glycosyltransferase	Both

Table S2: Comparative glycosyl composition analysis of p25.C2 (WT) LPS and the O-antigen mutants. The LPS was analyzed by the GC-MS after acidic methanolysis, and conversion of the monosaccharides to trimethylsilyl (TMS)-methyl glycosides.

Strain	***ΔwfgD***	***ΔrmlC***	***ΔtagG***	***ΔtagH***	***ΔepsE***	***ΔspsA***	**WT**
Sugar residue							
Rha	42.8	92.2	69.4	60.6	33.2	24.7	94.7
Glc	27.9	1.0	10.1	8.3	28.2	8.3	0.7
Hep*	0.0	0.0	0.0	0.0	0.0	0.0	0.0
Kdo	27.6	5.9	19.4	29.3	36.3	63.9	2.4
FucNAc**	0.2	0.6	0.1	0.0	0.0	0.0	2.0
QuiNAc**	tr.	tr.	tr.	tr.	tr.	0.0	tr.
GalNAc	0.1	tr.	0.1	0.1	0.1	0.2	0.0
GlcNAc	1.4	0.3	0.9	1.7	2.2	2.9	0.1
	Mol %						

Legend: tr.- below 0.1%; . Rha- rhamnose; ; FucNAc- N-acetyl-fucosamine; Glc-glucose; Kdo-3-deoxy-D-manno-octulosonic acid; GalNAc- N-acetyl galactosamine, Hep- heptose; GlcNAc- N-acetyl glucosamine; *- the detection of heptose in the applied hydrolytic condition (1M HCL-MeOH) was not possible due to the phosphorylation of the Hep residue in the LPS; **- due to unavailability of authentic standards of FucNAc, Ara4N, QuiNAc, we used the relative response factor of GlcNAc to calculate the relative mol %.

Table S3: Statistics associated with the growth curves of p25.C2 WT versus O-antigen mutants. Growth curve parameters *k*, *r* (growth rates), t_gen (generation time) and AUC (area under the curve) were extracted for each curve (Fig. S4). Statistical analysis was performed on the means of three independent biological replicates with 4 technical replicates each. Differences were assessed by one-way analysis of variance (ANOVA1) followed by Tukey's post hoc test for each parameter (p-values: *** < 0.001, ** < 0.01, * < 0.05).

PARAMETER	STRAIN	WT	*ΔepsE*	*ΔrmlC*	*ΔspsA*	*ΔtagG*	*ΔtagH*	*ΔwfgD*
k	WT							
	ΔepsE	**						
	ΔrmlC	NS	*					
	ΔspsA	**	NS	NS				
	ΔtagG	**	NS	NS	NS			
	ΔtagH	NS	NS	NS	NS	NS		
	ΔwfgD	**	NS	*	NS	NS	NS	
r	WT							
	ΔepsE	NS						
	ΔrmlC	NS	NS					
	ΔspsA	*	NS	**				
	ΔtagG	NS	NS	NS	*			
	ΔtagH	NS	NS	**	NS	*		
	ΔwfgD	NS	NS	*	NS	NS	NS	
t_gen	WT							
	ΔepsE	NS						
	ΔrmlC	NS	NS					
	ΔspsA	*	NS	*				
	ΔtagG	NS	NS	NS	*			
	ΔtagH	NS	NS	*	NS	*		
	ΔwfgD	NS	NS	NS	NS	NS	NS	
AUC	WT							
	ΔepsE	***						
	ΔrmlC	NS	**					
	ΔspsA	***	NS	***				
	ΔtagG	**	NS	*	NS			
	ΔtagH	***	NS	**	NS	NS		
	ΔwfgD	***	NS	**	NS	NS	NS	

Table S4: Hydrogen peroxide minimum inhibitory concentrations (MICs) for WT and O-antigen mutants. MICs were determined as the lowest concentration of hydrogen peroxide that inhibited growth after 24 h in liquid culture, based on OD_{600} measurements collected in triplicate using a Tecan plate reader. Values represent mean ± SD (mM). "MIC/WT (est.)" indicates the relative MIC compared to wild-type; p-values reflect pairwise t-tests between each mutant and WT.

Strain	MIC (mM, mean ± SD)	MIC/WT (est.)	p-value
WT	5.0 ± 0.6	1.00	–
Δ*epsE*	6.9 ± 2.7	1.26	0.48
Δ*rmlC*	5.3 ± 0.6	1.06	0.17
Δ*spsA*	6.4 ± 2.7	1.26	0.55
Δ*tagG*	4.3 ± 0.6	0.87	0.27
Δ*tagH*	5.2 ± 0.6	1.03	0.87
Δ*wfgD*	6.6 ± 4.3	1.18	0.72

Table S5: Plasmids used in this study for Gateway cloning.

Product	**Sequence**	**Additional information**
p25.C2ΔwfgD attB DNA fragment	5'-GGGGACAAGTTTGTACAAAAAAGCAGGCTAACAGCGCCAAGGCTGGAAAGTGGCCTGCCTCGAAGAAATCGCGTACACCAATGGCTGGATCACACCAGAACAACTCGGCGCGCAAGCGCAGAAGCTGAAAAAAACCGGTTACGGTCAGTACCTGCAAAAACTGCTGGATCTGGGATCGTTCTGATTTCCGGCGCCTCTTTACACTTCATACCGCAAGGCGATGGACAGCTGACACGCTCATCCGCCTCCGTGGCATGAAAGCGCCTAGCCAGTACAAGCCATTGATAAATAAGGTCAATGCCTGCGCGAGAAGATTCACGACCGCCAGCTAAGCCCTGAACAGAATTGTCGGGAACGAGCAAACACCTAGCGATCCTATGGTTAAATTCCCGCCATCGAATGTTCTCCGAAGGCCGCCTATGTTAATGTACCCAGCTTTCTTGTACAAAGTGGTCCCC-3'	
p25.C2ΔrmlC attB DNA	5'-GGGGACAAGTTTGTACAAAAAAGCAGGCTATGACTCCCGCTCTCCACGCCGTGCAGAAGCCTTTCGC	

fragment	CGGAATCGTTCGTCTGCGCTTCCATCGCGCATGTC ATACCTCTTCAAAGTGCTTTTTCCATATGCCCTCAC ACGTCGGGCAGCAAGCATCCATTATCAGACGCTTT TCCAAACCAGTGCCGCACGAGTCTGCGCTGGTCA GTTTTTCGGAGATACCCTACGTATGAATCCCCATAT GACGCCATCTGCCGGCCCCTTGAGACTGGTGCAC AGCCTCTGGACGAACCGCTCGTTGATTTCACAGAT GACCCGACGCGAAGTCATCGGTCGGTATCGCGGC TCCGTCATGGGGCTGGCCTGGTCATTCTTCAACC CGGTTCTGATGCTGGCGGTATACACCTTCGTCTTT TCCGAAATTTTCAGTACCCAGCTTTCTTGTACAAAG TGGTCCCC-3’	
p25.C2ΔtagG attB DNA fragment	5’-GGGGACAAGTTTGTACAAAAAAGCAGGCTTTCG CCCATGGCTTCGTGGTGTTATCCGAAAGCGCCGA GTTCCTGTACAAGACCACGGATTACTGGGCGCCA GAGCATGAACGCAGTCTGGCCTGGAACGATTCGA GCGTAGCTATCCAATGGCCCATGAGCGAGCAGCC TGCGCTGTCCGCCAAGGATCAGAACGCTGTGCGT TTCGAAGACGCCGAGGTGTTCGCTTAAATGTCATC TGATCAACCGGTTATCAGCGTAAACAACGTCTCCA AGTGTTTTTACACCTACGACAAGCCCCATGAGCGT CTCAAACAGGCCCTGGTGCCGAGACTGCAGCGTT GGGCAGGCAAACAGGCCACTACCACGTACGGTAA AGAGTTCTGGGCGCTGCGAGACATCAGCTTCCAT GTCAACAAAGGCGAGACTGTGGGCATTGTCGACC CAGCTTTCTTGTACAAAGTGGTCCCC-3’	
p25.C2ΔtagH	pTB041	Ordered from TWIST
p25.C2ΔepsE_4 attB DNA fragment	5’-GGGGACAAGTTTGTACAAAAAAGCAGGCTAAGG CATGCCTGAAATTCAAGAGCTCTTTGGCAACCGGC GATTACTTCATATCCGTCGGGATTGCTTCCCGAGA AGGTGAAGAAATCGTCCCTCATGACAGACGCTAC GACTCCATACATTTCGTCGTAGAGCCCACCCCCAA CCTCCTTGGTTTGATCGACCTGGGTGCGTCCATG GATATCGAACCGGTAACAGTTAATGCTTGAACATGA ATATATTCCCCATATCCATTATGCCAAATACGAATAG CAAAGGTATGCAATGAACGTAGTGCAGAGACGTCC CGAAAAAATCGTCACGATGCTAAGGCTGATACTTAT ACTATTACCGGTCGTGAGCTTCTTAATAAGCGTATG GTCATGGCTGAGGTACGGCGTTGACATTCCAGTTT ATGATGACTGGCGTCACCCAGCTTTCTTGTACAAA GTGGTCCCC-3’	
p25.C2ΔspsA	pTB043	Ordered from TWIST

Flanking arm screening amplification	• p25.C2ΔwfgD F: 5'-AACAGCGCCAAGGCTGGAAA-3', R: 3'-ACATTAACATAGGCGGCCTTCGG-5', • p25.C2ΔrmlC_1 F: 5'-ATGACTCCCGCTCTCCACGC-3', R: 3'-ACTGAAAATTTCGGAAAAGACGAAGGTGT-5', • p25.C2ΔtagG_2 F: 5'-TTCGCCCATGGCTTCGTGG-3', R: 3'-CGACAATGCCCACAGTCTCGC-5', • p25.C2ΔtagH_2 F: 5'-TCTATCCAATCGCCGCGCTG-3', R: 3'-ACGTCAGGTGATAAAGCTTTGGCC-5', • p25.C2ΔepsE_4 F: 5'-AAAGGCATGCCTGAAATTCAAGAGCT-3', R: 3'-GACGCCAGTCATCATAAACTGGAATGT-5', • p25.C2ΔspsA F: 5'-TCCCTTACAGTGGAACATTCGCG-3', R: 3'-ACACACAGACCGGCACGTG-5'	wfgD WT= 1309bp rmlC WT= 946bp tagG W = 1228bp tagH W = 1772bp epsE WT= 5227bp spsA WT= 1374bp
sacB screening amplification	F: 5'-tgatttctccggtaaacattacggc-3', R: 3'-cctctgtttgtcatatagcttgtaatcac-5'	762bp
tetR screening amplification	F: 5'-accctggatgctgtaggcatagg-3', R: 3'-gccggaagcgagaagaatcataatg-5'	897bp

Table S6: qPCR primers and amplification program used in this study.

PRIMERS		
Gene	**Sequence 5'-3'**	**Amplicon length**
PP2A	FOR: TAACGTGGCCAAAATGATGC REV: GTTCTCCACAACCGCTTGGT	61 bp
FRK1	FOR: TTCGGATTCGGCGTTTGTTG REV: GCTTCTCTTGCTTTGAGGGA	118 bp

WRKY29	FOR: AGAATCTGTTGTCGGACGCA REV: TGCCAAACACCCTTTTGAGC	113 bp
NHL10	FOR: ATCGAAGCTCATGCCTACTACG REV: TTGGCTTCTCGCACAACTTC	113 bp
PAD3	FOR: TTGTGCTAAAGGCTGAAGCG REV: ACCGGAGATACAGTCGATGAAC	92 bp
PDF1.2	FOR: ACCCTTATCTTCGCTGCTCTTG REV: TTGGCTTCTCGCACAACTTC	85 bp
PR1	FOR: CTCATACACTCTGGTGGG REV: TTGGCACATCCGAGTC	191 bp

AMPLIFICATION PROGRAM			
	40X		**Up to 95 °C**
95 °C	95 °C	62 °C	62 °C + 0.3 °C/cycle
3'	30"	30"	30"

Table S7: Historical sample metadata.

*** Herbarium: KBI** = Komarov Botanical Institute of RAS (Russia); **KEW** = Kew Botanical Garden (United Kingdom); **LND** = Lund University Botanical Museum (Sweden); **MGC** = Herbario de Málaga (Spain); **NHM** = The Natural History Museum (United Kingdom); **OHN** = Biological Museum Oskarshamn (Sweden); **RJB** = Real Jardin Botanico (Spain); **STG** = Staatliches Museum für Naturkunde Stuttgart (Germany); **TUE** = Herbarium Tubingense University of Tübingen (Germany); **UOS** = University of Oslo (Norway)

SAMPLE	TYPE	YEAR	COUNTRY	At_proportion	At_covered_proportion	At_average_depth	Ps_proportion	Ps_covered_proportion	Ps_average_depth	GROUP	HERBARIUM*	SOURCE
PL0001	Plant tissue herbarium	1966	Spain	61.00%	87.61%	8.76	1.31%	90.66%	4.58	ATUE5	MGC	This study. ENA: PRJEB98841

PL0026	Plant tissue herbarium	2002	Sweden	50.00%	89.86%	12.01	0.50%	72.29%	1.58	ATUE5	OHN	This study. ENA: PRJEB98841
PL0059	Plant tissue herbarium	1985	Spain	12.10%	87.14%	6.85	31.47%	92.87%	137.41	ATUE5	RJB	This study. ENA: PRJEB98841
PL0073	Plant tissue herbarium	1991	Spain	56.30%	88.14%	8.13	1.05%	83.24%	2.83	ATUE5	RJB	This study. ENA: PRJEB98841
PL0087	Plant tissue herbarium	NA	Spain	44.00%	88.46%	8.37	0.33%	62.29%	1.13	ATUE5	RJB	This study. ENA: PRJEB98841
PL0102	Plant tissue herbarium	1888	Germany	25.60%	89.59%	7.46	6.34%	95.09%	31.13	ATUE5	TUE	This study. ENA: PRJEB98841
PL0105	Plant tissue herbarium	1920	Sweden	51.90%	89.42%	8.6	0.48%	64.37%	1.18	ATUE5	LND	This study. ENA: PRJEB98841
PL0108	Plant tissue herbarium	1946	Sweden	19.60%	89.74%	9.05	0.82%	80.50%	4.89	nonATUE5	LND	This study. ENA: PRJEB98841
PL0131	Plant tissue herbarium	1980	Spain	18.00%	87.70%	6.55	9.59%	92.67%	53.07	ATUE5	RJB	This study. ENA: PRJEB98841
PL0139	Plant tissue herbarium	1996	Sweden	13.90%	79.11%	2.36	0.48%	70.92%	1.52	ATUE5	OHN	This study. ENA: PRJEB98841
PL0185	Plant tissue herbarium	1994	Germany	43.20%	89.06%	8.35	0.60%	81.74%	2.7	ATUE5	STG	This study. ENA: PRJEB98841
PL0203	Plant tissue herbarium	1880	United Kingdom	54.80%	88.49%	8.06	0.50%	72.39%	1.68	nonATUE5	NHM	This study. ENA: PRJEB98841
PL0210	Plant tissue herbarium	1838	United Kingdom	30.30%	84.96%	4.18	3.70%	87.36%	10.36	ATUE5	NHM	This study. ENA: PRJEB98841
PL0220	Plant tissue herbarium	1946	United Kingdom	48.60%	88.47%	5.84	8.37%	89.32%	18.44	ATUE5	NHM	This study. ENA: PRJEB98841
PL0222	Plant tissue herbarium	1887	United Kingdom	42.10%	89.12%	8.55	0.36%	64.92%	1.23	ATUE5	NHM	This study. ENA: PRJEB98841
PL0224	Plant tissue herbarium	1889	United Kingdom	20.20%	89.01%	6.4	1.36%	93.00%	7.01	ATUE5	NHM	This study. ENA: PRJEB98841
PL0230	Plant tissue herbarium	1851	United Kingdom	57.30%	90.32%	8.68	0.73%	78.60%	2.01	ATUE5	NHM	This study. ENA: PRJEB98841
PL0235	Plant tissue herbarium	1905	United Kingdom	40.30%	86.39%	4.54	3.90%	91.81%	8.56	ATUE5	NHM	This study. ENA: PRJEB98841
PL0240	Plant tissue herbarium	1875	United Kingdom	66.70%	88.97%	7.57	2.02%	84.63%	7.38	ATUE5	NHM	This study. ENA: PRJEB98841

PL0258	Plant tissue herbarium	1913	United Kingdom	49.90%	88.39%	6.42	1.15%	83.22%	2.75	nonATUE5	NHM	This study. ENA: PRJEB98841
PL0027	Plant tissue herbarium	1939	Sweden	48.30%	89.78%	8.85	0.33%	65.78%	1.27	ATUE5	OHN	This study. ENA: PRJEB98841
PL0042	Plant tissue herbarium	1982	Spain	28.20%	88.62%	8.49	15.37%	93.77%	76.14	ATUE5	RJB	This study. ENA: PRJEB98841
PL0046	Plant tissue herbarium	1974	Spain	49.00%	88.93%	12.17	4.31%	89.76%	19.52	ATUE5	RJB	This study. ENA: PRJEB98841
PL0051	Plant tissue herbarium	1983	Spain	1.50%	20.73%	0.26	4.89%	89.92%	18.44	ATUE5	RJB	This study. ENA: PRJEB98841
PL0053	Plant tissue herbarium	1987	Spain	7.70%	64.01%	1.3	2.68%	94.16%	11.72	ATUE5	RJB	This study. ENA: PRJEB98841
PL0065	Plant tissue herbarium	2015	Spain	39.90%	88.61%	12.35	0.21%	68.88%	1.35	ATUE5	RJB	This study. ENA: PRJEB98841
PL0066	Plant tissue herbarium	2015	Spain	43.40%	89.49%	14.32	0.32%	70.50%	1.61	nonATUE5	RJB	This study. ENA: PRJEB98841
PL0068	Plant tissue herbarium	1986	Spain	17.20%	89.28%	8.43	1.04%	91.81%	12.58	ATUE5	RJB	This study. ENA: PRJEB98841
PL0080	Plant tissue herbarium	1985	Spain	1.90%	39.76%	0.58	4.23%	94.48%	29.67	ATUE5	RJB	This study. ENA: PRJEB98841
PL0127	Plant tissue herbarium	1979	Spain	9.10%	45.22%	0.68	4.61%	93.15%	8.63	ATUE5	RJB	This study. ENA: PRJEB98841
PL0137	Plant tissue herbarium	1961	Sweden	1.30%	1.89%	0.02	36.32%	89.29%	16.67	ATUE5	OHN	This study. ENA: PRJEB98841
27.ESP_1975	Plant tissue herbarium	1975	Spain	5.50%	7.22%	0.64	0.76%	75.00%	1.71	ATUE5	RJB	(Lopez et al., 2025)
30.ESP_1983b	Plant tissue herbarium	1983	Spain	4.70%	47.14%	0.81	0.54%	75.39%	1.74	ATUE5	RJB	(Lopez et al., 2025)
33.ESP_1985b	Plant tissue herbarium	1985	Spain	0.80%	13.26%	0.16	8.86%	91.39%	31.62	ATUE5	RJB	(Lopez et al., 2025)
34.ESP_1985c_S36	Plant tissue herbarium	1985	Spain	22.30%	81.36%	2.4	19.98%	89.98%	41.23	ATUE5	RJB	(Lopez et al., 2025)
64.GBR_1933b_S36	Plant tissue herbarium	1933	UK	39.50%	74.18%	1.95	5.71%	86.42%	5.51	ATUE5	KEW	(Lopez et al., 2025)
75.LTU_1894_S30	Plant tissue herbarium	1894	Lithuania	40.20%	87.96%	3.56	3.67%	90.64%	6.43	ATUE5	KBI	(Lopez et al., 2025)
76.LTU_2009_S19	Plant tissue herbarium	2009	Lithuania	0.20%	3.36%	0.04	26.02%	89.20%	65.73	ATUE5	RJB	(Lopez et al., 2025)
86.NOR_1911_S7	Plant tissue herbarium	1911	Norway	31.60%	83.44%	3.75	0.60%	67.85%	1.35	ATUE5	UOS	(Lopez et al., 2025)

109.NOR_1990	Plant tissue herbarium	1990	Norway	4.80%	30.04%	0.42	11.96%	91.97%	26.84	ATUE5	UOS	(Lopez et al., 2025)
120.RUS_1860	Plant tissue herbarium	1860	Russia	35.70%	70.54%	1.75	5.96%	89.46%	5.59	ATUE5	KBI	(Lopez et al., 2025)
HB0737	Plant tissue herbarium	1937	Germany	40.80%	88.15%	4.52	3.95%	90.08%	9.5	ATUE5	TUE	(Lang et al., 2024)
HB0766	Plant tissue herbarium	1846	Germany	48.90%	88.31%	5.87	2.85%	88.03%	8.16	ATUE5	STG	(Lang et al., 2024)
HB0808	Plant tissue herbarium	1817	Germany	55.10%	88.06%	5.33	0.56%	59.81%	1.06	ATUE5	STG	(Lang et al., 2024)
HB0814	Plant tissue herbarium	1882	Germany	19.20%	88.51%	5.05	1.82%	93.44%	8.98	ATUE5	STG	(Lang et al., 2024)
HB0828	Plant tissue herbarium	1890	Germany	39.10%	89.47%	6.34	0.52%	73.53%	1.74	nonATUE5	STG	(Lang et al., 2024)
HB0840	Plant tissue herbarium	1851	Germany	49.70%	89.45%	6.09	0.73%	76.28%	1.78	ATUE5	STG	(Lang et al., 2024)
HB0841	Plant tissue herbarium	1875	Germany	49.40%	89.21%	5.68	0.71%	73.19%	1.59	ATUE5	STG	(Lang et al., 2024)
HB0863	Plant tissue herbarium	1954	Somalia	23.20%	76.88%	3.05	0.51%	65.01%	1.49	nonATUE5	STG	(Lang et al., 2024)

Table S8: Summary of tailocin coverage, HTF haplotype assignment, and O-antigen presence in historical samples.

SAMPLE	Tailocin_cov_prop	Tailocin_depth	HTF_haplotype_bykmer	HTF_haplotype_bylocalassembly	HTFgroup_Oantigen_PA	wfgD_PA	rmlC_1_PA	tagG_2_PA	tagH_2_PA	spsA_PA	epsE_4_PA	epsE_4_length
109.NOR_1990	0.9662	28.26	HTF_p5.D5 (1803)	HTF_p5.D5 (1803)	OBC_present	1	1	1	1	1	1	4665
120.RUS_1860	0.9371	5.91	HTF_p5.D5 (1803)	HTF_p5.D5 (1803)	OBC_present	0	1	1	1	1	1	4665
27.ESP_1975	0.7961	1.88	HTF_p21.F9 (1245)	NA	OBC_present	1	1	1	1	1	NA	NA
30.ESP_1983b	0.8016	1.99	HTF_p25.A12 (1383)	NA	OBC_absent	0	0	0	0	0	0	0
33.ESP_1985b	0.9636	34.78	HTF_p23.B8 (1803)	HTF_p26.D6 (1803)	OBC_present	1	1	1	1	1	1	4827
34.ESP_1985c_S36	0.8867	42.57	HTF_p21.F9 (1245)	HTF_p21.F9 (1245)	OBC_present	1	1	1	1	1	1	4665
64.GBR_1933b_S36	0.8298	6.03	NA	NA	NA	0	0	0	0	0	0	0
75.LTU_1894_S30	0.9479	7.24	HTF_p25.A12 (1383)	HTF_p25.A12 (1383)	OBC_absent	0	0	0	0	0	0	0
76.LTU_2009_S19	0.8864	65.25	HTF_p21.F9 (1245)	HTF_p21.F9 (1245)	OBC_present	1	1	1	1	1	1	4665
86.NOR_1911_S7	0.7649	1.66	HTF_p23.B8 (1803)	NA	OBC_present	1	0	1	1	1	NA	NA
HB0737	0.9488	12.32	HTF_p23.B8 (1803)	HTF_p26.D6 (1803)	OBC_present	1	1	1	1	1	1	4827
HB0766	0.8935	8.33	HTF_p21.F9 (1245)	HTF_p21.F9 (1245)	OBC_present	1	1	1	1	1	1	4665
HB0808	0.6299	1.24	HTF_p25.A12 (1383)	NA	OBC_absent	0	0	0	0	0	0	0
HB0814	0.9414	10.22	HTF_p25.A12 (1383)	HTF_p25.A12 (1383)	OBC_absent	0	0	0	0	0	0	0
HB0840	0.8095	1.76	HTF_p7.G11 (1830)	NA	OBC_absent	0	0	0	0	0	0	0
HB0841	0.7612	1.69	HTF_p7.G11 (1830)	NA	OBC_absent	0	0	0	0	0	0	0
p1.G2	0.9472	46.84	HTF_p25.A12 (1383)	HTF_p25.A12 (1383)	OBC_absent	0	0	0	0	0	0	0
p12.A11	0.9066	42.92	HTF_p21.F9 (1245)	HTF_p21.F9 (1245)	OBC_present	1	1	0	1	1	1	4827
p12.E2	0.9965	119.05	HTF_p25.C2 (1803)	HTF_p26.D6 (1803)	OBC_present	1	1	1	1	1	1	4827
p12.G7	0.9472	25.53	HTF_p25.A12 (1383)	HTF_p25.A12 (1383)	OBC_absent	0	0	0	0	0	0	0
p13.C1	0.908	80.79	HTF_p21.F9 (1245)	HTF_p21.F9 (1245)	OBC_present	1	1	1	1	1	1	4665

p13.D10	0.9421	82.2	HTF_p25.A12 (1383)	HTF_p25.A12 (1383)	OBC_absent	0	0	0	0	0	0	0
p13.F3	0.9032	149.3	HTF_p7.G11 (1830)	HTF_p7.G11 (1830)	OBC_absent	0	0	0	0	0	0	0
p20.D4	0.985	27.7	HTF_p25.C2 (1803)	HTF_p26.D6 (1803)	OBC_present	1	1	1	1	1	1	4830
p20.F10	0.8983	25.66	HTF_p21.F9 (1245)	HTF_p21.F9 (1245)	OBC_present	1	1	0	1	1	1	4827
p20.G9	0.8983	23.34	HTF_p21.F9 (1245)	HTF_p21.F9 (1245)	OBC_present	1	1	0	1	1	1	4827
p21.A8	0.899	47.84	HTF_p21.F9 (1245)	HTF_p21.F9 (1245)	OBC_present	1	1	0	1	1	1	4827
p21.E3	0.8894	36.2	HTF_p21.F9 (1245)	HTF_p21.F9 (1245)	OBC_present	1	1	1	1	1	1	4665
p21.F1	0.9455	55.85	HTF_p5.D5 (1803)	HTF_p26.D6 (1803)	OBC_present	1	1	1	1	1	1	4665
p21.F9	0.915	40.89	HTF_p21.F9 (1245)	HTF_p21.F9 (1245)	OBC_present	1	1	0	1	1	1	4827
p22.A8	0.8847	35.76	HTF_p21.F9 (1245)	HTF_p21.F9 (1245)	OBC_present	1	1	1	1	1	1	4665
p22.B5	0.9002	27.86	HTF_p21.F9 (1245)	HTF_p21.F9 (1245)	OBC_present	1	1	1	1	1	1	4665
p22.C1	0.9312	40.68	HTF_p25.A12 (1383)	HTF_p25.A12 (1383)	OBC_absent	0	0	0	0	0	0	0
p22.D1	0.8985	9.41	HTF_p21.F9 (1245)	HTF_p21.F9 (1245)	OBC_present	1	1	1	1	1	1	4740
p22.D4	0.9494	7.01	HTF_p26.D6 (1803)	HTF_p26.D6 (1803)	OBC_present	1	1	1	1	1	1	4827
p23.A3	0.8558	85.83	HTF_p7.G11 (1830)	HTF_p7.G11 (1830)	OBC_absent	0	0	0	0	0	0	0
p23.B2	0.8543	49.68	HTF_p7.G11 (1830)	HTF_p7.G11 (1830)	OBC_absent	1	0	0	0	0	0	0
p23.B8	0.9671	26.47	HTF_p23.B8 (1803)	HTF_p26.D6 (1803)	OBC_present	1	1	1	1	1	1	4827
p24.B5	0.9463	23.21	HTF_p25.A12 (1383)	HTF_p25.A12 (1383)	OBC_absent	0	0	0	0	0	0	0
p24.H2	0.8291	28.8	HTF_p7.G11 (1830)	HTF_p7.G11 (1830)	OBC_absent	0	0	0	0	0	0	0
p25.A12	0.8627	6.84	HTF_p25.A12 (1383)	HTF_p25.A12 (1383)	OBC_absent	1	0	0	0	0	0	0
p25.B2	0.9983	9.65	HTF_p25.C2 (1803)	HTF_p26.D6 (1803)	OBC_present	1	1	1	1	1	1	4827
p25.C11	0.9102	8.22	HTF_p21.F9 (1245)	HTF_p21.F9 (1245)	OBC_present	1	1	1	1	0	NA	NA
p25.C2	1	42.26	HTF_p25.C2 (1803)	HTF_p26.D6 (1803)	OBC_present	1	1	1	1	1	1	4827
p25.D2	1	11.66	HTF_p25.C2 (1803)	HTF_p26.D6 (1803)	OBC_present	1	1	1	1	1	1	4827
p26.B7	0.9848	18.48	HTF_p25.C2 (1803)	HTF_p26.D6 (1803)	OBC_present	1	1	1	1	1	1	4773
p26.D6	0.9423	10.85	HTF_p26.D6 (1803)	HTF_p26.D6 (1803)	OBC_present	1	1	1	1	1	1	4827
p26.E7	0.9665	26.22	HTF_p23.B8 (1803)	HTF_p26.D6 (1803)	OBC_present	1	1	1	1	1	1	4827
p27.D6	0.8839	56.04	HTF_p21.F9 (1245)	HTF_p21.F9 (1245)	OBC_present	1	1	1	1	1	1	4665
p27.F2	0.9471	28.34	HTF_p25.A12 (1383)	HTF_p25.A12 (1383)	OBC_absent	0	0	0	0	0	0	0
p3.A3	1	13.74	HTF_p25.C2 (1803)	HTF_p26.D6 (1803)	OBC_present	1	1	1	1	1	1	4827
p3.F12	1	67.93	HTF_p25.C2 (1803)	HTF_p26.D6 (1803)	OBC_present	1	1	1	1	1	1	4827
p3.F8	0.9725	14.7	HTF_p26.D6 (1803)	HTF_p26.D6 (1803)	OBC_present	1	1	1	1	1	1	4827
p3.G9	0.9641	38.83	HTF_p25.A12 (1383)	HTF_p25.A12 (1383)	OBC_absent	0	0	0	0	0	0	0
p4.A6	1	12.73	HTF_p25.C2 (1803)	HTF_p26.D6 (1803)	OBC_present	1	1	1	0	1	1	4827
p4.D2	0.9521	41.7	HTF_p25.A12 (1383)	HTF_p25.A12 (1383)	OBC_absent	0	0	0	0	0	0	0
p4.E5	0.8841	8.28	HTF_p21.F9 (1245)	HTF_p21.F9 (1245)	OBC_present	1	1	1	1	1	1	4665
p4.E6	0.8915	24.02	HTF_p21.F9 (1245)	HTF_p21.F9 (1245)	OBC_present	1	1	1	1	1	1	4665
p5.C1	0.9244	81.52	HTF_p21.F9 (1245)	HTF_p21.F9 (1245)	OBC_present	1	1	1	1	1	1	4740
p5.C3	0.8853	52.84	HTF_p21.F9 (1245)	HTF_p21.F9 (1245)	OBC_present	1	1	1	1	1	1	4665
p5.D5	0.9405	51.93	HTF_p5.D5 (1803)	HTF_p26.D6 (1803)	OBC_present	1	1	1	1	1	1	4665
p5.H11	0.81	20.36	HTF_p7.G11 (1830)	HTF_p7.G11 (1830)	OBC_absent	0	0	0	0	0	0	0
p6.B9	0.9682	44.69	HTF_p26.D6 (1803)	HTF_p26.D6 (1803)	OBC_present	1	1	1	1	1	1	4827
p7.G11	0.8663	51.55	HTF_p7.G11 (1830)	HTF_p7.G11 (1830)	OBC_absent	0	0	0	0	0	0	0
p8.B3	1	81.84	HTF_p25.C2 (1803)	HTF_p26.D6 (1803)	OBC_present	1	1	1	1	1	1	4827
p8.B9	0.9546	50.02	HTF_p5.D5 (1803)	HTF_p26.D6 (1803)	OBC_present	1	1	1	1	1	1	4665
p8.C7	0.9228	47.55	HTF_p21.F9 (1245)	HTF_p21.F9 (1245)	OBC_present	1	1	1	1	1	1	4665

p8.E4	0.8831	33.34	HTF_p25.A12 (1383)	HTF_p25.A12 (1383)	OBC_absent	1	0	0	0	0	0	0
p8.H7	0.8614	57.78	HTF_p7.G11 (1830)	HTF_p7.G11 (1830)	OBC_absent	0	0	0	0	0	0	0
PL0001	0.8967	5.13	HTF_p21.F9 (1245)	NA	OBC_present	1	1	1	1	1	1	4740
PL0026	0.8111	1.85	NA	NA	NA	1	0	1	1	1	0	0
PL0027	0.6808	1.37	NA	NA	NA	1	1	1	1	1	0	0
PL0042	0.9445	81.1	HTF_p25.A12 (1383)	HTF_p25.A12 (1383)	OBC_absent	0	0	0	0	0	0	0
PL0046	0.8973	18.89	HTF_p21.F9 (1245)	HTF_p21.F9 (1245)	OBC_present	1	1	1	1	1	1	4665
PL0051	0.945	19.86	HTF_p25.A12 (1383)	HTF_p25.A12 (1383)	OBC_absent	0	0	0	0	0	0	0
PL0053	0.903	11.25	NA	HTF_p7.G11 (1830)	NA	0	0	0	0	0	1	4740
PL0059	0.9773	147.81	HTF_p23.B8 (1803)	HTF_p21.F9 (1245)	OBC_present	1	1	1	1	1	1	4827
PL0065	0.7115	1.47	NA	NA	NA	0	0	1	1	1	0	0
PL0068	0.9509	13.96	HTF_p23.B8 (1803)	HTF_p26.D6 (1803)	OBC_present	1	1	1	1	1	1	4827
PL0073	0.8247	2.85	HTF_p7.G11 (1830)	NA	OBC_absent	0	0	0	0	0	0	0
PL0080	0.9335	28.2	HTF_p25.A12 (1383)	HTF_p25.A12 (1383)	OBC_absent	0	0	0	0	0	0	0
PL0087	0.706	1.36	HTF_p5.D5 (1803)	NA	OBC_present	1	1	1	1	0	NA	NA
PL0102	0.9598	35.59	HTF_p25.A12 (1383)	HTF_p25.A12 (1383)	OBC_absent	0	0	0	0	0	0	0
PL0105	0.6913	1.4	HTF_p21.F9 (1245)	NA	OBC_present	0	1	1	1	1	NA	NA
PL0127	0.9203	8.31	HTF_p7.G11 (1830)	HTF_p7.G11 (1830)	OBC_absent	0	0	0	0	0	0	0
PL0131	0.972	55	HTF_p5.D5 (1803)	HTF_p5.D5 (1803)	OBC_present	1	1	1	1	1	1	4665
PL0137	0.9291	17.56	HTF_p26.D6 (1803)	HTF_p26.D6 (1803)	OBC_present	1	1	1	1	1	1	4827
PL0139	0.7523	1.74	HTF_p21.F9 (1245)	NA	OBC_present	1	1	0	1	1	NA	NA
PL0185	0.8486	2.92	HTF_p25.A12 (1383)	NA	OBC_absent	0	0	0	0	0	0	0
PL0210	0.8408	9.75	HTF_p7.G11 (1830)	HTF_p7.G11 (1830)	OBC_absent	0	0	0	0	0	0	0
PL0220	0.873	19.29	HTF_p25.A12 (1383)	HTF_p25.A12 (1383)	OBC_absent	0	0	0	0	0	0	0
PL0222	0.5953	1.1	HTF_p7.G11 (1830)	NA	OBC_absent	0	0	0	0	0	0	0
PL0224	0.9083	7.46	HTF_p21.F9 (1245)	HTF_p21.F9 (1245)	OBC_present	0	1	1	1	1	1	4665
PL0230	0.7933	2.03	HTF_p7.G11 (1830)	NA	OBC_absent	1	0	0	0	0	0	0
PL0235	0.9158	9.25	HTF_p21.F9 (1245)	HTF_p21.F9 (1245)	OBC_present	1	1	0	1	1	1	NA
PL0240	0.8604	8.04	HTF_p21.F9 (1245)	HTF_p21.F9 (1245)	OBC_present	0	0	0	0	0	0	0

Key Resources Table

RESOURCE	SOURCE	IDENTIFIER
Deposited Data		
1524 *Pseudomonas* genomes	Karasov et al. 2018	ENA: PRJEB24450
Experimental Models: Organisms/Strains		
1524 Modern *Pseudomonas* strains	Karasov et al. 2018	ENA: PRJEB24450
49 Historical strains	Lopez et al., 2025; Lang et al., 2024; This study	In supplementary info (Sample)/zenodo id ENA: PRJEB98841
p25.C2ΔwfgD, p25.C2ΔrmlC, p25.C2ΔtagG, p25.C2ΔtagH, p25.C2ΔepsE, p25.C2ΔspsA	This study	NA
Software and Algorithms		
BWA aln v0.7.17	Li & Durbin, 2009	
mapDamage2 v2.2.0	Jónsson et al., 2013	
IQ-TREE2 v2.1.4	Minh et al., 2020	
AdapterRemoval v2.3.3	Schubert et al., 2016	

SPAdes v3.15.0	Prjibelski et al., 2020	
Minimap2 v2.28	Li, 2018	
Jellyfish v2.2.10	Marçais & Kingsford, 2011	
ggplot2 v3.5.2	Wickham, 2009	
ExPASy	Gasteiger et al., 2003	
EMBOSS Transeq	Rice et al., 2000	
Clustal Omega	Sievers et al., 2011	
R v4.x	R Core Team, 2024	
BLAST+ v2.14	Camacho et al., 2009	
DESeq2 v1.30.1	Love et al., 2014	
lme4 v1.1-34	Bates et al., 2015	
emmeans v1.10.0	Lenth, 2020	
growthcurver v0.3.1	Sprouffske & Wagner, 2016	
lmerTest v3.1.3	Kuznetsova et al., 2017	
qpcR v1.4-2	Spiess, 2025	

Modern sample metadata.

SAMPLE	TYPE*	YEAR	COUNTRY	LOCATION	LAT	LON	Pseudomonas_Genome_Coverage_Prop.	Pseudomonas_Genome_Average_Depth_MQ30
p12.A11	Modern	2018	Germany	Eyach	48.446111	8.781611	0.955211	43.2805
p12.A9	Modern	2018	Germany	Eyach	48.446111	8.781611	0.385298	2.68517
p12.E2	Modern	2018	Germany	Eyach	48.446111	8.781611	0.946364	124.361
p12.F2	Modern	2018	Germany	Det-2	48.556255	9.135424	0.941151	61.1632
p12.G7	Modern	2018	Germany	Det-2	48.556255	9.135424	0.942483	26.1727
p12.H7	Modern	2018	Germany	Det-2	48.556255	9.135424	0.703408	7.44366
p13.C1	Modern	2018	Germany	Eyach	48.446111	8.781611	0.919667	91.4711

p13.C7	Modern	2018	Germany	Eyach	48.446111	8.781611	0.915668	30.2041
p13.D10	Modern	2018	Germany	Eyach	48.446111	8.781611	0.917782	83.4618
p13.D5	Modern	2018	Germany	Eyach	48.446111	8.781611	0.373545	3.2645
p13.F1	Modern	2018	Germany	Eyach	48.446111	8.781611	0.548638	9.89508
p13.F3	Modern	2018	Germany	Eyach	48.446111	8.781611	0.930129	180.182
p13.F5	Modern	2018	Germany	Eyach	48.446111	8.781611	0.486993	7.68403
p20.B10	Modern	2018	Germany	Eyach	48.446111	8.781611	0.362051	6.0333
p20.D4	Modern	2018	Germany	Eyach	48.446111	8.781611	0.965996	26.275
p20.F10	Modern	2018	Germany	Eyach	48.446111	8.781611	0.951949	27.3486
p20.G9	Modern	2018	Germany	Eyach	48.446111	8.781611	0.951606	25.8164
p21.A8	Modern	2018	Germany	Eyach	48.446111	8.781611	0.951989	50.4423
p21.E3	Modern	2018	Germany	Eyach	48.446111	8.781611	0.912764	42.5976
p21.F1	Modern	2018	Germany	Eyach	48.446111	8.781611	0.921125	54.2176
p21.F9	Modern	2018	Germany	Eyach	48.446111	8.781611	0.951456	43.9553
p22.A8	Modern	2018	Germany	Eyach	48.446111	8.781611	0.910773	42.5346
p22.B5	Modern	2018	Germany	Eyach	48.446111	8.781611	0.908795	31.8141
p22.C1	Modern	2018	Germany	Eyach	48.446111	8.781611	0.910697	44.4703
p22.D1	Modern	2018	Germany	Eyach	48.446111	8.781611	0.93509	9.86993
p22.D4	Modern	2018	Germany	Eyach	48.446111	8.781611	0.901368	6.48617
p23.A3	Modern	2018	Germany	Det-2	48.556255	9.135424	0.922147	90.3312
p23.A5	Modern	2018	Germany	Det-2	48.556255	9.135424	0.355851	5.69028
p23.B4	Modern	2018	Germany	Det-2	48.556255	9.135424	0.353754	10.3529
p23.B8	Modern	2018	Germany	Pfrondorf2	48.561087	9.109294	0.915323	25.8754
p24.B5	Modern	2018	Germany	Eyach	48.446111	8.781611	0.906998	24.3191
p24.H2	Modern	2018	Germany	Eyach	48.446111	8.781611	0.919194	36.961
p25.A12	Modern	2018	Germany	Eyach	48.446111	8.781611	0.904389	8.27369
p25.B2	Modern	2018	Germany	Eyach	48.446111	8.781611	0.99527	9.73957
p25.C11	Modern	2018	Germany	Eyach	48.446111	8.781611	0.936486	7.67613
p25.C2	Modern	2018	Germany	Eyach	48.446111	8.781611	0.999957	38.9734
p25.D2	Modern	2018	Germany	Eyach	48.446111	8.781611	0.997331	11.0366
p26.B7	Modern	2018	Germany	Pfrondorf2	48.561087	9.109294	0.918811	18.5831
p26.C10	Modern	2018	Germany	Det-2	48.556255	9.135424	0.532614	7.27294
p26.D6	Modern	2018	Germany	Eyach	48.446111	8.781611	0.907977	10.1768

p26.E7	Modern	2018	Germany	Pfrondorf2	48.561087	9.109294	0.915118	26.4647
p26.F6	Modern	2018	Germany	Pfrondorf2	48.561087	9.109294	0.263831	1.09767
p27.C5	Modern	2018	Germany	Pfrondorf2	48.561087	9.109294	0.33096	4.98267
p27.D6	Modern	2018	Germany	Pfrondorf2	48.561087	9.109294	0.915116	62.9111
p27.F2	Modern	2018	Germany	Pfrondorf2	48.561087	9.109294	0.908864	30.4347
p3.A3	Modern	2018	Germany	Eyach	48.446111	8.781611	0.999479	12.1995
p3.F12	Modern	2018	Germany	Eyach	48.446111	8.781611	0.999766	64.6266
p3.F8	Modern	2018	Germany	Eyach	48.446111	8.781611	0.910145	14.5013
p3.G11	Modern	2018	Germany	Eyach	48.446111	8.781611	0.405107	35.7165
p3.G9	Modern	2018	Germany	Eyach	48.446111	8.781611	0.936757	40.7657
p4.A6	Modern	2018	Germany	Eyach	48.446111	8.781611	0.999359	11.257
p4.A8	Modern	2018	Germany	Eyach	48.446111	8.781611	0.317566	8.57523
p4.C5	Modern	2018	Germany	Eyach	48.446111	8.781611	0.281958	2.19208
p4.D11	Modern	2018	Germany	Eyach	48.446111	8.781611	0.329928	7.72875
p4.D2	Modern	2018	Germany	Eyach	48.446111	8.781611	0.903089	43.5342
p4.E5	Modern	2018	Germany	Eyach	48.446111	8.781611	0.905147	9.07888
p4.E6	Modern	2018	Germany	Eyach	48.446111	8.781611	0.907851	26.4274
p4.H3	Modern	2018	Germany	Det-2	48.556255	9.135424	0.359271	11.1964
p5.A5	Modern	2018	Germany	Eyach	48.446111	8.781611	0.569164	20.9644
p5.C1	Modern	2018	Germany	Eyach	48.446111	8.781611	0.940631	83.5842
p5.C3	Modern	2018	Germany	Eyach	48.446111	8.781611	0.911686	61.8474
p5.D5	Modern	2018	Germany	Eyach	48.446111	8.781611	0.908126	47.1102
p5.F2	Modern	2018	Germany	Eyach	48.446111	8.781611	0.355109	10.8067
p5.H11	Modern	2018	Germany	Eyach	48.446111	8.781611	0.912223	24.6014
p6.A10	Modern	2018	Germany	Eyach	48.446111	8.781611	0.967914	86.1443
p6.B5	Modern	2018	Germany	Eyach	48.446111	8.781611	0.377432	8.17665
p6.B9	Modern	2018	Germany	Eyach	48.446111	8.781611	0.915641	40.9034
p6.D10	Modern	2018	Germany	Eyach	48.446111	8.781611	0.362251	6.29957
p6.E9	Modern	2018	Germany	Eyach	48.446111	8.781611	0.348102	5.45088
p6.F1	Modern	2018	Germany	Det-2	48.556255	9.135424	0.441901	14.1066
p6.G2	Modern	2018	Germany	Det-2	48.556255	9.135424	0.591204	22.8581
p6.G3	Modern	2018	Germany	Det-2	48.556255	9.135424	0.374359	12.0216
p7.F2	Modern	2018	Germany	Eyach	48.446111	8.781611	0.420044	6.6193